

## GROUNDED EO: Data-driven Sentinel-2 LAI and FAPAR retrieval using Gaussian processes trained with extensive fiducial reference measurements

Luke A. Brown<sup>a,\*</sup>, Richard Fernandes<sup>b</sup>, Jochem Verrelst<sup>c</sup>, Harry Morris<sup>d</sup>, Najib Djamai<sup>b</sup>, Pablo Reyes-Muñoz<sup>c</sup>, Dávid Kovács<sup>c</sup>, Courtney Meier<sup>e</sup>

<sup>a</sup> School of Science, Engineering & Environment, University of Salford, Manchester M5 4WT, United Kingdom

<sup>b</sup> Canada Centre for Remote Sensing, Natural Resources Canada, Ottawa K1A 0E4, Canada

<sup>c</sup> Image Processing Laboratory, University of Valencia, Paterna 46980, Spain

<sup>d</sup> Climate and Earth Observation Group, National Physical Laboratory, Teddington TW11 0LW, United Kingdom

<sup>e</sup> National Ecological Observatory Network, Battelle, Boulder, CO 80301, United States

### ARTICLE INFO

Editor: Jing M. Chen

**Keywords:**

Leaf area index  
Fraction of absorbed photosynthetically active radiation  
FRM  
GPR  
Machine learning  
S2

### ABSTRACT

Due to their importance in monitoring and modelling Earth's climate, the Global Climate Observing System (GCOS) designates leaf area index (LAI) and the fraction of absorbed photosynthetically active radiation (FAPAR) as essential climate variables (ECVs). The Simplified Level 2 Biophysical Processor (SL2P) has proven particularly popular for decametric (i.e. 10 m to 100 m) retrieval of these ECVs. Comprehensive validation has shown that due to simplifying assumptions in the underlying radiative transfer models (RTMs), biases persist in SL2P retrievals. To avoid RTM assumptions altogether, an empirical data-driven approach might be considered. Yet, such a strategy has historically been prevented by the limited quantity and quality of available in situ reference measurements, as well as the large number of training samples traditionally required by machine learning regression algorithms. New opportunities are now offered by recently established continental-scale environmental monitoring networks, advances in automated data processing and uncertainty evaluation, and machine learning regression algorithms that require many fewer training samples. The Ground Reference Observations Underlying Novel Decametric Vegetation Data Products from Earth Observation (GROUNDED EO) project was initiated to take advantage of these opportunities. We describe the empirical data-driven LAI and FAPAR retrieval approach adopted within the project, involving i) generation of a database containing over 16,000 fiducial reference measurements covering 81 National Ecological Observatory Network (NEON), Integrated Carbon Observation System (ICOS), and Terrestrial Ecosystem Research Network (TERN) sites between 2013 and 2022, ii) development of an empirical data-driven algorithm for Sentinel-2 LAI and FAPAR retrieval based on Gaussian processes, and iii) evaluation of GROUNDED EO retrievals through intercomparison with the current state-of-the-art in decametric retrieval (i.e. SL2P, and a modified version of SL2P developed by the Canada Centre for Remote Sensing – SL2P-CCRS), as well as validation against unseen fiducial reference measurements. In the majority of cases (and despite not making use of ancillary data such as land cover), the empirical data-driven GROUNDED EO retrievals were subject to reduced bias than those from SL2P and SL2P-CCRS, as well as increased fulfilment of user requirements (i.e. 74% of LAI and 69% of FAPAR retrievals overall). Consequently, the approach has potential to reduce uncertainty in key inputs for climate monitoring and modelling, agricultural and forest management, and biodiversity assessment.

### 1. Introduction

Due to their fundamental importance in monitoring and modelling Earth's climate, the Global Climate Observing System (GCOS, 2019) designates leaf area index (LAI) and the fraction of absorbed

photosynthetically active radiation (FAPAR) as essential climate variables (ECVs). LAI is defined as half the total green leaf area per unit horizontal ground area, whilst FAPAR is defined as the fraction of photosynthetically active radiation (PAR, i.e. radiation between 400 nm and 700 nm) absorbed by vegetation for a specified illumination. In

\* Corresponding author.

E-mail address: [l.a.brown4@salford.ac.uk](mailto:l.a.brown4@salford.ac.uk) (L.A. Brown).

addition to climate monitoring and modelling, these biophysical variables are widely used for agricultural and forest management, as well as biodiversity assessment, forming a crucial input into models of vegetation productivity and crop yield, and representing a useful indicator of landscape disturbance (Ogutu et al., 2013; Richardson et al., 2013; Sellers et al., 1997). Over the last 25 years, a range of operational algorithms and products have been developed to retrieve LAI and FAPAR from optical satellite remote sensing data, with a primary focus on hectometric (i.e. 100 m to 1 km) and kilometric (i.e. > 1 km) spatial resolution instruments such as the Advanced Very High Resolution Radiometer (García-Haro et al., 2018), Moderate Resolution Imaging Spectroradiometer and successor Visible Infrared Imaging Radiometer Suite (Yan et al., 2016a, 2018), and Ocean and Land Colour Instrument (Gobron et al., 2022; Kovács et al., 2023; Reyes-Muñoz et al., 2022). With  $\leq 3$  day repeat global coverage, these products have proven invaluable for regional and global monitoring. Nevertheless, higher spatial resolution retrievals are required in applications including precision agriculture, forest management, and climate adaptation (Clevers and Gitelson, 2013; GCOS, 2019; Majasalmi and Rautiainen, 2016).

Within the last decade, the advent of analysis ready data (ARD) from instruments such as the Landsat 8/9 Operational Land Imager (OLI) (Vermote et al., 2016) and the Sentinel-2 Multispectral Instrument (MSI) (Drusch et al., 2012) has led to an increased focus on decametric (i.e. 10 m to 100 m) biophysical retrieval. Indeed, for LAI and FAPAR, GCOS currently specifies threshold, breakthrough, and target spatial resolution requirements of 250 m, 100 m and 10 m, respectively. The Simplified Level 2 Prototype Processor (SL2P) retrieval algorithm (Weiss and Baret, 2016) has proven particularly popular for generating 'L2B' products (including LAI and FAPAR) from OLI and MSI surface reflectance data, owing to its widespread availability and ease of adoption. Free and open implementations are available within the European Space Agency's (ESA's) Sentinel Application Platform (SNAP) (<https://step.esa.int/main/toolboxes/sentinel-2-toolbox/sentinel-2-toolbox-features>), as well as in Google Earth Engine via the Landscape Evolution and Forecasting (LEAF) Toolbox (<https://github.com/rfernand387/leaf-toolbox>). SL2P adopts a hybrid retrieval approach, using simulations from the coupled Leaf Optical Properties Spectra (PROSPECT) (Feret et al., 2008; Jacquemoud and Baret, 1990) and Scattering by Arbitrarily Inclined Leaves (SAIL) (Verhoef, 1984; Verhoef et al., 2007) radiative transfer models (RTMs) to train artificial neural networks for retrieval. Notably, SAIL represents the canopy as a horizontally homogeneous turbid medium, and is known to perform poorly in heterogeneous canopies that deviate strongly from this assumption (Richter et al., 2009; Verger et al., 2011).

Comprehensive validation of SL2P LAI and FAPAR retrievals has demonstrated acceptable performance over homogeneous canopies (e.g. cultivated crops, grasslands, pasture/hay, and shrub/scrub vegetation), but biases over heterogeneous canopies (e.g. forests and woodlands) (Brown et al., 2019, 2021b; Djamai et al., 2019; Fernandes et al., 2023, 2024; Hassampour et al., 2024; Hu et al., 2020; Putzenlechner et al., 2019; Uperti et al., 2019; Vanino et al., 2018; Vuolo et al., 2016; Xie et al., 2019). For example, Fernandes et al. (2024), report that SL2P LAI retrievals meet user requirements over  $> 90\%$  of non-forest sites, but only 50% of forest sites, indicating that algorithm improvements are clearly required. In an attempt to address the issue, several strategies have been tested, including empirical bias correction of SL2P LAI retrievals (Fernandes et al., 2023), as well as the replacement of SAIL with a heterogeneous canopy RTM (Fernandes et al., 2024). A version of SL2P using the 4SAIL2 heterogeneous RTM, SL2P-CCRS, was found to reduce the bias of LAI retrievals over forests, but the overall difference with respect to fiducial reference measurements was virtually unchanged due to lower precision (Fernandes et al., 2024).

To avoid the assumptions associated with RTM simulations altogether, an empirical data-driven approach might be considered, in which machine learning regression algorithms are trained with a large number of high-quality in situ reference and contemporaneous satellite observations. So far, however, such a strategy has been difficult to

implement globally. This has primarily been due to the limited quantity and quality of representative in situ reference measurements, which have historically been collected during one-off field campaigns (typically during the peak of the growing season, thereby representing a limited range of vegetation condition), and have been subject to unquantified measurement uncertainties (Camacho et al., 2013; Fang et al., 2019; Garrigues et al., 2008; Weiss et al., 2014; Yan et al., 2016b). These factors have been compounded by the nature of the machine learning regression algorithms themselves, which traditionally required a vast number of training samples to achieve acceptable levels of performance over large or diverse domains (Combal et al., 2003; Weiss et al., 2000).

In recent years, new continental-scale environmental monitoring networks have been established and are now collecting long-term in situ reference observations over permanent measurement sites on a routine basis. Examples include the National Ecological Observatory Network (NEON) in the United States (Kao et al., 2012; Meier et al., 2023), the Integrated Carbon Observation System (ICOS) in Europe (Gielen et al., 2018), and the Terrestrial Ecosystem Research Network (TERN) in Australia (Cleverly et al., 2019; Karan et al., 2016). Crucially, these networks adopt standard data collection protocols, ensuring the data they provide is consistent. Whilst several of these networks only provide raw observations, automated data processing tools now enable the derivation of biophysical variables including LAI and FAPAR from their archives using a common processing chain (Brown et al., 2020b, 2023; Brown and Leblanc, 2024; Chianucci et al., 2022; Chianucci and Macek, 2023; Serouart et al., 2022). In addition, developments under ESA's Fiducial Reference Measurements for Vegetation (FRM4VEG) programme provide the means to quantify the uncertainty of the derived measurements in a metrologically robust manner (Brown et al., 2021a; Camacho et al., 2024; Goryl et al., 2023; Niro et al., 2021).

In parallel to substantial increases in the availability of in situ reference observations, and in particular, fiducial reference measurements, new retrieval algorithm training strategies such as active learning have been gaining popularity. Through the use of uncertainty- and diversity-based criteria, active learning aims to select only the most informative samples for training (Berger et al., 2021; Verrelst et al., 2020; Verrelst et al., 2016). When coupled with machine learning regression algorithms, these methods have been demonstrated to require many fewer training samples (i.e. hundreds) (Berger et al., 2021; Estévez et al., 2022; Verrelst et al., 2020) than for traditional training strategies (i.e. tens of thousands to hundreds of thousands) (Combal et al., 2003; Weiss et al., 2000). Meanwhile, alternative non-parametric machine learning regression algorithms such as Gaussian process regression (GPR) (also termed Gaussian processes) have risen to prominence (Rasmussen and Williams, 2006). Due to the adoption of a Bayesian approach to the regression problem, GPR inherently provides retrieval (i.e. model-based) uncertainty estimates in the form of a posterior probability distribution (whose mean and standard deviation represent the retrieved value and its uncertainty, respectively) (Verrelst et al., 2013, 2015b). Retrieval uncertainty estimates are a growing requirement, for example in data assimilation schemes (Chernetskiy et al., 2017; Lewis et al., 2012; Mathieu and O'Neill, 2008), enabling users to weight observations on the basis of their confidence (Demarty et al., 2007; Raupach et al., 2005; Richardson et al., 2011), making such a feature particularly attractive. Indeed, per-pixel retrieval uncertainty estimates are a goal of the Committee on Earth Observation Satellites (CEOS, 2024) ARD standard.

Within the framework of ESA's Living Planet Fellowship programme, the Ground Reference Observations Underlying Novel Decametric Vegetation Data Products from Earth Observation (GROUNDED EO) project (<https://eo4society.esa.int/projects/grounded-eo>) was initiated to take advantage of opportunities afforded by new continental-scale environmental monitoring networks, automated data processing and uncertainty evaluation methods, as well as advances in machine learning regression techniques. In this paper, we describe the empirical

data-driven LAI and FAPAR retrieval approach developed within the project for application to Sentinel-2. We focus on Sentinel-2 due to the extensive validation of existing retrieval algorithms for Sentinel-2 products, the operational availability of free and open data, and the similarities between Sentinel-2 and upcoming missions such as Landsat Next (Wulder et al., 2022). The specific objectives of the paper are to:

1. Describe the generation of an extensive database suitable for calibration and validation of decametric LAI and FAPAR retrieval algorithms and products, containing fiducial reference measurements from 81 NEON, ICOS, and TERN sites (hereafter termed the GROUNDED EO database);
2. Detail the development of a new empirical data-driven biophysical retrieval algorithm for Sentinel-2 LAI and FAPAR, based on Gaussian processes (hereafter termed the GROUNDED EO retrieval algorithm);
3. Provide a comprehensive evaluation of GROUNDED EO LAI and FAPAR retrievals through intercomparison with the current state-of-the-art in decametric retrieval approaches (i.e. SL2P and SL2P-CCRS) as well as validation against unseen fiducial reference measurements.

By adopting an empirical data-driven approach that utilises consistent, representative fiducial reference measurements with characterised uncertainties, and by avoiding assumptions associated with RTM simulations, it is hypothesised that GROUNDED EO will reduce biases associated with existing decametric LAI and FAPAR retrieval algorithms. For downstream applications, which typically involve spatiotemporal synthesis, reducing bias is critical, since random errors are suppressed by averaging, whereas systematic errors are not (Brown et al., 2024a; Fernandes et al., 2024). In this respect, the approach has potential to reduce uncertainty in key inputs for climate monitoring and modelling, agricultural and forest management, and biodiversity assessment.

## 2. Materials and methods

### 2.1. Overview

An overview of the applied workflow is provided in Fig. 1. This relied upon the generation of fiducial reference measurements from raw in situ digital hemispherical photography (DHP) and digital cover photography (DCP) data collected at 81 NEON, ICOS, and TERN sites (1–2), which were then matched to spatiotemporally coincident Sentinel-2 L2A surface reflectance observations (3). Matched pairs of fiducial reference measurements and L2A observations were used to train GPR models (4), and the trained models were applied for LAI and FAPAR retrieval (5). Intercomparison against SL2P and SL2P-CCRS was carried out (6–7), and all retrieval algorithms were validated against unseen fiducial reference measurements (8). A detailed description of each step is provided in the following sub-sections.

### 2.2. Study sites and generation of the GROUNDED EO fiducial reference database

To train the empirical data-driven GROUNDED EO retrieval algorithm, an extensive database of in situ reference measurements was required. One of the largest reference datasets for biophysical variables is the DIRECT database maintained by the Land Product Validation (LPV) sub-group of the CEOS Working Group on Calibration and Validation (WGCV). In its latest version (2.1), it contains 280 LAI and 128 FAPAR samples from 176 sites, but unfortunately, it was designed for the calibration and validation of kilometric products, and features only 3 km × 3 km averages, making it ill-suited for decametric remote sensing data (Camacho, 2021). In terms of decametric LAI and FAPAR products, two in situ reference datasets widely used for calibration and validation were developed respectively under the Implementing Multiscale Agricultural Indicators Exploiting Sentinels (ImagineS) project and

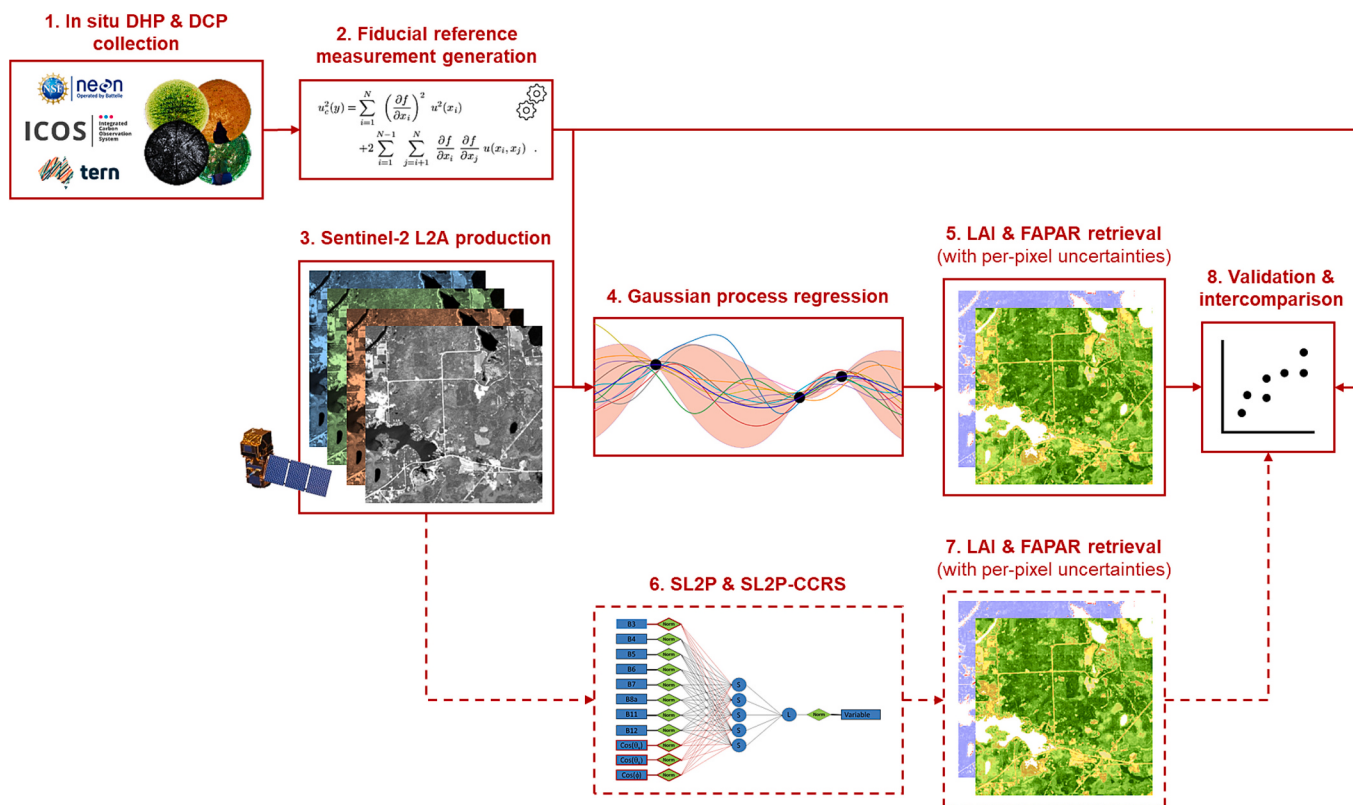


**Fig. 1.** Overview of the training and evaluation of the empirical data-driven GROUNDED EO retrieval algorithm (including intercomparison with SL2P and SL2P-CCRS – shown with dashed lines).

Copernicus Ground Based Observations for Validation (GBOV) service. Whilst useful for Landsat 8, ImagineS, covering 15 sites, contains few observations since the launch of the Sentinel-2 missions in 2015 (Camacho et al., 2021; Fuster et al., 2020). The GBOV dataset, on the other hand, contains a greater number of observations from within Sentinel-2's lifetime, but has been primarily restricted to a subset of NEON sites (Brown et al., 2021b; Brown et al., 2020a).

For the purposes of this study, we expanded upon the NEON data included within the GBOV dataset, making full use of all 47 terrestrial NEON sites, as well as data from an additional 20 ICOS and 14 TERN sites (Fig. 2 and Appendix A). These networks were selected because they operate free and open data policies and adopt standardised and documented data collection protocols, allowing consistent *in situ* reference measurements to be generated. We note that data from one-off field campaigns were not considered, as they would not allow seasonal variations in the reflectance-biophysical variable relationship to be captured, nor would they enable assessment of retrieval temporal stability (Djamai et al., 2025). Networks with restrictions on data use were also disregarded, as were as networks that did not provide access to raw data. Access to raw data was critical because i) it was necessary to derive uncertainties in an end-to-end manner, and ii) our aim was to apply common automated processing chains to achieve a greater degree of consistency in the derived *in situ* reference measurements than has been possible in previous datasets, which have been compiled from different groups using a range of data processing methods. The 81 sites spanned cultivated crops, deciduous broadleaf forest, evergreen broadleaf forest, evergreen needleleaf forest, grasslands, mixed forest, pasture/hay, shrub/scrub and woody wetlands over the United States, Europe, and Australia, covering the period from 2013 to 2022 (Fig. 2 and Appendix A).

To monitor vegetation biophysical properties, NEON and ICOS make use of DHP, whereas TERN uses a mixture of DHP and DCP depending on the site in question. Whilst DHP makes use of a fisheye lens with a 180° field-of-view, only a standard digital camera with a 15° to 30° field-of-view is required by DCP. Crucially, this smaller field-of-view is known to result in more even sky luminance, less sensitivity to exposure, and a stronger contrast between the sky and vegetation, facilitating successful classification even for images captured under sub-optimal illumination conditions (i.e. non-uniform skies and outside of dawn/dusk) (Macfarlane et al., 2007b; Macfarlane et al., 2007a; Pekin and Macfarlane, 2009). This greatly simplifies logistics associated with field data collection. All networks sample multiple times per year within elementary sampling units (ESUs) suitable for the calibration and

validation of decametric remote sensing data (Table 1). Neither NEON nor TERN process their DHP or DCP data, whilst ICOS provide only site-level averages as opposed to values at the ESU level. Thus, full processing of all images was required. The quantity of data to be handled necessitated a fully automated approach.

The HemiPy (Brown et al., 2023) and CoverPy (Brown and Leblanc, 2024) modules were utilised for automated processing of DHP and DCP images, respectively. They calculate estimates of gap fraction to derive overstory plant area index (PAI), understory green area index (GAI), the fraction of vegetation cover (FCOVER), and for HemiPy, the fraction of intercepted photosynthetically active radiation (FIPAR). Note that GAI incorporates all green plant elements (e.g. stems), not only leaves (Baret et al., 2010a). Critically, HemiPy and CoverPy adopt the recommendations of the FRM4VEG project (Brown et al., 2021a; Camacho et al., 2024), propagating uncertainties (due to variability in gap fraction) through the derivation of the considered variables, in line with the International Standards Organisation (ISO) Guide to the Expression of Uncertainty in Measurement (GUM) (Working Group 1 of the Joint Committee for Guides in Metrology, 2008). Over 280,000 individual DHP or DCP images were processed, yielding a database containing more than 16,000 unique ESU-level observations between 2013 and 2022 (Table 1).

Note that HemiPy and CoverPy account for clumping at both the within- and between-crown scales, allowing PAI to be computed (as opposed to effective PAI ( $PAI_e$ ), in which a random distribution of plant material is assumed). To achieve this, HemiPy makes use of Lang and Yueqin's (1986) method, in which PAI is derived from the mean of the natural logarithm of gap fraction values over all azimuth cells and images within an ESU (as opposed to the natural logarithm of mean gap fraction values). Leblanc and Fournier (2014) evaluated several clumping correction approaches using three-dimensional forest simulations, finding that although the method of Leblanc et al. (2005) was the best performing, the performance of Lang and Yueqin's (1986) approach was comparable when calculated using an azimuth cell size of 15°, which is very close to the 10° adopted by HemiPy (both methods led to an RMSD in PAI of between 1.0 and 1.1). Meanwhile, CoverPy accounts for clumping through calculation of mean crown cover and crown porosity over all images within an ESU, which themselves are determined on the basis of the number of small, within-crown, and large, between-crown gaps (Brown and Leblanc, 2024; Chianucci et al., 2022; Macfarlane et al., 2007a, 2007b). Full details on the processing algorithms adopted by HemiPy and CoverPy are available in Brown et al. (2023) and Brown and Leblanc (2024).

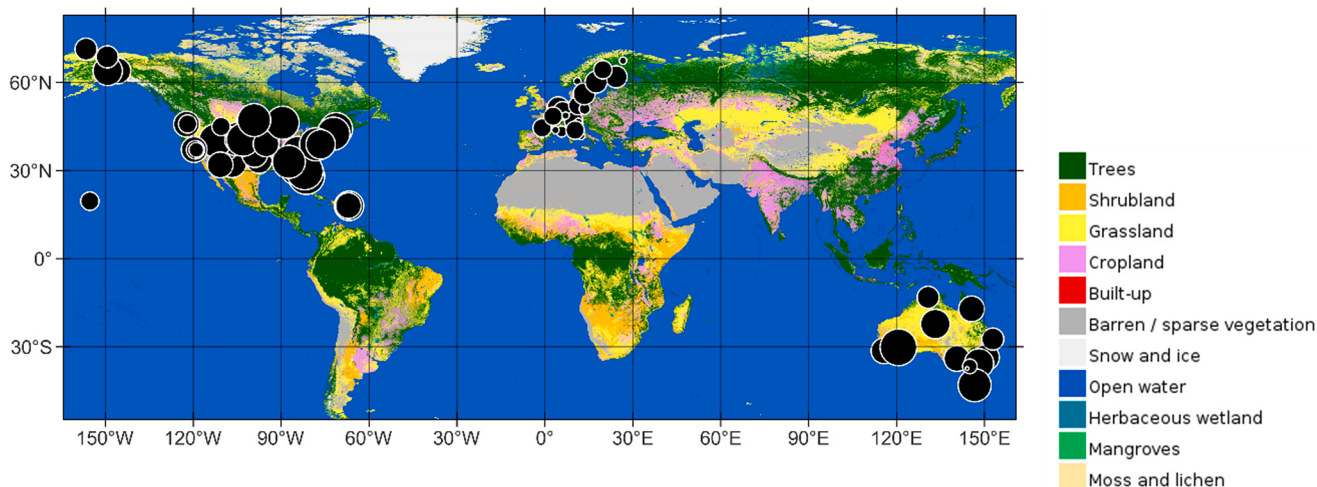


**Fig. 2.** Location of the 81 NEON, ICOS, and TERN sites from which raw *in situ* data were obtained and processed to derive fiducial reference measurements (black circles). The circle size is proportional to the number of years (1 to 10) of data available at each site. Background land cover data are from WorldCover 2020 (ESA, 2021). Please refer to Appendix A for site-specific land cover information.

**Table 1**

Overview of in situ sampling conducted by NEON, ICOS and TERN.

Network	Sites	Method	Temporal frequency	ESU extent	Sampling points per ESU	Unique ESU-level observations	Approximate number of images
NEON	47	DHP	Every two weeks within the growing season	20 m × 20 m to 40 m × 40 m	12	14,141	258,216
ICOS	20	DHP	Six times per year	30 m × 30 m	9	1776	15,984
TERN	14	DHP & DCP	Site dependent, up to five times per year	100 m × 100 m	36	169	6084

To account for shoot-scale clumping in needleleaf canopies, a multiplicative correction is often applied based on destructively sampled shoots, corresponding to

$$\gamma = \frac{1}{4 \text{STAR}} \quad (1)$$

where STAR is the shoot silhouette-to-total needle area ratio, with values typically ranging from 0.13 to 0.20 (Pisek et al., 2025; Stenberg, 1996). However, this correction was considered liable to overestimate PAI for three reasons. Firstly, image resolution is usually insufficient to resolve gaps within small or far-away shoots, leading to an overestimation of PAI that partly compensates for underestimation due to shoot-scale clumping. This implies that, for photographic methods, the average imaged shoot silhouette-to-total needle area ratio should be used in place of STAR. Secondly, STAR is only applicable to shoots – no correction should be applied to viewed woody area (Stenberg, 1996). This implies that the correction factor should be reduced as a function of the woody-to-total ratio. Thirdly, the correction assumes a random distribution of shoots, whereas recent work has indicated that shoots may not be randomly distributed at the scale of a 10° zenith and azimuth cell (as is adopted by HemiPy). Using terrestrial laser scanning and a 0.8 m length scale (approximately equivalent to a 10° zenith and azimuth cell at a 5 m distance), Schraik et al. (2021) found a within-crown STAR of 0.20 to 0.25 ( $\gamma = 1$  to 1.25) for Norway spruce, where STAR reportedly ranges from 0.14 to 0.18 ( $\gamma = 1.39$  to 1.79) (Pisek et al., 2025). These issues all suggest that the applied correction factor should, in fact, be substantially less than  $\frac{1}{4 \text{STAR}}$ . Considering the large natural variability in STAR (Pisek et al., 2025; Stenberg, 1996) and the lack of knowledge of each factor for a given measurement, we assumed  $\gamma = 1$ . This likely led to some degree of underestimation of PAI for needleleaf canopies, but more research is required to confirm and quantify the extent of this underestimation.

It should be noted that the quality of DHP-derived biophysical variables is strongly dependent on the illumination conditions under which images are captured (Bréda, 2003; Chianucci and Cutini, 2012; Jonckheere et al., 2004). As a result, in parallel to the automated derivation of PAI, GAI, and FIPAR, manual inspection of each set of DHP images (corresponding to a single ESU) was undertaken to assign a quality flag. As in previous validation studies, we discarded all ESUs containing DHP images that demonstrated fixed pattern noise, overexposure, colour balance issues, variable illumination, or foreign objects within the field-of-view from further analysis (Brown et al., 2021b; Brown et al., 2020a).

### 2.3. Correcting the GROUNDED EO database for missing understory measurements and overstory woody area

Although the majority of sites considered in this study routinely collect both upwards- and downwards-facing DHP and DCP images, enabling the understory and overstory to be characterised, only upwards-facing DHP images are provided by ICOS (despite the documented presence of understory vegetation) (George et al., 2021; Gielen et al., 2018). Previous work has shown that the understory may represent a substantial proportion of the total canopy, particularly at forest sites, and that biases of  $> 0.5$  in PAI may be observed if in situ measurements neglect the understory layer (Brown et al., 2020a). Discarding

forest observations lacking understory data within the database, as has previously been recommended as good practice (Brown et al., 2020a; Camacho et al., 2013; Weiss et al., 2014), would have led to no coverage over Europe. Instead, we made use of previously published information available at the considered ICOS sites, in which the effective GAI (GAI<sub>e</sub>) of the understory layer had been quantified using DCP and two radiometric methods (George et al., 2021). The inter-method uncertainty in the understory GAI<sub>e</sub> values was computed as the standard deviation of the mean over the three measurement approaches (Appendix B). It is worth noting that these observations were, in some cases, obtained from different moments in the season, and the resulting mismatch between the fixed understory and temporally resolved overstory observations must be acknowledged as a source of uncertainty. In the absence of other available information, however, it was judged that use of these site-specific values was superior to assuming no understory (which would have led to a gross error of greater magnitude).

Empirical relationships were used to transform the observed understory GAI<sub>e</sub> at each ICOS site to understory GAI and FIPAR. These were derived from those observations within the GROUNDED EO database containing all three variables (Appendix B). Following FRM4VEG recommendations (Brown et al., 2021a), orthogonal distance regression (ODR) was used to establish these relationships. ODR accounts for uncertainties in both predictor and response variables (Boggs et al., 1987), and enabled random error within the understory GAI<sub>e</sub>, GAI, and FIPAR values to be largely suppressed. Meanwhile, ODR prediction uncertainties associated with the understory GAI and FIPAR estimates could be propagated through all subsequent calculations, thereby enabling quantification of uncertainty in the results due to use of these understory estimates.

In addition to a lack of understory measurements at forest sites, a further issue that had to be corrected for prior to training the GROUNDED EO retrieval algorithm was the influence of woody material. Woody material is known to represent up to 35% of total plant area in forests (Gower et al., 1999), and recent work has demonstrated errors of up to 61% when no correction for woody material is undertaken (Brown et al., 2024b). Unless near-infrared cameras (which are not currently utilised by NEON, ICOS, or TERN) are adopted (Brown et al., 2024b), foliage and woody material is difficult to automatically distinguish in upwards-facing DHP and DCP data, as RGB images correctly exposed for gap fraction estimation typically demonstrate little contrast between the two canopy elements (Woodgate et al., 2016). Nevertheless, with high resolution and bit-depth DSLR cameras such as those adopted by NEON, careful manual interpretation of enhanced raw images is possible.

For the purposes of this study, baseline wood area index (WAI) values and uncertainties were determined from manually classified early spring images from at least one ESU at each NEON site (Appendix C). Raw images were enhanced in Nikon NX Studio prior to classification, to maximise the contrast between green foliage and woody material by increasing the ‘shadow protection’ setting. Where WAI values were available for multiple ESUs within a site, the mean was computed. In this case, the uncertainty associated with each WAI value was propagated through the calculation of the mean (representing observation-level uncertainty), which was added in quadrature to the standard deviation of the mean (representing uncertainty due to variability between observations) to obtain the total uncertainty in site-level WAI. A per-

observation woody-to-total ratio ( $\alpha$ ) was then computed as the ratio of the baseline WAI to the observed PAI.

The WAI estimation approach relied on high resolution ( $\geq 24$  MP) and bit-depth ( $\geq 14$ -bit) cameras adopted by NEON and so could not be consistently applied to the lower resolution images at ICOS and TERN sites. Instead, to enable a first-order woody area correction for these networks, the mean  $\alpha$  was computed from the NEON data to provide values representative of each forest type (Appendix C). Again, the uncertainty associated with each  $\alpha$  value was propagated through the calculation of the mean, which was added in quadrature to the associated standard deviation. Since the  $\alpha$  values for each forest type were seasonally varying and covered multiple sites spanning a variety of eco-climatic conditions, uncertainty due to both seasonal and site-related variability was captured by this latter term.

By implementing the woody area corrections, we could derive LAI and FAPAR from the values obtained from HemiPy and CoverPy as

$$LAI = PAI_{up} (1 - \alpha) + GAI_{down} \quad (2)$$

$$FAPAR = FIPAR_{up} (1 - \alpha) + [1 - FIPAR_{up} (1 - \alpha)] FIPAR_{down} \quad (3)$$

where  $PAI_{up}$ ,  $GAI_{down}$ ,  $FIPAR_{up}$ , and  $FIPAR_{down}$  represent overstory (*up*) and understory (*down*) PAI, GAI, and FIPAR values, respectively. Uncertainties in  $PAI_{up}$ ,  $GAI_{down}$ ,  $FIPAR_{up}$ ,  $FIPAR_{down}$ , and  $\alpha$  were propagated through Eqs. 2 and 3 according to the law of propagation of uncertainty, following Brown et al. (2021b). Our corrections assumed no woody material in values derived from downwards-facing images, as unlike the upwards-facing image classification, the downwards-facing image classification adopted by HemiPy and CoverPy is sensitive to green elements only (Brown et al., 2023; Brown and Leblanc, 2024; Meyer and Neto, 2008). Note Eq. 3 assumes that, because of strong absorption by photosynthetic pigments, the difference between FAPAR and FIPAR is negligible for green foliage (Li et al., 2015; Weiss et al., 2014). It is known that differences of up to 0.1 can occur over very bright backgrounds (i.e. snow), but Gobron et al. (2006) demonstrated that such differences can be neglected in the overall FAPAR uncertainty budget under usual conditions and where a vegetated understory is present.

#### 2.4. Sentinel-2 data processing and spatiotemporal matchup procedure

All Sentinel-2 L2A observations available over our study sites since launch of Sentinel-2A (June 2015) and within the period during which fiducial reference measurements were available (i.e. until the end of 2022) were obtained. Unfortunately, the Sentinel-2 Collection 1 reprocessing had not been completed at the time of data curation (ESA, 2024), and L2A products were not available prior to 24th March 2018 in Europe and 13th December 2018 for the rest of the world (ESA, 2018). Thus, all L1C top-of-atmosphere reflectance scenes prior to these dates were locally processed to L2A using Sen2Cor (Müller-Wilm, 2018). The L2A scene classification map was used to mask invalid pixels due to cloud, cloud shadow, thin cirrus, water, or snow, as well as dark, saturated, or defective pixels. Fiducial reference measurements were paired with corresponding Sentinel-2 observations acquired within one day (yielding 4167 matchups). For ESUs larger than a Sentinel-2 pixel, the mean of the corresponding pixels was computed. Recent work used a larger temporal window of one week (Fernandes et al., 2024; Fernandes et al., 2023), as has also been adopted in several previous studies (Baret et al., 2005; Brown et al., 2021a; De Kauwe et al., 2011). Whilst a larger temporal window would have arguably provided a greater number of matchups, it would have also resulted in greater potential mismatch due to phenological variations. This is particularly true over deciduous forest, where changes in biophysical variables occur very rapidly at the start and end of the growing season (Brown et al., 2020b; Brown et al., 2019), but also over cultivated crops, where rapid changes may occur due to harvesting and management activities. Whilst such variations may not be a major concern in studies using data from the peak of the

growing season (Brown et al., 2021a), they were of increased importance here given the multitemporal nature of the fiducial reference measurements utilised.

#### 2.5. Training the GROUNDED EO retrieval algorithm with Gaussian processes and active learning

Unlike artificial neural networks, in which sample size primarily impacts the computation time of the training rather than the retrieval phase, for Gaussian processes, retrieval time grows cubically with sample size (Berger et al., 2021; Rivera-Caicedo et al., 2017). A small but high-quality training dataset is therefore desirable. To optimise the matchup database so that it contained only the most informative samples, five active learning methods implemented within the ‘Machine Learning Regression Algorithm’ toolbox of the Automated Radiative Transfer Models Operator (ARTMO) were applied (Verrelst et al., 2015a, 2015b). These included the angle-based diversity (ABD), cluster-based diversity (CBD), and Euclidean distance-based diversity (EBD) methods, which rely on diversity-based criteria, as well as variance-based pool of regressors (PAL), and residual regression active learning (RSAL), which rely on uncertainty-based criteria. Samples were sequentially added according to these criteria and kept if they led to an improvement (assessed against a testing dataset). A full description of each method is provided by Verrelst et al. (2016). Random sampling was also implemented in addition to the active learning methods. In the interests of computational efficiency, kernel ridge regression was adopted for matchup database optimisation, as it is closely related to Gaussian processes (Verrelst et al., 2020), but proved substantially less computationally demanding. Given the same kernel and hyperparameters, the prediction of kernel ridge regression is identical to the mean of the posterior probability distribution provided by GPR (Kanagawa et al., 2018).

To apply the active learning methods, the overall matchup database was randomly divided into initialisation (1%), ‘pool’ (49%), and testing (50%) sets. Samples were iteratively added from the ‘pool’ to the initialisation set according to the ABD, CBD, EBD, RSAL, PAL, and random sampling criteria, until the root mean square difference (RMSD), as assessed against the testing set, stabilised. Finally, the set of observations with the lowest RMSD for each method was deemed the optimised matchup dataset. Python’s ‘scikit-learn’ (Pedregosa et al., 2011) implementation of GPR, which enables per-observation uncertainties to be accounted for within the training process, was used to train the empirical data-driven GROUNDED EO retrieval algorithm. This was achieved by passing the square of the standard uncertainty (i.e. variance) associated with each fiducial reference measurement to the ‘GaussianProcessRegressor’ function via the ‘alpha’ parameter, which represents the variance of Gaussian measurement noise on the training observations (Schraik et al., 2021). The radial basis function was selected as the kernel, and Sentinel-2 bands 1 to 8A, 9, 11, and 12, as well as the cosine of the solar zenith, view zenith, and relative azimuth angle, were provided as inputs. As a consequence of the matchup database optimisation results (Section 3.1), a random sample of 400 observations was ultimately selected for training.

#### 2.6. Validation and intercomparison of GROUNDED EO, SL2P, and SL2P-CCRS retrievals

To assess the GROUNDED EO retrieval algorithm against the current state-of-the-art in decametric LAI and FAPAR retrieval, intercomparison against Python implementations (<https://github.com/djamaainajib/SL2P-SL2PCCRS PYTHON>) of SL2P (Weiss and Baret, 2016) and SL2P-CCRS (Fernandes et al., 2024) was undertaken using valid matchups (i.e. those not flagged by SL2P or SL2P-CCRS to indicate inputs/outputs were out of domain/range). To ensure they were comparable, only retrievals valid for both SL2P and SL2P-CCRS were used in the calculation of statistics ( $n = 3226$ ). Both SL2P and SL2P-CCRS rely on artificial

neural networks for retrieval: SL2P uses the homogeneous SAIL RTM for training, whilst SL2P-CCRS makes use of the heterogeneous 4SAIL2 RTM for forest pixels and SAIL for non-forest pixels. Only pixels corresponding to fiducial reference measurement matchups were considered, as the objective of intercomparison was solely to better contextualise our validation results. Our study was concerned with thematic uncertainty (assessment of which can be considered a prerequisite to the computationally demanding and costly nature of global application). A more comprehensive intercomparison between GROUNDED EO, SL2P, and SL2P-CCRS using global, seasonally representative sampling was beyond the scope of our work.

It is worth noting that we did not undertake intercomparison against hectometric or kilometric LAI and FAPAR products. This was motivated by two key factors. Firstly, because of landscape heterogeneity and the non-linear nature of the reflectance-biophysical variable relationship, it is widely known that such products are subject to scaling errors. In principle, LAI retrieved from coarser spatial resolution data should equal the arithmetic mean of that derived from finer spatial resolution data. In practice, the coarser spatial resolution estimates tend to underestimate LAI due to these scaling errors (Garrigues et al., 2006; Tian et al., 2002). Comparison against hectometric or kilometric products, was, therefore, likely to lead to discrepancies indicative of scaling errors as opposed to useful information on the performance of the GROUNDED EO, SL2P, and SL2P-CCRS retrievals. Secondly, our study was explicitly focussed on decametric retrievals required in applications such as precision agriculture, forest management, and climate adaptation, where current hectometric or kilometric products are of little use, failing to comply with GCOS spatial resolution requirements for LAI and FAPAR (see Section 1).

Since only a small subset (i.e. 400 observations) of the entire matchup database was used to train the GPR models, GROUNDED EO LAI and FAPAR retrievals could be validated against fiducial reference measurements that were not used for training (hereafter termed the validation dataset). However, because it was recognised that the performance for sites included within both the training and validation datasets might be unfairly advantaged, a leave-site-out validation scheme was adopted. Within this scheme, each site was sequentially removed from the training dataset, a GPR model was trained, and observations from that site within the validation dataset were then used to assess the resulting retrievals, providing information on the capability of the model to generalise to unseen sites. To enable comparison, validation of SL2P and SL2P-CCRS LAI and FAPAR retrievals was carried out using the same validation dataset.

Agreement between LAI and FAPAR retrievals and the validation dataset was assessed using the RMSD, normalised RMSD (NRMSD), bias, precision, and user agreement ratio (UAR). The slope and coefficient of determination ( $r^2$ ) were also determined using ordinary least square regression. The RMSD, NRMSD, bias, and precision were computed as

$$RMSD = \sqrt{\frac{1}{n} \sum_{i=1}^n (p_i - o_i)^2} \quad (4)$$

$$NRMSD = \frac{RMSD}{\frac{1}{n} \sum_{i=1}^n (o_i)} \quad (5)$$

$$Bias = \frac{1}{n} \sum_{i=1}^n (p_i - o_i) \quad (6)$$

$$Precision = \sqrt{\frac{1}{n} \sum_{i=1}^n (p_i - o_i - Bias)^2} \quad (7)$$

where  $p_i$  represents the retrieval,  $o_i$  represents the fiducial reference measurement, and  $n$  represents the number of comparisons. Using uncertainty propagation, the standard uncertainty in the RMSD, NRMSD, bias, and precision values resulting from the uncertainties associated with the retrievals and fiducial reference measurements was computed. The UAR, which corresponds to the percentage of retrievals meeting user requirements, was determined as

$$UAR = \frac{1}{n} \sum_{i=1}^n I[ (|p_i - o_i| \leq \varepsilon_{abs}) \vee (|p_i - o_i| \leq \varepsilon_{rel} o_i) ] \quad (8)$$

where  $I[x]$  is the indicator function,  $\varepsilon_{abs}$  is the absolute requirement, and  $\varepsilon_{rel}$  is the relative requirement. For comparability with Djamai et al. (2019) and Brown et al. (2021b, 2020a), we used user requirements of 1 unit (absolute) or 20% (relative) for LAI and 0.1 unit (absolute) or 20% (relative) for FAPAR. For LAI, these correspond to the Sentinels for Science (SEN4SCI, 2011) requirements. The stricter GCOS threshold requirements were not considered because uncertainties associated with fiducial reference measurements typically approach 1 unit for LAI and 0.1 unit for FAPAR (Camacho et al., 2013; Fang et al., 2019; Garrigues et al., 2008) – a point highlighted in a recent study on conformity testing (Camacho et al., 2024). This makes compliance with the GCOS threshold requirements difficult to assess, as the reference data should ideally have a smaller uncertainty than the requirement (Widłowski, 2015). Additionally, the GCOS requirements have not been revised for decametric sensors, whilst the SEN4SCI requirements used here as specific to Sentinel-2. Moreover, as they were applied to all investigated algorithms, the SEN4SCI requirements were sufficient for the purposes of algorithm comparison.

In addition to overall values, statistics were calculated for land cover type and LAI and FAPAR magnitude subsets following validation good practices (Fernandes et al., 2014). RMSD, bias, and precision were modelled as a function of fiducial reference LAI and FAPAR magnitude using third-order polynomial weighted least squares regression (Fernandes et al., 2023), with weights determined as the standard uncertainty (derived according to the law of propagation of uncertainty). Since performance has previously been shown to vary between canopies with homogeneous and heterogeneous radiative transfer regimes, this was carried out for subsets representing only homogeneous (i.e. cultivated crops, grassland/herbaceous, shrub/scrub, and pasture/hay) or heterogeneous (i.e. deciduous broadleaf forest, evergreen broadleaf forest, evergreen needleleaf forest, mixed forest, and woody wetland) canopies.

### 3. Results

#### 3.1. Performance of active learning and random sampling

The results of matchup database optimisation demonstrated similar performance amongst the active learning methods, with the optimised matchup datasets all consisting of less than ~ 400 samples (Fig. 3 and Table 2). For LAI, the active learning approaches achieved RMSD values of 0.75 to 0.80 with between 182 and 288 samples. However, they were outperformed by random sampling, which achieved an RMSD of 0.73 using 403 samples (Fig. 3a and Table 2). Similar results were obtained for FAPAR, where the active learning approaches achieved RMSD values of 0.12 to 0.15 with between 31 and 355 samples. In this case, random sampling performed almost as well as the best active learning methods, achieving an RMSD of 0.13 using 269 samples (Fig. 3b and Table 2). It is worth noting that all samples within the ‘pool’ dataset were analysed against the testing dataset – the role of the active learning algorithms lies in selection/discard of samples. Based on these results, the ultimate

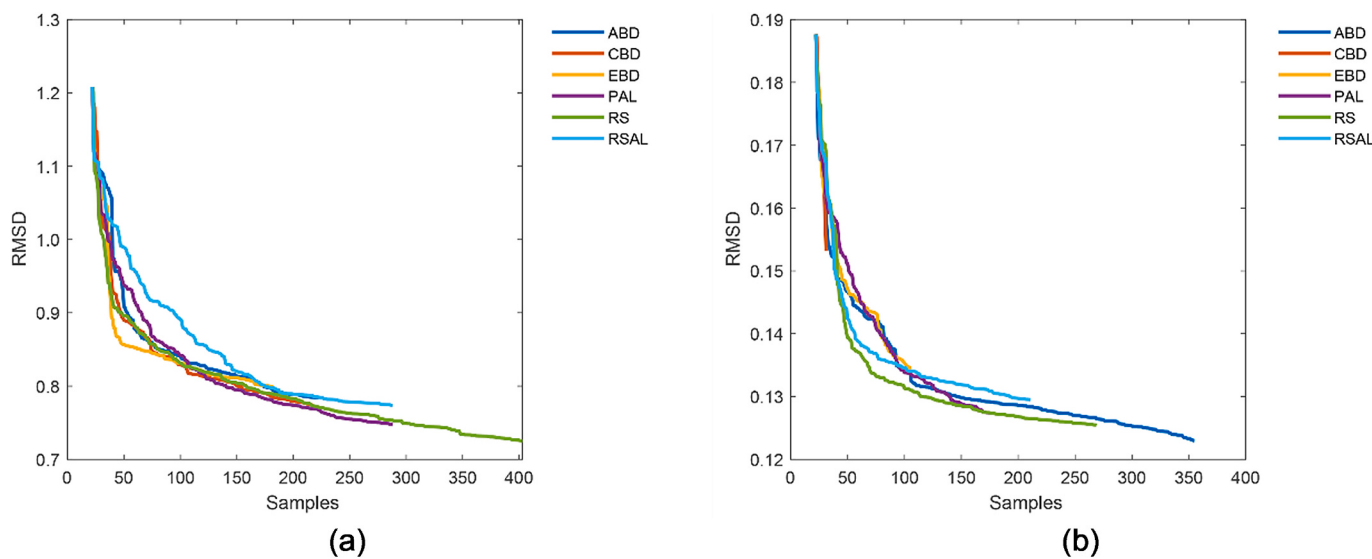


**Fig. 3.** RMSD as a function of the number of samples selected from the matchup database for the five active learning methods (ABD, CBD, EBD, PAL, and RSAL) and random sampling (RS) for LAI (a) and FAPAR (b). Note that ARTMO's 'Machine Learning Regression Algorithm' toolbox, which implements the active learning methods, only outputs the RMSD associated with the selected (not discarded) samples.

**Table 2**

Performance statistics associated with optimised matchup datasets according to the five active learning methods (ABD, CBD, EBD, PAL, and RSAL) as well as random sampling (RS).

Variable	Method	RMSD	NRMSD (%)	Bias	Samples
LAI	ABD	0.78	46.76	-0.01	226
	CBD	0.77	46.25	0.02	217
	EBD	0.80	47.62	0.00	182
	PAL	0.75	44.65	0.02	288
	RS	0.73	43.32	0.01	403
	RSAL	0.77	46.20	-0.07	288
FAPAR	ABD	0.12	29.42	0.00	355
	CBD	0.15	36.63	-0.03	31
	EBD	0.13	32.19	0.01	106
	PAL	0.13	30.47	0.00	175
	RS	0.13	30.00	0.00	269
	RSAL	0.13	30.97	0.00	211

decision to train the GROUNDED EO retrieval algorithm on 400 random samples was taken (Section 2.5).

### 3.2. Intercomparison of retrievals

Intercomparison revealed that GROUNDED EO and SL2P retrievals were well correlated ( $r^2 = 0.94$  and 0.92 for LAI and FAPAR, respectively), but subject to clear differences in absolute terms, with an overall RMSD (NRMSD) of 0.69 (41%) observed for LAI and 0.14 (33%) for FAPAR (Fig. 4). For LAI, the greatest differences were over deciduous broadleaf forest, evergreen needleleaf forest, mixed forest, and woody wetlands (RMSD = 0.69 to 0.91), where GROUNDED EO retrievals were substantially higher than their SL2P counterparts (bias = 0.31 to 0.71) (Fig. 4a and Appendix D). Similar results were obtained for FAPAR, with the greatest differences observed over deciduous broadleaf forest, evergreen broadleaf forest, evergreen needleleaf forest, and woody wetlands (RMSD = 0.14 to 0.18, bias = 0.09 to 0.15) (Fig. 4b and Appendix D).

Much smaller differences were observed over cultivated crops, grassland/herbaceous, pasture/hay, and shrub/scrub (RMSD = 0.38 to 0.58 for LAI and 0.08 to 0.13 for FAPAR), where GROUNDED EO retrievals were slightly lower than their SL2P counterparts (bias = -0.08 to -0.36 for LAI and -0.03 to -0.07 for FAPAR) (Fig. 4 and Appendix D). Differences between GROUNDED EO and SL2P retrievals appeared nearly linearly proportional to magnitude (slope = 1.39 for LAI and 1.28 for FAPAR), though with clearly apparent land cover dependencies (Fig. 4). When assessed by SL2P retrieval magnitude, the greatest differences between SL2P and GROUNDED EO retrievals were observed for LAI values > 2 and FAPAR values > 0.4 (Fig. 4 and Appendix D).

Intercomparison of GROUNDED EO and SL2P-CCRS retrievals revealed increased overall agreement when compared to SL2P for LAI (RMSD = 0.70, NRMSD = 33%, bias = -0.29) despite a slightly reduced  $r^2$  (0.92), but reduced overall agreement for FAPAR ( $r^2 = 0.85$ , RMSD = 0.17, NRMSD = 42%, bias = 0.06) (Fig. 4). SL2P-CCRS and GROUNDED EO retrievals were subject to reduced differences over deciduous broadleaf forest for both variables (RMSD = 0.72, bias = -0.24 for LAI and RMSD = 0.12, bias = 0.06 for FAPAR), and over evergreen broadleaf forest for FAPAR only (RMSD = 0.12, bias = 0.16) (Fig. 4 and Appendix D). This was not the case over evergreen needleleaf forest, mixed forest, or woody wetlands (RMSD = 0.74 to 1.32, bias = -0.37 to -1.08 for LAI and RMSD = 0.22 to 0.26, bias = 0.17 to 0.23 for FAPAR) (Fig. 4 and Appendix D). When assessed by SL2P-CCRS retrieval magnitude, the greatest differences between SL2P-CCRS and GROUNDED EO retrievals were observed for LAI values of 5 to 8 and FAPAR values between 0.5 and 0.8 (Fig. 4 and Appendix D).

### 3.3. Overall performance of retrievals

Validation revealed that GROUNDED EO LAI and FAPAR retrievals were very strongly correlated to fiducial reference measurements ( $r^2 = 0.84$  to 0.89) demonstrating good overall agreement, with an RMSD (NRMSD) of 0.96 (51%) for LAI and 0.15 (31%) for FAPAR. User requirements were met for 74% of LAI and 69% of FAPAR retrievals (Fig. 5). Biases were small in both cases (-0.06 for LAI and 0.00 for

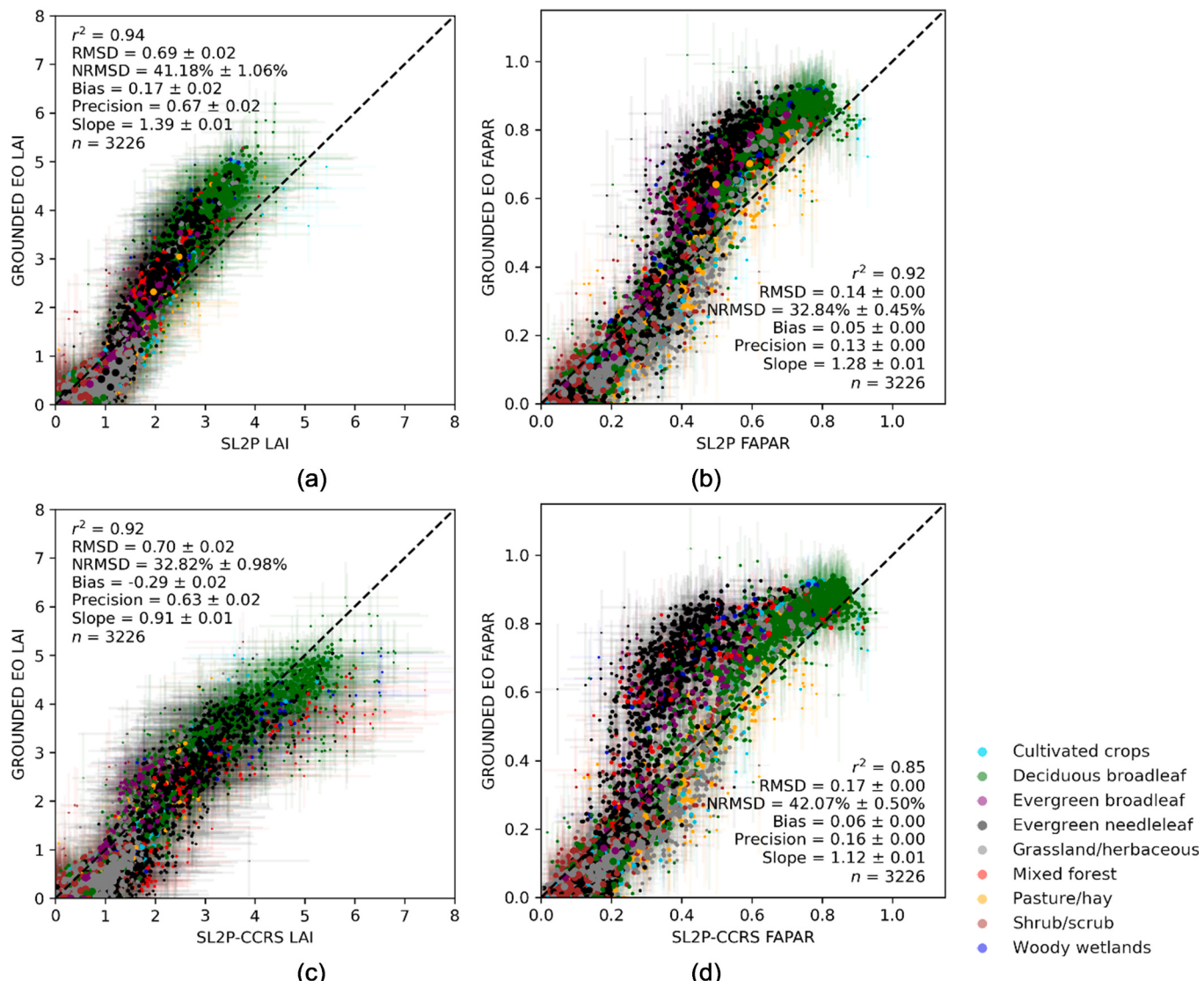


**Fig. 4.** Intercomparison of GROUNDED EO vs. SL2P (a-b) and SL2P-CCRS (c-d) LAI (a, c) and FAPAR (b, d) retrievals. Error bars represent standard uncertainties. The dashed line represents a 1:1 relationship.

FAPAR), with differences being driven primarily by random rather than systematic error (precision = 0.96 for LAI and 0.15 for FAPAR) (Fig. 5). Assessed qualitatively, good temporal consistency between GROUNDED EO retrievals and fiducial reference measurements was also observed over sites representative of a broad range of vegetation types (i.e. grassland/herbaceous, shrub/scrub, deciduous broadleaf forest, cultivated crops, mixed forest, and evergreen needleleaf forest). Seasonal peaks and troughs of GROUNDED EO retrievals and fiducial reference measurements were in phase, and the magnitudes of these were similar, though retrievals during low LAI conditions outside of the growing season (for which there were no fiducial reference measurements) appeared slightly noisier (Fig. 6).

When compared to GROUNDED EO retrievals, a reduced correlation with fiducial reference measurements was observed for SL2P LAI and FAPAR retrievals ( $r^2 = 0.84$  to  $0.86$ ), which demonstrated worse overall agreement, with an RMSE (NRMSE) of 1.07 (57%) for LAI and 0.18 (37%) FAPAR (Fig. 5). This led to a reduced proportion of SL2P retrievals meeting user requirements (69% for LAI and 53% for FAPAR). In this case, larger biases were observed ( $-0.23$  for LAI and  $-0.04$  for FAPAR), with the tendency of SL2P retrievals to underestimate larger

values, as reflected by the slope of 0.50 for LAI and 0.60 for FAPAR (Fig. 5), and as evident in time series of SL2P retrievals and fiducial reference measurements (Fig. 6). It is worth noting that random error associated with SL2P retrievals was also increased (precision = 1.05 for LAI and 0.17 for FAPAR) when compared to GROUNDED EO retrievals (Fig. 5). SL2P-CCRS retrievals demonstrated superior overall performance than SL2P retrievals for LAI (RMSE = 0.99, NRMSE = 53%, bias = 0.23, UAR = 71%), but worse overall performance than SL2P retrievals for FAPAR (RMSE = 0.20, NRMSE = 42%, bias =  $-0.06$ , UAR = 51%), with worse overall performance than GROUNDED EO retrievals occurring in both cases (Fig. 5). The poor performance of SL2P-CCRS for FAPAR was particularly apparent for evergreen needleleaf forest, and so may be related to the scaling of simulated leaf reflectance/transmittance as a function of the needle-to-shoot area ratio ( $\gamma$ ) within the algorithm (Fernandes et al., 2024) (i.e. the prior distribution of  $\gamma$  values adopted by SL2P-CCRS may result in biased retrievals and require revision). In terms of their temporal consistency with fiducial reference measurements, SL2P retrievals appeared qualitatively noisier than GROUNDED EO retrievals during the growing season and tended to underestimate peaks (Fig. 6).

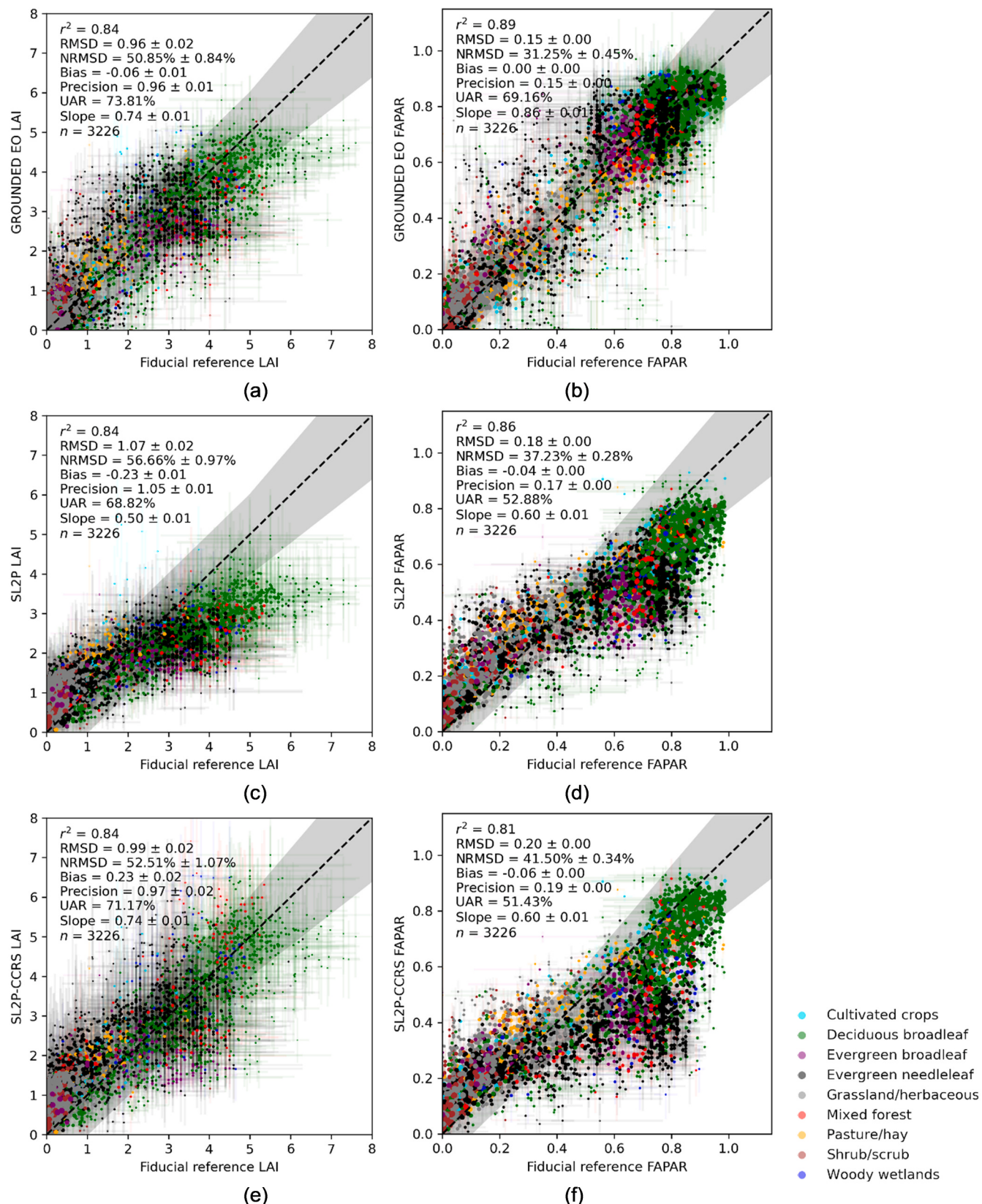


**Fig. 5.** Validation of GROUNDED EO (a-b), SL2P (c-d), and SL2P-CCRS (e-f) LAI (a, c, e) and FAPAR (b, d, f) retrievals against fiducial reference measurements. Error bars represent standard uncertainties. The dashed line represents a 1:1 relationship, whilst the shaded grey area represents user requirements.

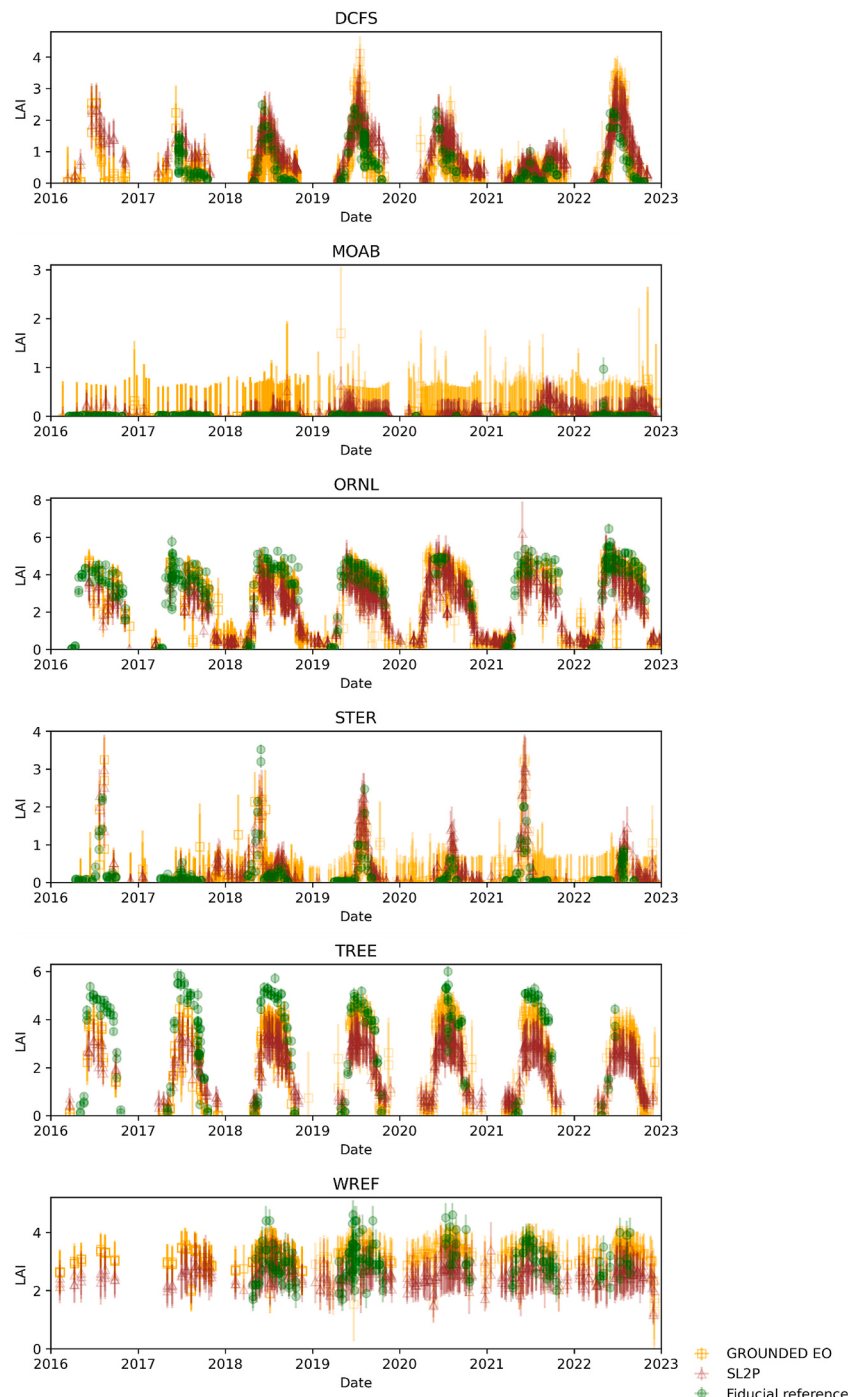


**Fig. 6.** Time series of GROUNDED EO, SL2P, and fiducial reference LAI at Dakota Coteau Field (DCFS), Moab (MOAB), Oak Ridge (ORNL), North Sterling (STER), Treehaven (TREE), and Wind River Experimental Forest (WREF). These sites were chosen to represent grassland/herbaceous, shrub/scrub, deciduous broadleaf forest, cultivated crops, mixed forest, and evergreen needleleaf forest, respectively.

Table 3

Performance of GROUNDED EO, SL2P, and SL2P-CCRS LAI and FAPAR retrievals with respect to fiducial reference measurements, by land cover type. The best performing results for each land cover type in terms of UAR are shown in bold and highlighted in grey.

Land cover	n	LAI							FAPAR							
		$r^2$	RMSD	NRMSD (%)	Bias	Precision	UAR (%)	Slope	$r^2$	RMSD	NRMSD (%)	Bias	Precision	UAR (%)	Slope	
GROUNDED EO	Cultivated crops	111	0.63	0.88±0.06	109.69±7.75	0.19±0.06	0.85±0.06	82.88	1.24±0.09	0.79	0.14±0.01	43.90±3.48	0.00±0.01	0.14±0.01	54.95	0.92±0.05
	Deciduous broadleaf	906	0.68	1.11±0.03	32.52±0.82	-0.53±0.03	0.98±0.03	67.00	0.73±0.02	0.69	0.15±0.00	21.46±0.55	-0.05±0.00	0.15±0.00	77.48	0.90±0.02
	Evergreen broadleaf	104	0.45	1.01±0.08	46.68±3.96	-0.19±0.08	0.99±0.08	69.23	0.39±0.04	0.55	0.17±0.02	34.38±3.48	0.06±0.012	0.16±0.01	63.46	0.55±0.05
	Evergreen needleleaf	845	0.42	1.11±0.03	56.92±1.63	0.15±0.03	1.10±0.03	62.01	0.64±0.03	0.58	0.18±0.00	34.23±0.91	0.03±0.004	0.18±0.00	55.98	0.77±0.02
	Grassland /herbaceous	576	0.60	0.69±0.03	131.51±5.13	0.24±0.03	0.65±0.03	87.85	1.10±0.04	0.76	0.12±0.00	48.71±1.71	0.03±0.004	0.12±0.00	70.66	0.89±0.02
	Mixed forest	124	0.62	1.13±0.09	36.28±2.54	-0.67±0.08	0.92±0.08	60.48	0.69±0.05	0.80	0.10±0.01	15.77±1.65	-0.01±0.01	0.10±0.01	84.68	0.87±0.04
	Pasture/ hay	191	0.68	0.60±0.05	77.63±6.27	0.28±0.05	0.53±0.05	89.01	1.13±0.06	0.70	0.14±0.01	35.62±2.04	-0.02±0.01	0.13±0.01	69.11	0.74±0.04
	Shrub/ scrub	319	0.33	0.52±0.05	300.26±26.46	0.17±0.04	0.49±0.04	95.30	0.72±0.06	0.67	0.10±0.01	133.19±8.24	0.05±0.01	0.09±0.01	77.74	1.02±0.04
	Woody wetlands	50	0.45	1.00±0.10	31.33±3.24	-0.14±0.10	0.99±0.10	62.00	0.66±0.10	0.55	0.14±0.02	19.35±2.37	0.01±0.02	0.14±0.02	74.00	0.72±0.09
	Cultivated crops	111	0.72	0.85±0.08	106.26±10.54	0.52±0.05	0.67±0.05	85.59	1.20±0.07	0.86	0.12±0.00	37.79±1.47	0.05±0.01	0.11±0.01	63.96	0.80±0.03
SL2P	Deciduous broadleaf	906	0.73	1.43±0.04	41.85±0.95	-1.02±0.03	1.00±0.03	50.77	0.50±0.01	0.68	0.19±0.00	26.98±0.31	-0.14±0.00	0.14±0.00	54.97	0.71±0.02
	Evergreen broadleaf	104	0.25	1.26±0.08	58.42±3.46	-0.50±0.08	1.16±0.08	50.96	0.18±0.03	0.33	0.22±0.01	44.20±1.82	-0.09±0.01	0.20±0.01	27.88	0.26±0.04
	Evergreen needleleaf	845	0.47	0.99±0.04	50.76±1.80	-0.17±0.03	0.98±0.03	69.59	0.40±0.02	0.49	0.20±0.00	38.54±0.54	-0.08±0.00	0.18±0.00	44.85	0.43±0.02
	Grassland /herbaceous	576	0.60	0.70±0.03	133.76±5.12	0.50±0.02	0.49±0.02	82.47	0.80±0.03	0.69	0.15±0.00	60.47±0.89	0.07±0.00	0.13±0.00	53.13	0.66±0.02
	Mixed forest	124	0.63	1.38±0.10	44.09±2.84	-0.98±0.09	0.97±0.09	47.58	0.44±0.03	0.72	0.16±0.01	24.77±1.23	-0.11±0.01	0.12±0.01	58.06	0.67±0.04
	Pasture/ hay	191	0.65	0.76±0.05	98.70±6.05	0.64±0.04	0.41±0.04	86.39	0.80±0.04	0.73	0.14±0.00	37.03±0.92	0.05±0.00	0.13±0.00	55.50	0.61±0.03
	Shrub/ scrub	319	0.41	0.47±0.03	27.61±17.74	0.24±0.02	0.40±0.02	92.79	0.67±0.04	0.67	0.12±0.00	148.17±4.18	0.08±0.00	0.08±0.00	70.53	0.89±0.04
	Woody wetlands	50	0.33	1.32±0.12	41.42±3.69	-0.85±0.12	1.01±0.12	58.00	0.35±0.07	0.39	0.21±0.01	29.67±1.20	-0.14±0.01	0.16±0.01	40.00	0.52±0.09
	Cultivated crops	111	0.72	0.85±0.08	106.26±10.54	0.52±0.05	0.67±0.05	85.59	1.20±0.07	0.86	0.12±0.00	37.79±1.47	0.05±0.01	0.11±0.01	63.96	0.80±0.03
	Deciduous broadleaf	906	0.68	1.05±0.03	30.65±0.94	-0.29±0.03	1.01±0.03	70.97	0.79±0.02	0.65	0.18±0.00	25.01±0.26	-0.10±0.00	0.14±0.00	65.56	0.76±0.02
SL2P-CCRS	Evergreen broadleaf	104	0.15	1.33±0.07	61.58±3.25	-0.53±0.07	1.22±0.07	53.85	0.18±0.04	0.24	0.23±0.01	46.62±1.62	-0.10±0.01	0.21±0.01	29.81	0.25±0.04
	Evergreen needleleaf	845	0.41	1.17±0.05	59.86±2.50	0.52±0.05	1.05±0.05	57.04	0.54±0.02	0.40	0.26±0.00	49.69±0.60	-0.17±0.00	0.20±0.00	30.89	0.34±0.01
	Grassland /herbaceous	576	0.60	0.70±0.03	133.76±5.12	0.50±0.02	0.49±0.02	82.47	0.80±0.03	0.69	0.15±0.00	60.47±0.89	0.07±0.00	0.13±0.00	53.13	0.66±0.02
	Mixed forest	124	0.46	1.29±0.12	41.34±3.63	0.42±0.12	1.22±0.12	46.77	0.72±0.07	0.53	0.24±0.01	37.36±1.50	-0.18±0.01	0.16±0.01	41.13	0.70±0.06
	Pasture/ hay	191	0.65	0.76±0.05	98.70±6.05	0.64±0.04	0.41±0.04	86.39	0.80±0.04	0.73	0.14±0.00	37.03±0.92	0.05±0.00	0.13±0.00	55.50	0.61±0.03
	Shrub/ scrub	319	0.41	0.47±0.03	271.61±17.74	0.24±0.02	0.40±0.02	92.79	0.67±0.04	0.67	0.12±0.00	148.17±4.18	0.08±0.00	0.08±0.00	70.53	0.89±0.04
	Woody wetlands	50	0.29	1.46±0.18	45.85±5.87	0.52±0.17	1.36±0.17	52.00	0.68±0.15	0.30	0.29±0.01	41.05±1.77	-0.22±0.01	0.18±0.01	28.00	0.56±0.12
	Cultivated crops	111	0.72	0.85±0.08	106.26±10.54	0.52±0.05	0.67±0.05	85.59	1.20±0.07	0.86	0.12±0.00	37.79±1.47	0.05±0.01	0.11±0.01	63.96	0.80±0.03
	Deciduous broadleaf	906	0.68	1.05±0.03	30.65±0.94	-0.29±0.03	1.01±0.03	70.97	0.79±0.02	0.65	0.18±0.00	25.01±0.26	-0.10±0.00	0.14±0.00	65.56	0.76±0.02
	Evergreen broadleaf	104	0.15	1.33±0.07	61.58±3.25	-0.53±0.07	1.22±0.07	53.85	0.18±0.04	0.24	0.23±0.01	46.62±1.62	-0.10±0.01	0.21±0.01	29.81	0.25±0.04
	Evergreen needleleaf	845	0.41	1.17±0.05	59.86±2.50	0.52±0.05	1.05±0.05	57.04	0.54±0.02	0.40	0.26±0.00	49.69±0.60	-0.17±0.00	0.20±0.00	30.89	0.34±0.01
	Grassland /herbaceous	576	0.60	0.70±0.03	133.76±5.12	0.50±0.02	0.49±0.02	82.47	0.80±0.03	0.69	0.15±0.00	60.47±0.89	0.07±0.00	0.13±0.00	53.13	0.66±0.02
	Mixed forest	124	0.46	1.29±0.12	41.34±3.63	0.42±0.12	1.22±0.12	46.77	0.72±0.07	0.53	0.24±0.01	37.36±1.50	-0.18±0.01	0.16±0.01	41.13	0.70±0.06
	Pasture/ hay	191	0.65	0.76±0.05	98.70±6.05	0.64±0.04	0.41±0.04	86.39	0.80±0.04	0.73	0.14±0.00	37.03±0.92	0.05±0.00	0.13±0.00	55.50	0.61±0.03
	Shrub/ scrub	319	0.41	0.47±0.03	271.61±17.74	0.24±0.02	0.40±0.02	92.79	0.67±0.04	0.67	0.12±0.00	148.17±4.18	0.08±0.00	0.08±0.00	70.53	0.89±0.04
	Woody wetlands	50	0.29	1.46±0.18	45.85±5.87	0.52±0.17	1.36±0.17	52.00	0.68±0.15	0.30	0.29±0.01	41.05±1.77	-0.22±0.01	0.18±0.01	28.00	0.56±0.12

### 3.4. Performance of retrievals as a function of land cover type

The greatest differences between GROUNDED EO LAI retrievals and fiducial reference measurements were observed over deciduous broadleaf forest, evergreen broadleaf forest, evergreen needleleaf forest, mixed forest, and woody wetlands (RMSD = 1.00 to 1.13, bias = 0.15 to -0.67), where 60% to 69% of retrievals met user requirements, whilst smaller differences were observed over cultivated crops, grassland/herbaceous, pasture/hay, and shrub/scrub (RMSD = 0.52 to 0.88, bias = 0.17 to 0.28), where 83% to 95% of GROUNDED EO retrievals met user requirements (Table 3). For FAPAR, the largest differences between retrievals and fiducial reference measurements occurred over evergreen broadleaf forest and evergreen needleleaf forest (RMSD = 0.17 to 0.18), where 56% to 63% of GROUNDED EO retrievals met user requirements, but these differences appeared to be primarily driven by random rather than systematic error (bias = 0.03 to 0.06, precision = 0.16 to 0.18) (Table 3). In terms of UAR, GROUNDED EO retrievals outperformed SL2P and SL2P-CCRS in all land cover types except cultivated crops, deciduous broadleaf forest, and evergreen needleleaf forest for LAI, and all land cover types except cultivated crops for FAPAR (Table 3).

For SL2P LAI retrievals, the greatest differences with respect to fiducial reference measurements were observed over deciduous broadleaf forest, evergreen broadleaf forest, evergreen needleleaf forest, mixed forest, and woody wetlands (RMSD = 0.99 to 1.43, bias = -0.17 to -1.02), where 48% to 70% of retrievals met user requirements. This was also true for FAPAR (RMSD = 0.16 to 0.22, bias = -0.08 to -0.14), where 28% to 58% of SL2P retrievals met user requirements (Table 3). In contrast, SL2P retrievals outperformed GROUNDED EO retrievals over cultivated crops (RMSD = 0.85, bias = 0.52, UAR = 86% for LAI and RMSD = 0.12, bias = 0.05, UAR = 64% for FAPAR) and evergreen needleleaf forest (for LAI only, RMSD = 0.99, bias = -0.17, UAR = 70%) (Table 3).

As with SL2P, the greatest differences between SL2P-CCRS LAI retrievals and fiducial reference measurements were observed for deciduous broadleaf forest, evergreen broadleaf forest, evergreen needleleaf forest, mixed forest, and woody wetlands (RMSD = 1.05 to 1.46, bias = -0.53 to 0.52, UAR = 47% to 71%). Except for evergreen broadleaf forest and evergreen needleleaf forest, these differences were smaller than observed for SL2P retrievals (though larger than observed for GROUNDED EO retrievals with the exception of deciduous broadleaf forest) (Table 3). The greatest differences between SL2P-CCRS FAPAR retrievals and fiducial reference measurements also occurred over these land cover types, but in this case, differences were larger than for SL2P (and GROUNDED EO) retrievals (RMSD = 0.18 to 0.29, bias = -0.10 to -0.22, UAR = 28% to 66%) (Table 3). Note that since SL2P-CCRS utilises the same algorithm as SL2P for non-forest land cover, results over cultivated crops, grassland/herbaceous, pasture/hay, and shrub/scrub were identical to those observed for SL2P (Table 3).

### 3.5. Performance of retrievals as a function of fiducial reference magnitude

Since they average over different canopy types, overall performance statistics (Appendix F) are not necessarily informative of the performance achieved over specific environments. When only homogeneous (i.e. cultivated crops, grassland/herbaceous, shrub/scrub, and pasture/hay) canopies were considered, compliance with user requirements in terms of RMSD was achieved by GROUNDED EO LAI retrievals at all LAI magnitudes, but only for LAI values  $\leq 4$  for SL2P and SL2P-CCRS (Fig. 7a). The performance of SL2P and SL2P-CCRS was identical (since they utilise the same algorithm for non-forest land cover). Similar patterns were observed in terms of bias and precision (Fig. 7a). GROUNDED EO retrievals were positively biased at LAI values  $\leq 4.5$  and negatively biased thereafter (with bias exceeding user requirements

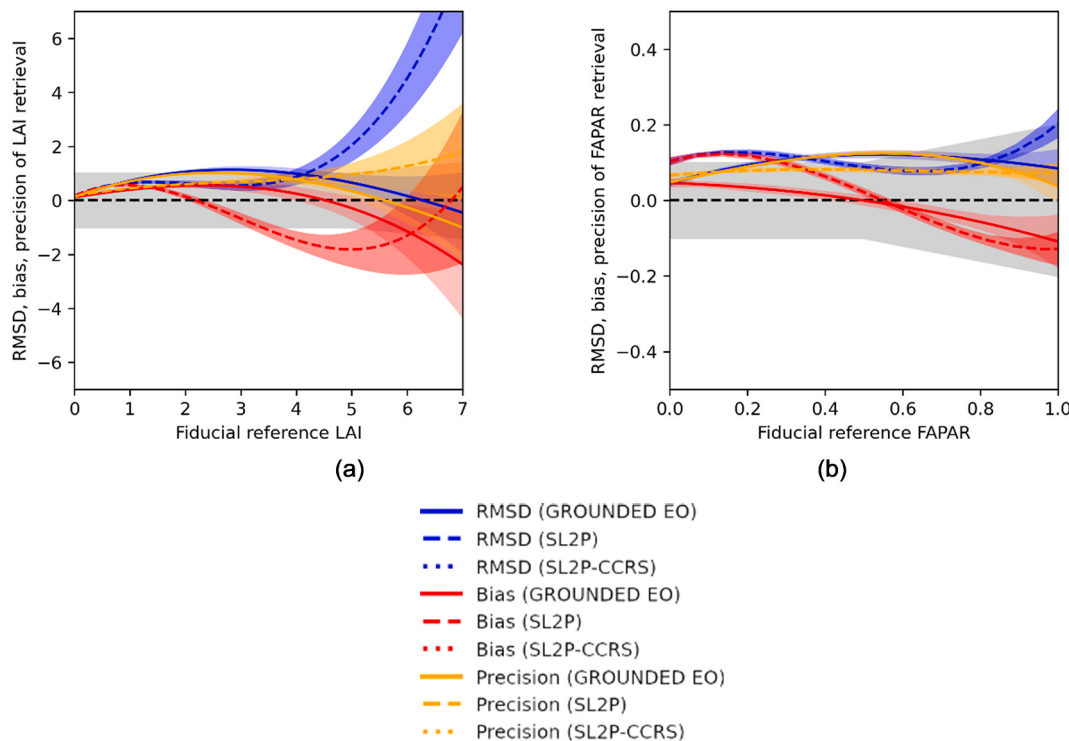


**Fig. 7.** Performance of GROUNDED EO, SL2P, and SL2P-CCRS LAI (a) and FAPAR (b) retrievals as a function of fiducial reference magnitude for homogeneous (i.e. cultivated crops, grassland/herbaceous, shrub/scrub, and pasture/hay) canopies. The dashed line represents a 1:1 relationship, whilst the shaded grey area represents user requirements. Error bands represent the 95% confidence interval.

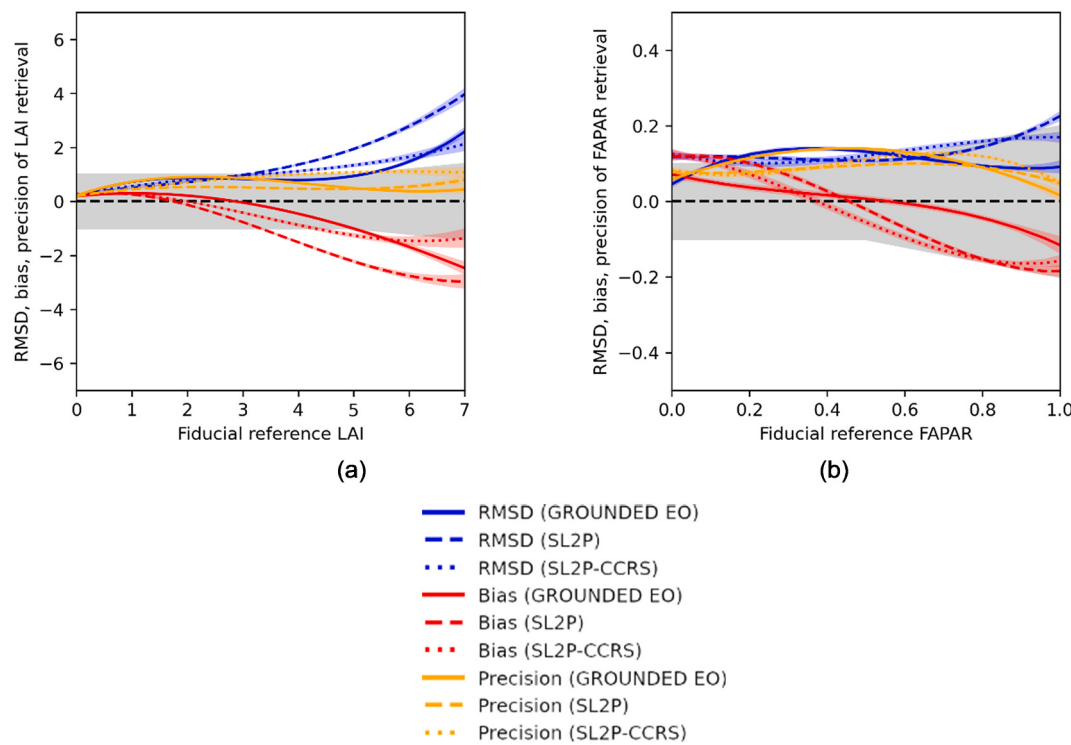


**Fig. 8.** Performance of GROUNDED EO, SL2P, and SL2P-CCRS LAI (a) and FAPAR (b) retrievals as a function of fiducial reference magnitude for heterogeneous (i.e. deciduous broadleaf forest, evergreen broadleaf forest, evergreen needleleaf forest, mixed forest, and woody wetland) canopies. The dashed line represents a 1:1 relationship, whilst the shaded grey area represents user requirements. Error bands represent the 95% confidence interval.

only for LAI values  $\geq 6$ ). SL2P and SL2P-CCRS retrievals had a similar positive bias to GROUNDED EO retrievals for LAI values  $\leq 2$ , but were negatively biased thereafter, exceeding user requirements for LAI values  $\geq 3$  and reaching a bias of  $-2$  at LAI = 5. The precision of GROUNDED EO retrievals remained below 1 unit at all LAI magnitudes, whereas the precision of SL2P and SL2P-CCRS retrievals exceeded user requirements for LAI values  $\geq 5$  (Fig. 7a).

GROUNDED EO FAPAR retrievals over homogeneous canopies were compliant with user requirements in terms of RMSD for FAPAR values  $\leq 0.35$  and  $\geq 0.55$ , whilst SL2P and SL2P-CCRS retrievals were compliant for FAPAR values  $\geq 0.35$  (Fig. 7b). All algorithms were positively biased for FAPAR values  $\leq 0.5$  and negatively biased thereafter, however the bias of GROUNDED EO retrievals was generally below  $\pm 0.05$ , whereas the bias of SL2P and SL2P-CCRS retrievals exceeded  $\pm 0.1$  at extreme FAPAR values. In terms of precision, GROUNDED EO retrievals were compliant with user requirements at FAPAR values  $\leq 0.35$  and  $\geq 0.55$ , whilst SL2P and SL2P-CCRS retrievals were compliant at all FAPAR magnitudes (Fig. 7b).

When only heterogeneous (i.e. deciduous broadleaf forest, evergreen broadleaf forest, evergreen needleleaf forest, mixed forest, and woody wetland) canopies were considered, GROUNDED EO LAI retrievals were compliant with user requirements in terms of RMSD for LAI values  $\leq 5.5$ , whilst SL2P and SL2P-CCRS retrievals were only compliant for LAI values  $\leq 3$  and 3.5, respectively (Fig. 8a). For all retrieval algorithms, a negative relationship between LAI magnitude and bias was observed, with a bias of  $\sim 0.5$  at LAI = 0, reaching  $-1.5$ ,  $-2.5$ , and  $-3$  at LAI = 7 for SL2P-CCRS, GROUNDED EO, and SL2P retrievals, respectively. The bias of GROUNDED EO retrievals exceeded user requirements for LAI values  $\geq 5$ , whereas SL2P and SL2P-CCRS biases exceeded requirements for LAI values  $\geq 3$  and 4.5, respectively (Fig. 8a). In terms of precision, GROUNDED EO and SL2P retrievals achieved compliance with user

requirements for all LAI magnitudes, whilst SL2P-CCRS retrievals were non-compliant for LAI values  $\geq 3.5$  and  $\leq 5.5$ , respectively, though the requirements were only very slightly exceeded in this case (Fig. 8a).

GROUNDED EO FAPAR retrievals over heterogeneous canopies were compliant with user requirements in terms of RMSD for FAPAR values  $\leq 0.1$  and  $\geq 0.5$ , whilst SL2P and SL2P-CCRS retrievals were compliant for FAPAR values  $\geq 0.2$  (Fig. 8b). GROUNDED EO, SL2P, and SL2P-CCRS retrievals had similar positive biases for FAPAR values  $\leq 0.5$ , 0.45, and 0.4, respectively, with negative biases thereafter. SL2P and SL2P-CCRS retrievals were compliant with user requirements in terms of precision at all FAPAR magnitudes, whereas GROUNDED EO retrievals were non-compliant for FAPAR values  $\geq 0.2$  and  $\leq 0.5$  (Fig. 8b).

## 4. Discussion

### 4.1. Empirical data-driven vs. hybrid biophysical variable retrieval

Existing decametric biophysical variable retrieval algorithms such as SL2P and SL2P-CCRS adopt a ‘hybrid’ retrieval approach, in that they combine RTMs and machine learning regression algorithms to facilitate computationally efficient retrieval (Verrelst et al., 2015a). The performance of such retrieval algorithms is dependent on the extent to which the adopted RTM can adequately represent the canopy of interest, the selected prior distributions of RTM input parameters, and the regression algorithm utilised. SAIL, which is used by SL2P, describes the canopy as a horizontally homogeneous turbid medium, and is known to perform poorly in heterogeneous canopies that deviate strongly from this assumption (Brown et al., 2024a; Richter et al., 2009; Verger et al., 2011). We found that over heterogeneous canopies such as deciduous broadleaf forest, evergreen broadleaf forest, mixed forest and woody wetlands, substantial underestimation (negative biases of up to  $-1.02$

for LAI and  $-0.14$  for FAPAR) were observed. This explains the apparent overestimation of SL2P retrievals by GROUNDED EO at higher values corresponding to these vegetation types (Fig. 4). Our results are consistent with a wide range of previously published validation efforts (Brown et al., 2021b; Brown et al., 2019; Djamai et al., 2019; Fernandes et al., 2024; Fernandes et al., 2023; Hu et al., 2020; Putzenlechner et al., 2019; Upreti et al., 2019; Vanino et al., 2018; Vuolo et al., 2016; Xie et al., 2019).

Despite the known limitations of SAIL, adopting more complex RTMs with a greater degree of realism is not straightforward. As the number of input parameters increase (Roberts, 2001; Schlerf and Atzberger, 2006), their specification becomes more challenging. Retrieval also becomes ill-posed, in that i) multiple combinations of input parameters may lead to similar reflectance spectra, and ii) there may be more input parameters (i.e. unknowns) than information contained within the limited number of spectral bands available, confounding retrieval (Combal et al., 2003; Gobron et al., 1997; Verger et al., 2011; Verrelst et al., 2015a). It is worth recognising that due to data redundancy (whereby adjacent spectral bands contain limited additional information), hyperspectral observations from recent and upcoming spaceborne missions such as the Environmental Mapping and Analysis Program (EnMAP), Precursore Iperspettrale della Missione Applicativa (PRISMA), Copernicus Hyperspectral Imaging Mission for the Environment (CHIME), and Surface Biology Geology (SBG) may not solve this problem (Brown et al., 2024a; Verger et al., 2011).

In an attempt to overcome the ill-posed nature of the inverse problem, strategies involving the use of prior or ancillary information related to expected canopy conditions have been adopted. These have included prior distributions of RTM input parameters, land cover-specific algorithms, or cascaded approaches in which specific algorithms are applied on the basis of a variable that can be retrieved in a well-posed manner (Bacour et al., 2006; Baret et al., 2007; Brown et al., 2021b; Combal et al., 2003; Knyazikhin et al., 1998; Verger et al., 2011; Verrelst et al., 2015a). Despite the adoption of these strategies, the performance of decametric biophysical variable retrieval algorithms making use of more complex RTMs has been mixed. For example, SL2P-CCRS uses the heterogeneous 4SAIL2 RTM for training land cover-specific retrieval algorithms suitable for forest environments. Fernandes et al. (2024) found that whilst the increased complexity of the canopy representation in SL2P-CCRS did lead to reduced bias (as confirmed in this study), the overall difference with respect to fiducial reference measurements increased, due to a drop in the precision of retrievals (i.e. a bias-variance tradeoff).

For land cover-specific algorithms such as SL2P-CCRS, the need for an accurate and routinely updated land cover dataset is a non-trivial complication for operational application, since inaccuracies in the chosen decametric land cover product (e.g. due classification errors or changes in land cover) could lead to substantial uncertainty in the retrievals (Fang et al., 2013). In this study, we utilised ground-based land cover information available from NEON, ICOS and TERN as input to SL2P-CCRS for the considered ESUs. Even in this case, there was some degree of uncertainty in the land cover labels (e.g. due to ambiguity in the definition of land cover classes, as well as the presence of ESUs containing a mixture of land cover types). It is likely that the uncertainty associated with satellite-derived land cover products would be greater still, meaning that the results reported for SL2P-CCRS in this study may be somewhat optimistic.

Within GROUNDED EO, we bypassed RTMs, adopting an empirical data-driven retrieval approach utilising Gaussian processes trained and validated on extensive fiducial reference measurements. Crucially, and as discussed in Section 1, Gaussian processes require many fewer training samples than other machine learning regression techniques

such as artificial neural networks (Berger et al., 2021; Combal et al., 2003; Estévez et al., 2022; Verrelst et al., 2020; Weiss et al., 2000). Whilst the utility of Gaussian processes for hybrid biophysical variable retrieval has been known for some time (Verrelst et al., 2015a), due to the limited quantity and quality of available in situ reference measurements (Camacho et al., 2013; Fang et al., 2019; Garrigues et al., 2008; Weiss et al., 2014; Yan et al., 2016b), relatively few studies have attempted extensive empirical data-driven training of Gaussian processes over multiple sites or vegetation types (Amin et al., 2020; Camacho et al., 2021; Revill et al., 2019; Verrelst et al., 2013; Verrelst et al., 2012; Xie et al., 2021). It is only thanks to the recent emergence of i) continental-scale environmental monitoring networks (Cleverly et al., 2019; Gielen et al., 2018; Kao et al., 2012; Karan et al., 2016; Meier et al., 2023), ii) automated in situ data processing methods (Brown et al., 2023; Brown et al., 2020b; Brown and Leblanc, 2024; Chianucci et al., 2022; Chianucci and Macek, 2023), and iii) uncertainty evaluation approaches (Brown et al., 2021a; Camacho et al., 2024; Goryl et al., 2023; Niro et al., 2021), that such a strategy is now feasible.

Our results indicate that the empirical data-driven strategy was effective: in the majority of cases (and despite not making use of ancillary data such as land cover) GROUNDED EO LAI and FAPAR retrievals were subject to reduced bias than those from SL2P and SL2P-CCRS, leading to increased fulfilment of user requirements (i.e. 74% of LAI and 69% of FAPAR retrievals overall, compared to 71% of LAI and 51% of FAPAR retrievals for SL2P-CCRS, the best hybrid approach tested). These findings reflect the results of Camacho et al. (2021), who demonstrated better performance for Gaussian process-based cropland GAI and FAPAR retrieval algorithms trained with the ImagineS database than for those trained with SAIL simulations. In our case, SL2P and SL2P-CCRS provided slightly better performance over croplands than GROUNDED EO for both LAI and FAPAR. The weaker performance of the GROUNDED EO retrievals may be due to the relatively low number of fiducial reference measurements of this land cover type contained within the matchup database, whilst the stronger performance of the SL2P retrievals reflects the homogeneous nature of these canopies. Despite this, it is worth noting that for homogeneous canopies with high LAI and FAPAR values, GROUNDED EO outperformed SL2P and SL2P-CCRS retrievals, where the latter algorithms demonstrated large biases. Our results suggest there may be opportunity to further improve performance through fusion or ensemble retrieval approaches, leveraging the precision of the hybrid RTM-based approaches and the low bias of the GROUNDED EO solution (Baret et al., 2013). This may be particularly relevant for geographical regions not well-represented in the training dataset (Mederer et al., 2025).

#### 4.2. Treatment of uncertainties

In addition to the retrieved value, users of satellite-derived biophysical variables increasingly desire an estimate of retrieval uncertainty. As discussed in Section 1, uncertainty estimates are critical in allowing users to weight observations on the basis of their confidence (Demarty et al., 2007; Raupach et al., 2005; Richardson et al., 2011), and represent a growing requirement, particularly for application within data assimilation schemes (Chernetskiy et al., 2017; Lewis et al., 2012; Mathieu and O'Niell, 2008). Furthermore, recent work has explored the propagation of uncertainties in biophysical variable retrievals to downstream analyses, including the derivation of land surface phenology metrics (Graf et al., 2023), highlighting the crucial context such information can provide when assessing the impacts of environmental change. Gaussian processes, as adopted in the GROUNDED EO retrieval algorithm, inherently provide retrieval uncertainty estimates, whilst 'predicted uncertainties' may be produced in the case SL2P and

SL2P-CCRS, accounting for some, but not all, sources of uncertainty. These ‘predicted uncertainties’ are derived using a separate artificial neural network, which is trained to estimate the retrieval uncertainty that might be expected for a given satellite observation (itself assessed as the RMSD between the biophysical variable value and similar candidates within the training database) (Baret et al., 2010b; Brown et al., 2021b).

By making use of fiducial reference measurements with characterised uncertainties to train the GROUNDED EO retrieval algorithm, we attempted to move towards end-to-end uncertainty treatment, but further work is still necessary. Crucially, the Sentinel-2 L2A product does not yet provide per-pixel uncertainty estimates, so this source of uncertainty could not be explicitly considered in our work. Building on the radiometric uncertainty tool (RUT) already available for L1C products (Gorroño et al., 2018; Gorroño et al., 2017), a L2A RUT has recently been developed, but unfortunately is not yet suitable for operational per-pixel application (Gorroño et al., 2024), preventing its use in our study. Although alternative atmospheric correction approaches such as Sensor Invariant Atmospheric Correction (SIAC) do provide per-pixel uncertainties, they do not yet utilise per-pixel L1C uncertainties as input (instead relying on an assumed constant of 5%) (Yin et al., 2022), so these also cannot strictly be considered end-to-end. In the future, space agencies and data providers must invest in the provision of per-pixel uncertainties incorporating all substantial uncertainty components, including those from upstream input data. Additional experiments to assess the potential impact of L2A surface reflectance uncertainties revealed that whilst they are not the dominant driver of overall retrieval uncertainty, they still represent an important term, with a relative contribution of 33% on average, compared to 67% for GPR-derived (i.e. model-based) uncertainties (Appendix G). In addition to uncertainties associated with the atmospheric correction itself, uncertainties related to geolocation and the instrument point spread function may also play an important role (Choi et al., 2025) and should be considered in future work.

#### 4.3. Applicability of the GROUNDED EO approach to other sensors

Notwithstanding the strengths of the empirical data-driven strategy adopted in our study, a potential limitation for wider use is that the GROUNDED EO retrieval algorithm is, by its nature, specific to the spectral configuration of Sentinel-2’s MSI sensor. Differences in the number, position, and spectral response of MSI’s bands with respect to other sensors such as Landsat 8/9 OLI precludes direct application of the trained GPR models to these other sensors. In principle, separate GPR models could be trained using Landsat 8/9 OLI observations that are spatiotemporally coincident with fiducial reference measurements within the GROUNDED EO database, but this was beyond the scope of our study. Potential challenges include the lower temporal resolution of the Landsat 8/9 OLI archive, since only a single OLI sensor was in orbit for most of the time period covered by the fiducial reference measurements (Landsat 9 was launched only in 2021, and Landsat 8 alone has a repeat cycle of 16 days, as opposed to the 5-day repeat cycle of Sentinel-2A and —2B). The reduced spectral sampling of OLI in regions of the electromagnetic spectrum known to be important for vegetation biophysical variable retrieval (i.e. the red-edge) is a further potential challenge. Future work should investigate the consistency of LAI and FAPAR retrievals from separate GPR models trained with Landsat 8/9 OLI and Sentinel-2 MSI matchups, as well as the utility of products incorporating spectrally and spatially harmonised surface reflectance observations from the two missions (e.g. the Harmonised Landsat Sentinel (HLS) dataset) (Claverie et al., 2018). Comparison against further decametric LAI and FAPAR products including the High Resolution Global Land Surface Satellite (Hi-GLASS) suite (Jin et al., 2022), as well as other Landsat-based datasets (Kang et al., 2021; Wan et al., 2024), should also be prioritised.

#### 4.4. The need for continued provision and expansion of fiducial reference measurements

The efficacy of empirical data-driven approaches, such as the one adopted in this study, is ultimately dependent on the quality and representativeness of the observations used for training. Although it is clear that substantial advances in the availability of in situ reference observations (and fiducial reference measurements with characterised uncertainties) have been made, continued work is required. As discussed in Section 2.2, the GROUNDED EO database was constrained to a small number of continental-scale environmental monitoring networks (Cleverly et al., 2019; Gielen et al., 2018; Kao et al., 2012; Karan et al., 2016; Meier et al., 2023), because of the need for free and open data policies, standardised, documented data collection protocols, and provision of access to raw data. These requirements were crucial to maintaining consistency and enabling uncertainties to be derived in an end-to-end manner (Brown et al., 2021a). Containing more than 16,000 ESU-level observations derived from over 280,000 individual DHP or DCP images collected at 81 NEON, TERN, and ICOS sites between 2013 and 2022, GROUNDED EO is likely the most extensive decametric fiducial reference database of vegetation biophysical variables to date.

Despite the strengths of the GROUNDED EO database, for some sites, the lack of understory observations and ancillary data on woody material meant that several assumptions were still required, and we would urge the respective environmental monitoring networks to follow the example of NEON and consider the collection of these variables as a matter of priority. Additionally, the majority of incorporated sites represent semi-natural environments, with relatively few agricultural locations (Appendix A). Perhaps more importantly, the considered networks lack sites in the equatorial tropics (Fig. 2), which represent a high priority area for vegetation monitoring in the face of environmental change. Whilst our leave-site-out validation scheme provided information on the generalisation capabilities of the GROUNDED EO retrieval algorithm over unseen sites of sampled environments, further research will be required to determine how well the approach generalises to unsampled environments. The fact that the performance of the GROUNDED EO retrievals was worst at the highest LAI values, as might be experienced in equatorial regions, underscores the need for representative fiducial reference measurements – data-driven approaches cannot be expected to maintain the same performance for conditions beyond those represented in their training data. Co-ordinated effort and funding will be required to fill these data gaps, coverage of which is as important for validating existing hybrid retrieval algorithms as it is for training new or updated empirical data-driven ones (Cherif et al., 2023). Future work should focus on validating and refining the GROUNDED EO retrieval approach over regions not incorporated within the fiducial reference database through collection of additional independent in situ reference data.

#### 5. Conclusions

Algorithms such as SL2P have proven popular for decametric retrieval of LAI and FAPAR, yet comprehensive validation has shown that, due to simplifying assumptions in the underlying RTMs, biases persist in SL2P retrievals. RTM assumptions might be avoided altogether with an empirical data-driven approach, but such a strategy has historically been prevented by the limited quantity and quality of available in situ reference measurements, as well as the large number of training samples traditionally required by machine learning regression algorithms. Thanks to recently established continental-scale environmental monitoring networks, advances in automated data processing and uncertainty evaluation, and machine learning regression algorithms requiring many fewer training samples such as Gaussian processes, empirical data-driven retrieval is now a possibility.

In this study, we generated a database of more than 16,000 fiducial reference measurements from over 280,000 DHP or DCP images collected at 81 NEON, TERN, and ICOS sites between 2013 and 2022, which was then utilised to train Gaussian processes for Sentinel-2 LAI and FAPAR retrieval. Our results indicate that in the majority of cases (and despite not making use of ancillary data such as land cover), the empirical data-driven GROUNDED EO retrievals were subject to reduced bias than those from SL2P and SL2P-CCRS, leading to increased fulfilment of user requirements (i.e. 74% of LAI and 69% of FAPAR retrievals overall). Consequently, the approach has potential to reduce uncertainty in key inputs for climate monitoring and modelling, agricultural and forest management, and biodiversity assessment.

#### CRediT authorship contribution statement

**Luke A. Brown:** Writing – review & editing, Writing – original draft, Visualization, Validation, Supervision, Software, Resources, Project administration, Methodology, Investigation, Funding acquisition, Formal analysis, Data curation, Conceptualization. **Richard Fernandes:** Writing – review & editing, Validation, Software, Resources, Methodology, Investigation, Formal analysis, Data curation. **Jochem Verrelst:** Writing – review & editing, Supervision, Software, Resources, Methodology, Funding acquisition. **Harry Morris:** Writing – review & editing, Investigation, Formal analysis, Data curation. **Najib Djamai:** Writing – review & editing, Validation, Software, Methodology, Investigation, Formal analysis, Data curation. **Pablo Reyes-Muñoz:** Writing – review & editing, Investigation. **Dávid D.Kovács:** Writing – review & editing, Investigation. **Courtney Meier:** Writing – review & editing, Resources, Data curation.

#### Declaration of competing interest

The authors declare that they have no known competing financial interests or personal relationships that could have appeared to influence the work reported in this paper.

#### Acknowledgements

This activity was carried out under the Living Planet Fellowship, a programme of and funded by the European Space Agency. The view expressed in this publication can in no way be taken to reflect the official opinion of the European Space Agency. J. Verrelst, P. Reyes-Muñoz and D. D.Kovács were funded by the European Union (ERC, FLEXINEL, 101086622). Views and opinions expressed are however those of the author(s) only and do not necessarily reflect those of the European Union or the European Research Council. Neither the European Union nor the granting authority can be held responsible for them. The authors acknowledge Natural Resources Canada, Canada Centre for Mapping and Earth Observation for provision of SL2P and SL2P-CCRS code, and are grateful to Bert Gielen, Arne Iserbyt, and Dario Papale for provision of metadata associated with the ICOS DHP observations. The National Ecological Observatory Network is a program sponsored by the National Science Foundation and operated under cooperative agreement by Battelle. This material is based in part upon work supported by the National Science Foundation through the NEON Program. The authors thank the ICOS Principal Investigators, Ecosystem Thematic Centre, and Carbon Portal for providing DHP data. Work at Tharandt was funded by grant EUROFLUX (EN-VCT 0095-0078) from EU and grant Sicherstellung des Treibhausgasmonitorings an sächsischen ICOS-Standorten (65-0456/49/10) from Freistaat Sachsen. Work at Hyletmossa, Norunda, and Svarnberget was funded by grant National Research Infrastructure ICOS Sweden (2019-00205) from Swedish Research Council. Data were sourced from Terrestrial Ecosystem Research Network (TERN) infrastructure, which is enabled by the Australian Government's National Collaborative Research Infrastructure Strategy (NCRIS). TERN acknowledge the Traditional Owners and Custodians throughout Australia, New Zealand and all nations, honour their profound connections to land, water, biodiversity and culture, and pay respects to their Elders past, present and emerging. The authors also thank the Associate Editor and the four anonymous reviewers for their constructive comments, which helped to substantially improve the manuscript.

#### Appendix A. Study sites

**Table A1**

The 81 NEON, ICOS, and TERN sites from which raw in situ data were obtained and processed to derive fiducial reference measurements.

	Site	Modal land cover	Latitude	Longitude	Primary method	Dates	Reference
NEON	Abby Road	Evergreen forest	45.7624	-122.3303	DHP	2016 to 2022	National Ecological Observatory Network (2022)
	Utqiāġvik	Woody wetlands	71.2824	-156.6194	DHP	2017 to 2022	
	Bartlett Experimental Forest	Mixed forest	44.0639	-71.2874	DHP	2014 to 2022	
	Blandy Experimental Farm	Shrub/scrub	39.0337	-78.0418	DHP	2015 to 2022	
	Caribou-Poker Creeks Research Watershed	Deciduous forest	65.1540	-147.5026	DHP	2017 to 2022	
	Lyndon B. Johnson National Grassland	Deciduous forest	33.4012	-97.5700	DHP	2016 to 2022	
	Central Plains Experimental Range	Grassland/herbaceous	40.8155	-104.7456	DHP	2014 to 2022	
	Dakota Coteau Field	Grassland/herbaceous	47.1617	-99.1066	DHP	2017 to 2022	
	Delta Junction	Evergreen forest	63.8811	-145.7514	DHP	2016 to 2022	
	Dead Lake	Deciduous forest	32.5417	-87.8039	DHP	2016 to 2022	
	Disney Wilderness Preserve	Pasture/hay	28.1251	-81.4362	DHP	2013 to 2022	
	Great Smoky Mountains National Park	Deciduous forest	35.6890	-83.5020	DHP	2016 to 2022	
	Guanica Forest	Evergreen forest	17.9696	-66.8687	DHP	2015 to 2022	
	Harvard Forest & Quabbin Watershed	Mixed forest	42.5369	-72.1727	DHP	2014 to 2022	
	Healy	Shrub/scrub	63.8758	-149.2134	DHP	2015 to 2022	
	The Jones Center at Ichauway	Evergreen forest	31.1948	-84.4686	DHP	2013 to 2022	
	Jornada Experimental Range	Shrub/scrub	32.5907	-106.8425	DHP	2015 to 2022	
	Konza Prairie Agroecosystem	Cultivated crops	39.1105	-96.6129	DHP	2017 to 2022	
	Konza Prairie Biological Station	Grassland/herbaceous	39.1008	-96.5631	DHP	2016 to 2022	
	Lajas Experimental Station	Pasture/hay	18.0213	-67.0769	DHP	2016 to 2022	

(continued on next page)

**Table A1 (continued)**

	Site	Modal land cover	Latitude	Longitude	Primary method	Dates	Reference
	Lenoir Landing	Deciduous forest	31.8539	-88.1612	DHP	2016 to 2022	
	Mountain Lake Biological Station	Deciduous forest	37.3783	-80.5249	DHP	2017 to 2022	
	Moab	Shrub/scrub	38.2483	-109.3883	DHP	2015 to 2022	
	Niwot Ridge	Grassland/herbaceous	40.0543	-105.5824	DHP	2015 to 2022	
	Northern Great Plains Research Laboratory	Grassland/herbaceous	46.7697	-100.9154	DHP	2016 to 2022	
	Marvin Klemme Range Research Station	Shrub/scrub	35.4106	-99.0588	DHP	2016 to 2022	
	Onaqui	Shrub/scrub	40.1776	-112.4525	DHP	2014 to 2022	
	Oak Ridge	Deciduous forest	35.9641	-84.2826	DHP	2014 to 2022	
	Ordway-Swisher Biological Station	Evergreen forest	29.6893	-81.9934	DHP	2013 to 2022	
	Puu Makaala Natural Area Reserve	Evergreen forest	19.5531	-155.3173	DHP	2018 to 2022	
	Rocky Mountains	Evergreen forest	40.2759	-105.5460	DHP	2017 to 2022	
	Smithsonian Conservation Biology Institute	Deciduous forest	38.8929	-78.1395	DHP	2014 to 2022	
	Smithsonian Environmental Research Center	Deciduous forest	38.8901	-76.5600	DHP	2015 to 2022	
	San Joaquin Experimental Range	Evergreen forest	37.1088	-119.7323	DHP	2016 to 2022	
	Soaproot Saddle	Evergreen forest	37.0334	-119.2622	DHP	2018 to 2022	
	Santa Rita Experimental Range	Shrub/scrub	31.9107	-110.8355	DHP	2016 to 2022	
	Steigerwaldt-Chequamegon	Deciduous forest	45.5089	-89.5864	DHP	2015 to 2022	
	North Sterling	Cultivated crops	40.4619	-103.0293	DHP	2014 to 2022	
	Talladega National Forest	Evergreen forest	32.9505	-87.3933	DHP	2014 to 2022	
	Lower Teakettle	Evergreen forest	37.0058	-119.0060	DHP	2019 to 2022	
	Toolik Field Station	Grassland/herbaceous	68.6611	-149.3705	DHP	2017 to 2022	
	Treehaven	Mixed forest	45.4937	-89.5857	DHP	2015 to 2022	
	KU Field Station	Deciduous forest	39.0404	-95.1922	DHP	2016 to 2022	
	University of Notre Dame Environmental Research Center	Deciduous forest	46.2339	-89.5373	DHP	2014 to 2022	
	Chase Lake National Wildlife Refuge	Grassland/herbaceous	47.1282	-99.2413	DHP	2014 to 2022	
	Wind River Experimental Forest	Evergreen forest	45.8205	-121.9519	DHP	2018 to 2022	
	Yellowstone National Park	Evergreen forest	44.9535	-110.5391	DHP	2018 to 2022	
ICOS	Brasschaat	Evergreen forest	51.3076	4.5198	DHP	2017 to 2022	Janssens et al. (2022)
	Vielsalm	Mixed forest	50.3050	5.9981	DHP	2018 to 2022	Vincke et al. (2022)
	Davos	Evergreen forest	46.8153	9.8559	DHP	2018 to 2022	Feigenwinter et al. (2022)
	Hohes Holz	Deciduous forest	52.0866	11.2224	DHP	2018 to 2022	Rebmann et al. (2022)
	Tharandt	Evergreen forest	50.9626	13.5652	DHP	2020 to 2022	Bernhofer et al. (2021)
	Soroe	Deciduous forest	55.4859	11.6446	DHP	2020 to 2022	Ibrom et al. (2022)
	Hyytiälä	Evergreen forest	61.8474	24.2948	DHP	2017 to 2022	Mammarella et al. (2022)
	Sodankyla	Evergreen forest	67.3624	26.6386	DHP	2019 to 2020	Aurela et al. (2020)
	Bilos	Evergreen forest	44.4937	-0.9561	DHP	2018 to 2022	Loustau et al. (2022)
	Font-Blanche	Evergreen forest	43.2408	5.6787	DHP	2020 to 2022	Simioni et al. (2022)
	Fontainebleau-Barbeau	Deciduous forest	48.4764	2.7801	DHP	2018 to 2022	Berveiller et al. (2022)
	Hesse	Deciduous forest	48.6741	7.0647	DHP	2021 to 2022	Guntz et al. (2022)
	Puechabon	Evergreen forest	43.7413	3.5957	DHP	2021 to 2022	Limousin et al. (2022)
	Castelporziano	Mixed forest	41.7043	12.3573	DHP	2021 to 2022	Fares et al. (2022)
	Renon	Evergreen forest	46.5869	11.4337	DHP	2020 to 2021	Montagnani et al. (2021)
	San Rossore	Evergreen forest	43.7320	10.2909	DHP	2018 to 2022	Arriga et al. (2022)
TERN	Hurdal	Evergreen forest	60.3716	11.0795	DHP	2021 to 2022	Lange et al. (2022)
	Hyltemossa	Evergreen forest	56.0976	13.4190	DHP	2017 to 2022	Heliasz et al. (2022)
	Norunda	Evergreen forest	60.0865	17.4795	DHP	2017 to 2022	Mölder et al. (2022)
	Svartberget	Evergreen forest	64.2561	19.7745	DHP	2017 to 2021	Peichl et al. (2022)
	Alice Mulga	Shrub/scrub	-22.2828	133.2493	DCP	2011 to 2018	Cleverly et al. (2021)
	Boyagin	Evergreen forest	-32.4771	116.9386	DHP	2018 to 2021	Beringer et al. (2021a; 2021b)
	Calperum Malle	Shrub/scrub	-34.0027	140.5877	DCP	2013 to 2019	Meyer and Koerber (2021)
	Cumberland Plain	Evergreen forest	-33.6152	150.7236	DCP	2015 to 2021	Pendall et al. (2020)
	Gingin	Evergreen forest	-31.3764	115.7139	DCP	2015 to 2021	Silberstein et al. (2021)
	Great Western Woodlands	Evergreen forest	-30.1913	120.6541	DCP	2013 to 2022	Prober et al. (2020)
	Karawatha	Evergreen forest	-27.6333	153.0822	DCP	2015 to 2017	Hero and Lollback (2021)
	Litchfield	Evergreen forest	-13.1790	130.7945	DCP	2017 to 2022	Hutley et al. (2021)
	Robson Creek	Evergreen forest	-17.1175	145.6301	DHP	2014 to 2020	Liddell et al. (2016)
	Samford	Pasture/hay	-27.3881	152.8778	DCP	2017 to 2022	Grace et al. (2021)
	Tumbarumba	Evergreen forest	-35.6566	148.1517	DCP	2014 to 2021	Stol et al. (2021)
	Warra	Evergreen forest	-43.0950	146.6545	DHP	2015 to 2023	Wardlaw (2021)
	Whroo	Evergreen forest	-36.6732	145.0294	DHP	2014 to 2017	Beringer et al. (2021c)
	Wombat	Evergreen forest	-37.4222	144.0944	DHP	2015 to 2015	Arndt et al. (2021)

## Appendix B. Correcting for missing understory measurements at ICOS sites

At ICOS sites, understory GAI<sub>e</sub> was quantified using DCP and two radiometric methods (George et al., 2021). The inter-method uncertainty in the understory GAI<sub>e</sub> values was computed as the standard deviation of the mean over the three measurement approaches (Table B1). Empirical relationships were used to transform the observed understory GAI<sub>e</sub> at each ICOS site to understory GAI and FIPAR. These were derived from those observations within the GROUNDED EO database containing all three variables (Fig. B1). Following FRM4VEG recommendations (Brown et al., 2021a), orthogonal distance regression (ODR) was used to establish these relationships.

**Table B1**

Mean understory GAI<sub>e</sub> values reported by George et al. (2021), which were derived using three radiometric methods at each ICOS site.

Site	GAI <sub>e</sub>	
	Mean	Standard uncertainty
Brasschaat	0.34	0.20
Vielsalm	0.37	0.19
Davos	1.01	0.42
Hohes Holz	0.45	0.19
Tharandt	0.70	0.16
Soroe	0.57	0.21
Hyytiälä	1.50	0.10
Sodankylä	0.68	0.23
Bilos	1.85	0.32
Font-Blanche	0.97	0.15
Hesse	0.21	0.17
Puechabon	0.71	0.17
Castelporziano	0.36	0.23
Renon	1.23	0.15
San Rossore	0.44	0.26
Hurdal	1.61	0.04
Hyltemossa	1.22	0.12
Norunda	1.27	0.12
Svartherget	1.70	0.16

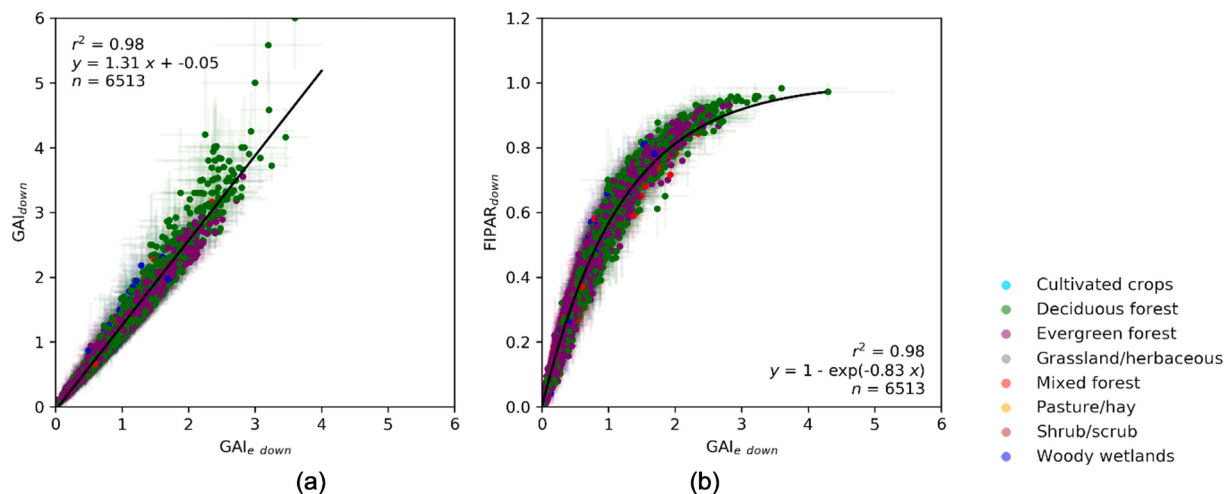


**Fig. B1.** Empirical relationships relating understory GAI<sub>e</sub> to understory GAI (a) and FIPAR (b), derived using ODR from those observations within the GROUNDED EO database containing all three variables.

## Appendix C. Overstory WAI at NEON sites

**Table C1**

Baseline WAI values determined from manually classified early spring images from at least one ESU at each NEON site where a vegetated overstory is present.

Site	WAI	
	Mean	Standard uncertainty
Abby Road	1.06	0.11
Bartlett Experimental Forest	1.09	0.04
Blandy Experimental Farm	1.02	0.06
Caribou-Poker Creeks Research Watershed	0.72	0.06
Lyndon B. Johnson National Grassland	0.96	0.13
Delta Junction	0.59	0.07
Dead Lake	0.88	0.05
Disney Wilderness Preserve	0.89	0.29
Great Smoky Mountains National Park	0.93	0.02
Guanica Forest	0.95	0.05
Harvard Forest & Quabbin Watershed	0.91	0.14
Healy	0.79	0.04
The Jones Center At Ichauway	1.10	0.25
Konza Prairie Biological Station	0.81	0.02
Lajas Experimental Station	0.84	0.03
Lenoir Landing	1.90	0.40
Mountain Lake Biological Station	0.93	0.02
Oak Ridge	0.90	0.05
Ordway-Swisher Biological Station	0.79	0.04
Puu Makaala Natural Area Reserve	1.70	0.40
Rocky Mountains	1.25	0.14
Smithsonian Conservation Biology Institute	0.97	0.03
San Joaquin Experimental Range	0.43	0.15
Soaproot Saddle	0.08	0.02
Steigerwaldt-Chequamegon	0.97	0.02
Talladega National Forest	1.27	0.13
Lower Teakettle	2.41	0.20
Treehaven	0.87	0.02
KU Field Station	1.21	0.18
University of Notre Dame Environmental Research Center	1.00	0.03
Wind River Experimental Forest	2.50	0.40
Yellowstone National Park	0.79	0.04

**Table C2**

Mean and standard uncertainty of woody-to-total ( $\alpha$ ) ratio values over all deciduous forest, evergreen forest, and mixed forest NEON ESUs.

Forest type	Woody-to-total ratio ( $\alpha$ )	
	Mean	Standard uncertainty
Deciduous forest	0.35	0.27
Evergreen forest	0.59	0.28
Mixed forest	0.33	0.22

## Appendix D. Intercomparison results by land cover and magnitude

**Table D1**

Intercomparison of GROUNDED EO vs. SL2P and SL2P-CCRS LAI and FAPAR retrievals, by land cover.

	Land cover	n	LAI					FAPAR						
			$r^2$	RMSD	NRMSD (%)	Bias	Precision	Slope	$r^2$	RMSD	NRMSD (%)	Bias	Precision	
GROUNDED EO vs. SL2P	Cultivated crops	111	0.89	0.56 ± 0.09	42.19 ± 6.44	-0.33 ± 0.08	0.45 ± 0.08	1.05 ± 0.04	0.91	0.11 ± 0.01	30.11 ± 2.90	-0.05 ± 0.01	0.10 ± 0.01	1.14 ± 0.04
	Deciduous broadleaf	906	0.88	0.82 ± 0.04	34.31 ± 1.76	0.49 ± 0.03	0.66 ± 0.03	1.41 ± 0.02	0.87	0.14 ± 0.00	23.55 ± 0.65	0.09 ± 0.00	0.10 ± 0.00	1.18 ± 0.02
	Evergreen broadleaf	104	0.81	0.50 ± 0.09	30.30 ± 5.96	0.31 ± 0.09	0.40 ± 0.09	1.46 ± 0.07	0.68	0.18 ± 0.01	46.24 ± 2.84	0.15 ± 0.01	0.11 ± 0.01	1.35 ± 0.09
	Evergreen needleleaf	845	0.87	0.72 ± 0.03	40.37 ± 2.20	0.32 ± 0.03	0.64 ± 0.03	1.58 ± 0.02	0.79	0.18 ± 0.00	40.62 ± 0.93	0.11 ± 0.00	0.14 ± 0.00	1.48 ± 0.03
	Grassland /herbaceous	579	0.76	0.58 ± 0.04	57.09 ± 3.67	-0.26 ± 0.03	0.52 ± 0.03	1.20 ± 0.03	0.83	0.11 ± 0.01	35.80 ± 1.42	-0.05 ± 0.00	0.10 ± 0.00	1.16 ± 0.02
	Mixed forest	124	0.87	0.69 ± 0.09	31.97 ± 4.95	0.31 ± 0.09	0.61 ± 0.09	1.49 ± 0.05	0.85	0.13 ± 0.01	24.72 ± 1.78	0.10 ± 0.01	0.09 ± 0.01	1.14 ± 0.04
	Pasture/hay	191	0.79	0.58 ± 0.06	41.10 ± 4.38	-0.36 ± 0.06	0.45 ± 0.06	1.23 ± 0.05	0.77	0.13 ± 0.01	29.27 ± 2.07	-0.07 ± 0.01	0.11 ± 0.01	1.10 ± 0.04
	Shrub/scrub	319	0.60	0.38 ± 0.05	90.49 ± 12.25	-0.08 ± 0.04	0.37 ± 0.04	0.93 ± 0.04	0.79	0.08 ± 0.01	49.22 ± 4.04	-0.03 ± 0.01	0.07 ± 0.01	1.03 ± 0.03
	Woody wetlands	50	0.87	0.91 ± 0.16	38.95 ± 8.09	0.71 ± 0.15	0.57 ± 0.15	1.51 ± 0.08	0.83	0.16 ± 0.02	29.14 ± 3.06	0.15 ± 0.02	0.08 ± 0.02	1.06 ± 0.07
	Cultivated crops	111	0.89	0.56 ± 0.09	42.19 ± 6.44	-0.33 ± 0.08	0.45 ± 0.08	1.05 ± 0.04	0.91	0.11 ± 0.01	30.11 ± 2.90	-0.05 ± 0.01	0.10 ± 0.01	1.14 ± 0.04
GROUNDED EO vs. SL2P-CCRS	Deciduous broadleaf	906	0.83	0.72 ± 0.04	22.98 ± 1.13	-0.24 ± 0.03	0.68 ± 0.03	0.84 ± 0.01	0.84	0.12 ± 0.00	19.64 ± 0.57	0.06 ± 0.00	0.12 ± 0.00	1.05 ± 0.02
	Evergreen broadleaf	104	0.64	0.57 ± 0.08	35.24 ± 5.49	0.34 ± 0.08	0.46 ± 0.08	1.02 ± 0.08	0.52	0.12 ± 0.01	50.48 ± 2.52	0.16 ± 0.01	0.12 ± 0.01	1.05 ± 0.10
	Evergreen needleleaf	845	0.76	0.74 ± 0.05	29.88 ± 1.70	-0.37 ± 0.05	0.64 ± 0.05	1.02 ± 0.02	0.60	0.26 ± 0.00	73.79 ± 1.47	0.19 ± 0.00	0.17 ± 0.00	1.45 ± 0.04
	Grassland /herbaceous	579	0.76	0.58 ± 0.04	57.09 ± 3.67	-0.26 ± 0.03	0.52 ± 0.03	1.20 ± 0.03	0.83	0.11 ± 0.01	35.80 ± 1.42	-0.05 ± 0.00	0.10 ± 0.00	1.16 ± 0.02
	Mixed forest	124	0.76	1.32 ± 0.12	37.38 ± 2.74	-1.08 ± 0.12	0.76 ± 0.12	0.72 ± 0.04	0.65	0.22 ± 0.01	47.14 ± 2.77	0.17 ± 0.01	0.13 ± 0.01	0.83 ± 0.05
	Pasture/hay	191	0.79	0.58 ± 0.06	41.10 ± 4.38	-0.36 ± 0.06	0.45 ± 0.06	1.23 ± 0.05	0.77	0.13 ± 0.01	29.27 ± 2.07	-0.07 ± 0.01	0.11 ± 0.01	1.10 ± 0.04
	Shrub/scrub	319	0.60	0.38 ± 0.05	90.49 ± 12.25	-0.08 ± 0.04	0.37 ± 0.04	0.93 ± 0.04	0.79	0.08 ± 0.01	49.22 ± 4.04	-0.03 ± 0.01	0.07 ± 0.01	1.03 ± 0.03
	Woody wetlands	50	0.80	0.97 ± 0.20	26.25 ± 4.76	-0.67 ± 0.19	0.71 ± 0.19	0.70 ± 0.05	0.69	0.25 ± 0.02	52.98 ± 4.70	0.23 ± 0.02	0.11 ± 0.02	0.79 ± 0.08

**Table D2**

Intercomparison of GROUNDED EO vs. SL2P and SL2P-CCRS LAI and FAPAR retrievals, by SL2P or SL2P-CCRS retrieval magnitude.

LAI									FAPAR								
	Value	n	$r^2$	RMSD	NRMSE (%)	Bias	Precision	Slope	Value	n	$r^2$	RMSD	NRMSE (%)	Bias	Precision	Slope	
GROUNDED EO vs. SL2P	0 to 1	973	0.13	0.40 ± 0.03	84.60 ± 4.89	-0.24 ± 0.02	0.32 ± 0.02	0.32 ± 0.03	0.0 to 0.1	261	0.12	0.05 ± 0.01	76.44 ± 11.78	-0.03 ± 0.01	0.04 ± 0.01	0.64 ± 0.11	
	1 to 2	1059	0.53	0.63 ± 0.03	42.19 ± 1.91	-0.10 ± 0.03	0.62 ± 0.03	2.03 ± 0.06	0.1 to 0.2	363	0.04	0.10 ± 0.01	64.22 ± 4.12	-0.06 ± 0.01	0.07 ± 0.01	0.57 ± 0.14	
	2 to 3	796	0.42	0.85 ± 0.04	34.41 ± 1.78	0.69 ± 0.04	0.50 ± 0.04	1.45 ± 0.06	0.2 to 0.3	367	0.17	0.13 ± 0.01	50.40 ± 2.45	-0.05 ± 0.01	0.12 ± 0.01	1.69 ± 0.20	
	3 to 4	360	0.31	0.98 ± 0.06	29.16 ± 2.14	0.88 ± 0.06	0.42 ± 0.06	1.12 ± 0.09	0.3 to 0.4	434	0.09	0.16 ± 0.01	44.15 ± 1.62	0.01 ± 0.01	0.16 ± 0.01	1.68 ± 0.25	
	4 to 5	35	0.01	0.84 ± 0.21	19.47 ± 5.39	0.51 ± 0.21	0.67 ± 0.21	0.20 ± 0.34	0.4 to 0.5	535	0.06	0.17 ± 0.01	37.50 ± 1.12	0.08 ± 0.01	0.15 ± 0.01	1.25 ± 0.22	
	5 to 6	3	0.96	1.0 ± 0.7	18.66 ± 12.65	-0.90 ± 0.70	0.40 ± 0.70	3.30 ± 0.60	0.5 to 0.6	480	0.16	0.17 ± 0.01	31.75 ± 0.94	0.14 ± 0.01	0.10 ± 0.01	1.53 ± 0.16	
	6 to 7	-	-	-	-	-	-	-	0.6 to 0.7	359	0.15	0.15 ± 0.01	23.47 ± 0.86	0.13 ± 0.01	0.08 ± 0.01	1.09 ± 0.14	
	7 to 8	-	-	-	-	-	-	-	0.7 to 0.8	347	0.04	0.12 ± 0.01	15.79 ± 0.72	0.10 ± 0.01	0.06 ± 0.01	0.43 ± 0.11	
	8 to 9	-	-	-	-	-	-	-	0.8 to 0.9	74	0.25	0.06 ± 0.01	7.47 ± 1.47	0.02 ± 0.01	0.06 ± 0.01	-0.69 ± 0.14	
	> 9	-	-	-	-	-	-	-	0.9 to 1.0	6	0.25	0.12 ± 0.06	13.39 ± 6.04	-0.11 ± 0.05	0.04 ± 0.05	-2.00 ± 1.70	
GROUNDED EO vs. SL2P-CCRS	0 to 1	891	0.12	0.39 ± 0.03	87.63 ± 5.52	-0.22 ± 0.03	0.32 ± 0.03	0.33 ± 0.03	0.0 to 0.1	254	0.06	0.06 ± 0.01	99.85 ± 15.81	-0.02 ± 0.01	0.06 ± 0.01	0.65 ± 0.16	
	1 to 2	876	0.26	0.75 ± 0.03	51.20 ± 2.05	-0.37 ± 0.03	0.66 ± 0.03	1.37 ± 0.08	0.1 to 0.2	418	0.05	0.13 ± 0.01	84.08 ± 4.35	-0.03 ± 0.01	0.12 ± 0.01	1.05 ± 0.22	
	2 to 3	602	0.20	0.66 ± 0.05	26.40 ± 1.94	-0.05 ± 0.05	0.66 ± 0.05	1.10 ± 0.09	0.2 to 0.3	532	0.11	0.20 ± 0.01	77.93 ± 2.38	0.05 ± 0.01	0.19 ± 0.01	2.13 ± 0.27	
	3 to 4	386	0.11	0.59 ± 0.07	16.84 ± 1.92	-0.04 ± 0.07	0.58 ± 0.07	0.70 ± 0.10	0.3 to 0.4	495	0.04	0.23 ± 0.01	65.32 ± 1.70	0.11 ± 0.01	0.20 ± 0.01	1.48 ± 0.31	
	4 to 5	281	0.05	0.78 ± 0.08	17.33 ± 1.67	-0.55 ± 0.08	0.56 ± 0.08	0.41 ± 0.11	0.4 to 0.5	456	0.01	0.23 ± 0.01	51.20 ± 1.36	0.12 ± 0.01	0.19 ± 0.01	0.60 ± 0.32	
	5 to 6	161	0.01	1.26 ± 0.11	23.39 ± 1.70	-1.04 ± 0.10	0.70 ± 0.10	-0.21 ± 0.18	0.5 to 0.6	321	0.08	0.17 ± 0.01	31.21 ± 1.23	0.12 ± 0.01	0.13 ± 0.01	1.26 ± 0.24	
	6 to 7	27	0.02	1.92 ± 0.27	29.92 ± 3.30	-1.80 ± 0.26	0.66 ± 0.26	0.40 ± 0.60	0.6 to 0.7	259	0.10	0.14 ± 0.01	22.28 ± 1.09	0.11 ± 0.01	0.09 ± 0.01	1.05 ± 0.19	
	7 to 8	-	-	-	-	-	-	-	0.7 to 0.8	256	0.12	0.10 ± 0.01	13.33 ± 0.83	0.08 ± 0.01	0.06 ± 0.01	0.76 ± 0.13	
	8 to 9	-	-	-	-	-	-	-	0.8 to 0.9	211	0.00	0.05 ± 0.01	6.42 ± 0.93	0.03 ± 0.01	0.05 ± 0.01	-0.11 ± 0.11	
	> 9	-	-	-	-	-	-	-	0.9 to 1.0	24	0.00	0.11 ± 0.03	12.23 ± 2.69	-0.11 ± 0.02	0.04 ± 0.02	-0.00 ± 0.60	

## Appendix E. Validation results by magnitude

**Table E1**

Performance of GROUNDED EO, SL2P, and SL2P-CCRS LAI and FAPAR retrievals with respect to fiducial reference measurements, by fiducial reference magnitude. The best performing results for each magnitude range in terms of UAR are shown in bold.

		LAI						FAPAR											
		Value	n	$r^2$	RMSD	NRMSD (%)	Bias	Precision	UAR (%)	Slope	Value	n	$r^2$	RMSD	NRMSD (%)	Bias	Precision	UAR (%)	Slope
GROUNDED EO	0 to 1	1449	0.21	<b>0.64 ± 0.02</b>	<b>209.12 ± 6.06</b>	<b>0.24 ± 0.02</b>	<b>0.59 ± 0.02</b>	<b>90.61</b>	<b>1.11 ± 0.06</b>		0.0 to 0.1	635	0.07	<b>0.12 ± 0.00</b>	<b>305.92 ± 12.00</b>	<b>0.05 ± 0.00</b>	<b>0.11 ± 0.00</b>	<b>81.26</b>	<b>0.99 ± 0.14</b>
	1 to 2	415	0.08	1.12 ± 0.04	76.44 ± 2.82	0.36 ± 0.04	1.06 ± 0.04	58.80	1.06 ± 0.18	<b>0.1 to 0.2</b>	296	0.04	<b>0.16 ± 0.01</b>	<b>107.77 ± 4.70</b>	<b>0.08 ± 0.01</b>	<b>0.13 ± 0.01</b>	<b>58.78</b>	<b>0.96 ± 0.27</b>	
	2 to 3	392	0.06	1.01 ± 0.04	40.68 ± 1.86	0.08 ± 0.04	1.01 ± 0.04	62.50	0.87 ± 0.18	0.2 to 0.3	254	0.06	0.15 ± 0.01	62.34 ± 2.77	0.04 ± 0.01	0.15 ± 0.01	54.33	1.29 ± 0.31	
	3 to 4	447	0.00	<b>1.00 ± 0.05</b>	<b>28.83 ± 1.22</b>	<b>-0.40 ± 0.04</b>	<b>0.92 ± 0.04</b>	<b>69.35</b>	<b>0.13 ± 0.15</b>	0.3 to 0.4	202	0.00	0.19 ± 0.01	54.69 ± 2.87	-0.01 ± 0.01	0.19 ± 0.01	38.12	-0.40 ± 0.50	
	4 to 5	346	0.04	<b>1.25 ± 0.06</b>	<b>28.33 ± 1.28</b>	<b>-0.85 ± 0.06</b>	<b>0.92 ± 0.06</b>	<b>60.12</b>	<b>0.73 ± 0.18</b>	0.4 to 0.5	184	0.05	0.17 ± 0.01	37.73 ± 2.03	-0.02 ± 0.01	0.17 ± 0.01	42.39	1.40 ± 0.50	
	5 to 6	134	0.03	1.39 ± 0.09	26.09 ± 1.50	-1.19 ± 0.10	0.73 ± 0.10	44.03	0.45 ± 0.23	0.5 to 0.6	244	0.03	0.19 ± 0.01	34.7 ± 2.14	0.04 ± 0.01	0.19 ± 0.01	41.39	1.20 ± 0.50	
	6 to 7	36	0.01	2.18 ± 0.12	34.16 ± 1.70	-2.05 ± 0.13	0.74 ± 0.13	5.56	0.20 ± 0.40	0.6 to 0.7	282	0.01	<b>0.16 ± 0.01</b>	<b>25.01 ± 1.02</b>	-0.01 ± 0.01	0.16 ± 0.01	<b>65.25</b>	<b>0.63 ± 0.34</b>	
	7 to 8	6	0.01	2.60 ± 0.28	35.54 ± 3.46	-2.58 ± 0.28	0.30 ± 0.28	0.00	0.10 ± 0.70	0.7 to 0.8	529	0.06	<b>0.13 ± 0.01</b>	<b>17.49 ± 0.71</b>	-0.02 ± 0.01	0.13 ± 0.01	<b>82.61</b>	<b>1.13 ± 0.20</b>	
	8 to 9	-	-	-	-	-	-	-	-	0.8 to 0.9	436	0.06	<b>0.13 ± 0.01</b>	<b>14.79 ± 0.61</b>	-0.06 ± 0.01	0.11 ± 0.01	<b>86.24</b>	<b>0.97 ± 0.19</b>	
	> 9	-	-	-	-	-	-	-	-	> 0.9	164	0.03	<b>0.14 ± 0.01</b>	<b>14.32 ± 0.89</b>	-0.11 ± 0.01	0.08 ± 0.01	91.46	0.55 ± 0.24	
SL2P	0 to 1	1449	0.38	0.66 ± 0.02	215.67 ± 5.60	0.50 ± 0.01	0.43 ± 0.01	85.85	1.20 ± 0.04	0.0 to 0.1	635	0.13	0.14 ± 0.00	368.60 ± 9.39	0.11 ± 0.00	0.09 ± 0.00	60.47	1.21 ± 0.13	
	1 to 2	415	0.09	<b>0.71 ± 0.04</b>	<b>48.37 ± 2.98</b>	<b>0.26 ± 0.04</b>	<b>0.66 ± 0.04</b>	<b>87.23</b>	<b>0.71 ± 0.11</b>	0.1 to 0.2	296	0.05	0.17 ± 0.00	113.71 ± 3.13	0.13 ± 0.00	0.10 ± 0.00	41.89	0.78 ± 0.20	
	2 to 3	392	0.03	<b>0.71 ± 0.04</b>	<b>28.69 ± 1.74</b>	<b>-0.38 ± 0.05</b>	<b>0.60 ± 0.05</b>	<b>84.18</b>	<b>0.36 ± 0.10</b>	0.2 to 0.3	254	0.06	0.13 ± 0.00	50.60 ± 1.76	0.08 ± 0.00	0.10 ± 0.00	56.30	0.81 ± 0.20	
	3 to 4	447	0.01	1.21 ± 0.05	34.76 ± 1.27	-1.05 ± 0.05	0.61 ± 0.05	47.20	0.24 ± 0.10	0.3 to 0.4	202	0.00	<b>0.13 ± 0.01</b>	<b>37.27 ± 1.98</b>	<b>0.02 ± 0.01</b>	<b>0.13 ± 0.01</b>	<b>55.94</b>	-0.20 ± 0.33	
	4 to 5	346	0.08	1.71 ± 0.06	38.57 ± 1.20	-1.58 ± 0.06	0.64 ± 0.06	18.79	0.67 ± 0.12	0.4 to 0.5	184	0.04	<b>0.11 ± 0.01</b>	<b>24.58 ± 1.18</b>	-0.04 ± 0.01	0.10 ± 0.01	<b>64.13</b>	<b>0.78 ± 0.28</b>	
	5 to 6	134	0.02	2.06 ± 0.11	38.57 ± 1.66	-1.97 ± 0.12	0.60 ± 0.12	5.97	0.30 ± 0.18	0.5 to 0.6	244	0.05	<b>0.14 ± 0.01</b>	<b>24.63 ± 1.16</b>	-0.08 ± 0.01	<b>0.11 ± 0.01</b>	<b>62.30</b>	<b>0.99 ± 0.29</b>	
	6 to 7	36	0.06	3.09 ± 0.18	48.39 ± 2.56	-3.06 ± 0.18	0.42 ± 0.18	0	0.34 ± 0.22	0.6 to 0.7	282	0.02	0.17 ± 0.01	26.68 ± 0.72	-0.13 ± 0.01	0.12 ± 0.01	52.84	0.51 ± 0.24	
	7 to 8	6	0.03	3.8 ± 0.4	51.77 ± 5.56	-3.80 ± 0.40	0.30 ± 0.40	0	-0.20 ± 0.60	0.7 to 0.8	529	0.04	0.22 ± 0.00	28.67 ± 0.48	-0.17 ± 0.00	0.13 ± 0.00	43.86	0.93 ± 0.20	
	8 to 9	-	-	-	-	-	-	-	-	0.8 to 0.9	436	0.06	0.23 ± 0.00	26.75 ± 0.33	-0.19 ± 0.00	0.12 ± 0.00	50.23	1.16 ± 0.21	
	> 9	-	-	-	-	-	-	-	-	> 0.9	164	0.05	0.23 ± 0.00	24.96 ± 0.35	-0.22 ± 0.00	0.09 ± 0.00	43.90	0.79 ± 0.27	
SL2P-CCRS	0 to 1	1449	0.39	0.79 ± 0.02	259.41 ± 8.12	0.59 ± 0.02	0.53 ± 0.02	79.43	1.47 ± 0.05	0.0 to 0.1	635	0.12	0.14 ± 0.00	358.72 ± 8.96	0.11 ± 0.00	0.09 ± 0.00	58.90	1.10 ± 0.12	
	1 to 2	415	0.10	0.98 ± 0.06	66.70 ± 4.35	0.56 ± 0.05	0.80 ± 0.05	72.53	0.93 ± 0.13	0.1 to 0.2	296	0.04	0.15 ± 0.00	102.57 ± 2.91	0.12 ± 0.00	0.10 ± 0.00	47.97	0.70 ± 0.19	
	2 to 3	392	0.06	0.97 ± 0.07	38.98 ± 2.84	0.21 ± 0.06	0.95 ± 0.06	70.92	0.81 ± 0.17	0.2 to 0.3	254	0.04	<b>0.11 ± 0.00</b>	<b>44.87 ± 1.58</b>	<b>0.06 ± 0.00</b>	<b>0.10 ± 0.00</b>	<b>64.17</b>	<b>0.61 ± 0.20</b>	
	3 to 4	447	0.01	1.16 ± 0.06	33.39 ± 1.56	-0.24 ± 0.06	1.14 ± 0.06	59.06	0.37 ± 0.19	0.3 to 0.4	202	0.00	0.13 ± 0.01	37.65 ± 1.89	-0.01 ± 0.01	0.13 ± 0.01	54.46	0.02 ± 0.34	
	4 to 5	346	0.07	1.27 ± 0.07	28.66 ± 1.42	-0.47 ± 0.07	1.18 ± 0.07	55.78	1.21 ± 0.23	0.4 to 0.5	184	0.05	0.14 ± 0.01	30.62 ± 1.34	-0.07 ± 0.01	0.12 ± 0.01	49.46	0.95 ± 0.32	
	5 to 6	134	0.01	<b>1.19 ± 0.10</b>	<b>22.27 ± 1.96</b>	<b>-0.59 ± 0.12</b>	<b>1.03 ± 0.12</b>	<b>72.39</b>	<b>0.44 ± 0.33</b>	0.5 to 0.6	244	0.06	0.18 ± 0.01	31.80 ± 1.26	-0.12 ± 0.01	0.13 ± 0.01	41.39	1.29 ± 0.32	
	6 to 7	36	0.06	<b>1.87 ± 0.17</b>	<b>29.37 ± 2.64</b>	<b>-1.75 ± 0.19</b>	<b>0.68 ± 0.19</b>	<b>27.78</b>	<b>0.60 ± 0.40</b>	0.6 to 0.7	282	0.01	0.22 ± 0.01	33.53 ± 0.80	-0.17 ± 0.01	0.14 ± 0.01	41.49	0.35 ± 0.29	
	7 to 8	6	0.21	<b>2.30 ± 0.40</b>	<b>31.72 ± 5.81</b>	<b>-2.20 ± 0.40</b>	<b>0.70 ± 0.40</b>	<b>33.33</b>	<b>-1.50 ± 1.40</b>	0.7 to 0.8	529	0.03	0.27 ± 0.01	35.60 ± 0.54	-0.20 ± 0.00	0.17 ± 0.00	39.89	1.17 ± 0.27	
	8 to 9	-	-	-	-	-	-	-	-	0.8 to 0.9	436	0.07	0.26 ± 0.00	30.28 ± 0.41	-0.19 ± 0.00	0.18 ± 0.00	55.96	1.69 ± 0.30	
	> 9	-	-	-	-	-	-	-	-	> 0.9	164	0.05	0.21 ± 0.00	22.64 ± 0.31	-0.18 ± 0.00	0.11 ± 0.00	64.63	0.98 ± 0.34	

## Appendix F. Performance of retrievals as a function of fiducial reference magnitude (all canopy types)

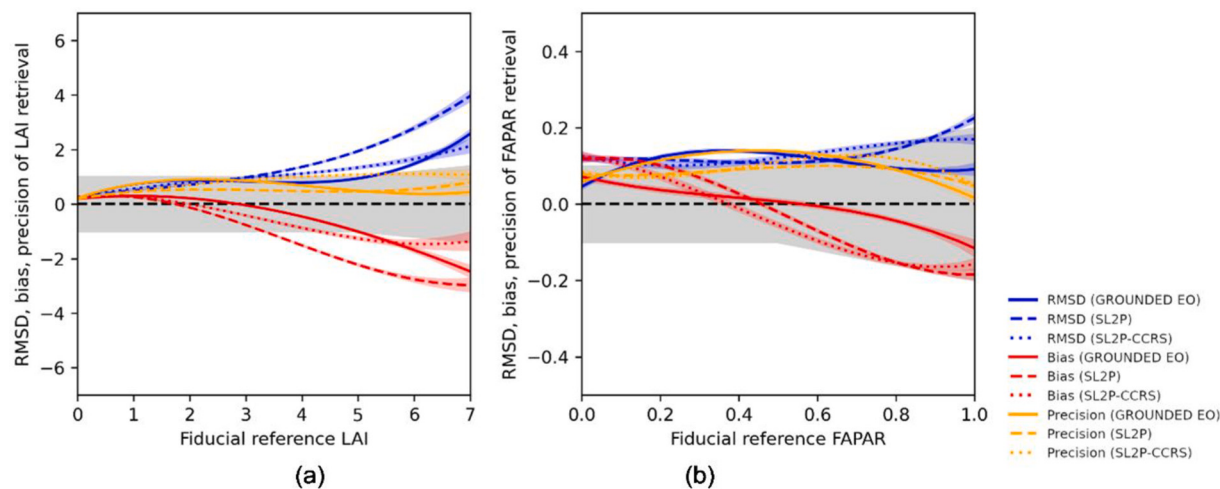


**Fig. F1.** Performance of GROUNDED EO, SL2P, and SL2P-CCRS LAI (a) and FAPAR (b) retrievals as a function of fiducial reference magnitude for all canopy types. The dashed line represents a 1:1 relationship, whilst the shaded grey area represents user requirements. Error bands represent the 95% confidence interval.

## Appendix G. Analysis of the potential impact of L2A surface reflectance uncertainty

In the absence of per-pixel uncertainties within the Sentinel-2 L2A product, we carried out an experiment to assess the potential contribution of L2A surface reflectance uncertainty to total LAI retrieval uncertainty. A Monte Carlo approach was adopted, in which 500 permutations of each GPR model were trained using the training dataset (see Section 2.5), but with surface reflectance values contaminated with Gaussian white noise consisting of multiplicative (2%) and additive (3%) components, assigned according to the expected L2A uncertainty of ~ 5% as demonstrated in previous surface reflectance intercomparison exercises (Djamai and Fernandes, 2018; Doxani et al., 2023, 2018). These trained GPR models were then applied to the reflectance observations within the validation dataset (see Section 2.6). From the 500 permutations of the trained GPR models, the standard deviation of the retrieved values was computed to represent the propagated L2A surface reflectance uncertainty. Total uncertainty in the retrieved values was determined by adding the GPR-derived (i.e. model-based) uncertainties and the propagated L2A surface reflectance uncertainties in quadrature, and the relative contribution of each component to the overall uncertainty budget was calculated. The results indicated that the GPR-derived (i.e. model-based) uncertainties were the dominant component, accounting for 67% of the total uncertainty on average, whereas the propagated L2A surface reflectance uncertainties accounted for 33% of the total uncertainty on average (Fig. G1).

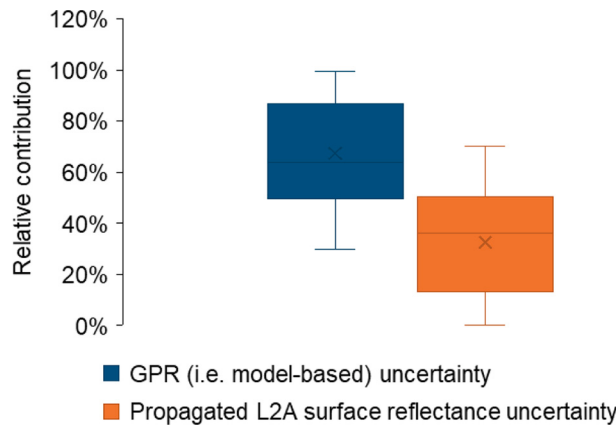


**Fig. G1.** Relative contribution of GPR (i.e. model-based) and propagated L2A surface reflectance uncertainties to the overall LAI retrieval uncertainty budget.

## Data availability

The GROUNDED EO fiducial reference database is archived on Zenodo: <https://doi.org/10.5281/zenodo.14293472>.

The GROUNDED EO retrieval algorithm is archived on GitHub: <https://github.com/luke-a-brown/grounded-eo>.

## References

- Amin, E., Verrelst, J., Rivera-Caicedo, J.P., Pipia, L., Ruiz-Verdú, A., Moreno, J., 2020. Prototyping Sentinel-2 green LAI and brown LAI products for cropland monitoring. *Remote Sens. Environ.* 112168. <https://doi.org/10.1016/j.rse.2020.112168>.
- Bacour, C., Baret, F., Béal, D., Weiss, M., Pavageau, K., 2006. Neural network estimation of LAI, fAPAR, fCover and LAIxCab, from top of canopy MERIS reflectance data: principles and validation. *Remote Sens. Environ.* 105, 313–325. <https://doi.org/10.1016/j.rse.2006.07.014>.
- Baret, F., Weiss, M., Allard, D., Garrigues, S., Leroy, M., Jeanjean, H., Fernandes, R., Myneni, R., Privette, J., Morisette, J., Bohbot, H., 2005. VALERI: A Network of Sites

- and a Methodology for the Validation of Medium Spatial Resolution Land Satellite Products. Institut National de la Recherche Agronomique, Avignon, France.
- Baret, F., Hagolle, O., Geiger, B., Bicheron, P., Miras, B., Huc, M., Berthelot, B., Niño, F., Weiss, M., Samain, O., Roujean, J.L., Leroy, M., 2007. LAI, fAPAR and fCover CYCLOPES global products derived from VEGETATION. *Remote Sens. Environ.* 110, 275–286. <https://doi.org/10.1016/j.rse.2007.02.018>.
- Baret, F., de Solan, B., Lopez-Lozano, R., Ma, K., Weiss, M., 2010a. GAI estimates of row crops from downward looking digital photos taken perpendicular to rows at 57.5° zenith angle: theoretical considerations based on 3D architecture models and application to wheat crops. *Agric. For. Meteorol.* 150, 1393–1401. <https://doi.org/10.1016/j.agrformet.2010.04.011>.
- Baret, F., Weiss, M., Berthelot, B., 2010b. Technical notes on error sensitivity analysis of the Sentinel-2 products level 2B. In: Institut National de la Recherche Agronomique, Avignon, France, 2.10. ed.
- Baret, F., Weiss, M., Lacaze, R., Camacho, F., Makhmara, H., Pacholczyk, P., Smets, B., 2013. GEOV1: LAI and FAPAR essential climate variables and FCOVER global time series capitalizing over existing products. Part 1: principles of development and production. *Remote Sens. Environ.* 137, 299–309. <https://doi.org/10.1016/j.rse.2012.12.027>.
- Berger, K., Rivera Caicedo, J.P., Martino, L., Wocher, M., Hank, T., Verrelst, J., 2021. A survey of active learning for quantifying vegetation traits from terrestrial earth observation data. *Remote Sens. (Basel)* 13, 287. <https://doi.org/10.3390/rs13020287>.
- Boggs, P.T., Byrd, R.H., Schnabel, R.B., 1987. A stable and efficient algorithm for nonlinear orthogonal distance regression. *SIAM J. Sci. Stat. Comput.* 8, 1052–1078. <https://doi.org/10.1137/0908085>.
- Bréda, N.J.J., 2003. Ground-based measurements of leaf area index: a review of methods, instruments and current controversies. *J. Exp. Bot.* 54, 2403–2417. <https://doi.org/10.1093/jxb/erg263>.
- Brown, L.A., Leblanc, S.G., 2024. CoverPy: automated estimates of plant area index, vegetation cover, crown cover, crown porosity, and uncertainties from digital cover photography in Python. *SoftwareX* 27, 101767. <https://doi.org/10.1016/j.softx.2024.101767>.
- Brown, L.A., Ogutu, B.O., Dash, J., 2019. Estimating Forest leaf area index and canopy chlorophyll content with Sentinel-2: an evaluation of two hybrid retrieval algorithms. *Remote Sens. (Basel)* 11, 1752. <https://doi.org/10.3390/rs11151752>.
- Brown, L.A., Meier, C., Morris, H., Pastor-Guzman, J., Bai, G., Lerebourg, C., Gobron, N., Lanconelli, C., Clerici, M., Dash, J., 2020a. Evaluation of global leaf area index and fraction of absorbed photosynthetically active radiation products over North America using Copernicus ground based observations for validation data. *Remote Sens. Environ.* 247, 111935. <https://doi.org/10.1016/j.rse.2020.111935>.
- Brown, L.A., Ogutu, B.O., Dash, J., 2020b. Tracking forest biophysical properties with automated digital repeat photography: a fisheye perspective using digital hemispherical photography from below the canopy. *Agric. For. Meteorol.* 287, 107944. <https://doi.org/10.1016/j.agrformet.2020.107944>.
- Brown, L.A., Camacho, F., García-Santos, V., Origo, N., Fuster, B., Morris, H., Pastor-Guzman, J., Sánchez-Zapero, J., Morrone, R., Ryder, J., Nightingale, J., Boccia, V., Dash, J., 2021a. Fiducial reference measurements for vegetation bio-geophysical variables: an end-to-end uncertainty evaluation framework. *Remote Sens. (Basel)* 13, 3194. <https://doi.org/10.3390/rs13163194>.
- Brown, L.A., Fernandes, R., Djamai, N., Meier, C., Gobron, N., Morris, H., Canisius, F., Bai, G., Lerebourg, C., Lanconelli, C., Clerici, M., Dash, J., 2021b. Validation of baseline and modified Sentinel-2 level 2 prototype processor leaf area index retrievals over the United States. *ISPRS J. Photogramm. Remote Sens.* 175, 71–87. <https://doi.org/10.1016/j.isprsjprs.2021.02.020>.
- Brown, L.A., Morris, H., Leblanc, S., Bai, G., Lanconelli, C., Gobron, N., Meier, C., Dash, J., 2023. Hemipy: a Python module for automated estimation of forest biophysical variables and uncertainties from digital hemispherical photographs. *Methods Ecol. Evol.* 14, 2329–2340. <https://doi.org/10.1111/2041-210X.14199>.
- Brown, L.A., Morris, H., MacLachlan, A., D'Adamo, F., Adams, J., Lopez-Baeza, E., Albero, E., Martínez, B., Sánchez-Ruiz, S., Campos-Taberner, M., Lidón, A., Lull, C., Bautista, I., Clewley, D., Llewellyn, G., Xie, Q., Camacho, F., Pastor-Guzman, J., Morrone, R., Sinclair, M., Williams, O., Hunt, M., Huén, A., Boccia, V., Dransfeld, S., Dash, J., 2024a. Hyperspectral leaf area index and chlorophyll retrieval over Forest and row-structured vineyard canopies. *Remote Sens. (Basel)* 16, 2066. <https://doi.org/10.3390/rs16122066>.
- Brown, L.A., Morris, H., Morrone, R., Sinclair, M., Williams, O., Hunt, M., Bandopadhyay, S., Guo, X., Akcay, H., Dash, J., 2024b. Near-infrared digital hemispherical photography enables correction of plant area index for woody material during leaf-on conditions. *Ecol. Inform.* 79, 102441. <https://doi.org/10.1016/j.ecoinf.2023.102441>.
- Camacho, F., 2021. CEOS WGVG LPV DIRECT V2.1 database [WWW document]. URL: <https://calvalportal.ceos.org/lpv-direct-v2.1> (accessed 8.9.24).
- Camacho, F., Cernicharo, J., Lacaze, R., Baret, F., Weiss, M., 2013. GEOV1: LAI, FAPAR essential climate variables and FCOVER global time series capitalizing over existing products. Part 2: validation and intercomparison with reference products. *Remote Sens. Environ.* 137, 310–329. <https://doi.org/10.1016/j.rse.2013.02.030>.
- Camacho, F., Fuster, B., Li, W., Weiss, M., Ganguly, S., Lacaze, R., Baret, F., 2021. Crop specific algorithms trained over ground measurements provide the best performance for GAI and fAPAR estimates from Landsat-8 observations. *Remote Sens. Environ.* 260, 112453. <https://doi.org/10.1016/j.rse.2021.112453>.
- Camacho, F., Martínez-Sánchez, E., Brown, L.A., Morris, H., Morrone, R., Williams, O., Dash, J., Origo, N., Sánchez-Zapero, J., Boccia, V., 2024. Validation and conformity testing of Sentinel-3 green instantaneous fAPAR and canopy chlorophyll content products. *Remote Sens. (Basel)* 16, 2698. <https://doi.org/10.3390/rs16152698>.
- CEOS, 2024. CEOS Analysis Ready Data [WWW Document]. URL: <https://ceos.org/ard/index.html> (accessed 12.10.24).
- Cherif, E., Feilhauer, H., Berger, K., Dao, P.D., Ewald, M., Hank, T.B., He, Y., Kovach, K. R., Lu, B., Townsend, P.A., Kattenborn, T., 2023. From spectra to plant functional traits: transferable multi-trait models from heterogeneous and sparse data. *Remote Sens. Environ.* 292, 113580. <https://doi.org/10.1016/j.rse.2023.113580>.
- Chernetskiy, M., Gómez-Dans, J., Gobron, N., Morgan, O., Lewis, P., Truckenbrodt, S., Schmullius, C., 2017. Estimation of FAPAR over croplands using MISR data and the earth observation land data assimilation system (EO-LDAS). *Remote Sens. (Basel)* 9, 656. <https://doi.org/10.3390/rs9070656>.
- Chianucci, F., Cutini, A., 2012. Digital hemispherical photography for estimating forest canopy properties: current controversies and opportunities. *iForest -Biogeosciences For.* 5, 290–295. <https://doi.org/10.3832/ifor0775-005>.
- Chianucci, F., Macek, M., 2023. hemispher: an R package for fisheye canopy image analysis. *Agric. For. Meteorol.* 336, 109470. <https://doi.org/10.1016/j.agrformet.2023.109470>.
- Chianucci, F., Ferrara, C., Puletti, N., 2022. coveR: an R package for processing digital cover photography images to retrieve forest canopy attributes. *Trees* 36, 1933–1942. <https://doi.org/10.1007/s00468-022-02338-5>.
- Choi, W., Ryu, Y., Kong, J., Jeong, S., Lee, K., 2025. Evaluation of spatial and temporal variability in Sentinel-2 surface reflectance on a rice paddy landscape. *Agric. For. Meteorol.* 363, 110401. <https://doi.org/10.1016/j.agrformet.2025.110401>.
- Claverie, M., Ju, J., Masek, J.G., Dungan, J.L., Vermote, E.F., Roger, J.-C., Skakun, S.V., Justice, C., 2018. The harmonized Landsat and Sentinel-2 surface reflectance data set. *Remote Sens. Environ.* 219, 145–161. <https://doi.org/10.1016/j.rse.2018.09.002>.
- Cleverly, J., Eamus, D., Edwards, W., Grant, M., Grundy, M.J., Held, A., Karan, M., Lowe, A.J., Prober, S.M., Sparrow, B., Morris, B., 2019. TERN, Australia's land observatory: addressing the global challenge of forecasting ecosystem responses to climate variability and change. *Environ. Res. Lett.* 14, 095004. <https://doi.org/10.1088/1748-9326/ab33cb>.
- Clevers, J.G.P.W., Gitelson, A.A., 2013. Remote estimation of crop and grass chlorophyll and nitrogen content using red-edge bands on Sentinel-2 and -3. *Int. J. Appl. Earth Obs. Geoinf.* 23, 344–351. <https://doi.org/10.1016/j.jag.2012.10.008>.
- Combal, B., Baret, F., Weiss, M., Trubuil, A., Macé, D., Pragnère, A., Myneni, R., Knyazikhin, Y., Wang, L., 2003. Retrieval of canopy biophysical variables from bidirectional reflectance. *Remote Sens. Environ.* 84, 1–15. [https://doi.org/10.1016/S0034-4252\(02\)00035-4](https://doi.org/10.1016/S0034-4252(02)00035-4).
- De Kauwe, M.G., Disney, M.I., Quaife, T., Lewis, P., Williams, M., 2011. An assessment of the MODIS collection 5 leaf area index product for a region of mixed coniferous forest. *Remote Sens. Environ.* 115, 767–780. <https://doi.org/10.1016/j.rse.2010.11.004>.
- Demarty, J., Chevallier, F., Friend, A.D., Viovy, N., Piao, S., Ciais, P., 2007. Assimilation of global MODIS leaf area index retrievals within a terrestrial biosphere model. *Geophys. Res. Lett.* 34, 1–6. <https://doi.org/10.1029/2007GL030014>.
- Djamai, N., Fernandes, R., 2018. Comparison of SNAP-derived sentinel-2A L2A product to ESA product over Europe. *Remote Sens. (Basel)* 10, 926. <https://doi.org/10.3390/rs10060926>.
- Djamai, N., Fernandes, R., Sun, L., Hong, G., Brown, L.A., Morris, H., Dash, J., 2025. On the consistency and stability of vegetation biophysical variables retrievals from Landsat-8/9 and Sentinel-2. *ISPRS J. Photogramm. Remote Sens.* 225, 329–347. <https://doi.org/10.1016/j.isprsjprs.2025.04.006>.
- Djamai, N., Fernandes, R., Weiss, M., McNairn, H., Goïta, K., 2019. Validation of the sentinel simplified level 2 product prototype processor (SL2P) for mapping cropland biophysical variables using Sentinel-2/MSI and Landsat-8/OLI data. *Remote Sens. Environ.* 225, 416–430. <https://doi.org/10.1016/j.rse.2019.03.020>.
- Doxani, G., Vermote, E., Roger, J., Gascon, F., Adriansen, S., Frantz, D., Hagolle, O., Hollstein, A., Kirches, G., Li, F., Louis, J., Mangin, A., Pahlevan, N., Pflug, B., Vanhellemont, Q., 2018. Atmospheric correction inter-comparison exercise. *Remote Sens.* 10, 352. <https://doi.org/10.3390/rs10020352>.
- Doxani, G., Vermote, E.F., Roger, J.-C., Skakun, S., Gascon, F., Collison, A., De Keukelaere, L., Desjardins, C., Frantz, D., Hagolle, O., Kim, M., Louis, J., Pacifici, F., Pflug, B., Poilvè, H., Ramon, D., Richter, R., Yin, F., 2023. Atmospheric correction inter-comparison exercise, ACIX-II land: an assessment of atmospheric correction processors for Landsat 8 and Sentinel-2 over land. *Remote Sens. Environ.* 285, 113412. <https://doi.org/10.1016/j.rse.2022.113412>.
- Drusch, M., Del Bello, U., Carlier, S., Colin, O., Fernandez, V., Gascon, F., Hoersch, B., Isola, C., Laberinti, P., Martimort, P., Meygret, A., Spoto, F., Sy, O., Marchese, F., Bargellini, P., 2012. Sentinel-2: ESA's optical high-resolution Mission for GMES operational services. *Remote Sens. Environ.* 120, 25–36. <https://doi.org/10.1016/j.rse.2011.11.026>.
- ESA, 2018. Sentinel-2 Mission Status Report 409. European Space Agency, Frascati, Italy.
- ESA, 2021. ESA WorldCover 2020 [WWW Document]. URL: <https://worldcover2020.esa.int/> (accessed 8.13.21).
- ESA, 2024. Copernicus Sentinel-2 Collection 1 MSI Level-2A (L2A) [WWW Document]. URL: <https://sentinels.copernicus.eu/web/sentinel/sentinel-data-access/sentinel-products/sentinel-2-data-products/collection-1-level-2a> (accessed 8.9.24).
- Estévez, J., Salinero-Delgado, M., Berger, K., Pipia, L., Rivera-Caicedo, J.P., Wocher, M., Reyes-Muñoz, P., Tagliabue, G., Boschetti, M., Verrelst, J., 2022. Gaussian processes retrieval of crop traits in Google earth engine based on Sentinel-2 top-of-atmosphere data. *Remote Sens. Environ.* 273, 112958. <https://doi.org/10.1016/j.rse.2022.112958>.
- Fang, H., Li, W., Myneni, R., 2013. The impact of potential land cover misclassification on MODIS leaf area index (LAI) estimation: a statistical perspective. *Remote Sens. (Basel)* 5, 830–844. <https://doi.org/10.3390/rs5020830>.

- Fang, H., Baret, F., Plummer, S., Schaepman-Strub, G., 2019. An overview of global leaf area index (LAI): methods, products, validation, and applications. *Rev. Geophys.* 57, 739–799. <https://doi.org/10.1029/2018RG000608>.
- Feret, J.-B., François, C., Asner, G.P., Gitelson, A.A., Martin, R.E., Bidel, L.P.R., Ustin, S. L., le Maire, G., Jacquemoud, S., 2008. PROSPECT-4 and 5: advances in the leaf optical properties model separating photosynthetic pigments. *Remote Sens. Environ.* 112, 3030–3043. <https://doi.org/10.1016/j.rse.2008.02.012>.
- Fernandes, R., Plummer, S., Nightingale, J., Baret, F., Camacho, F., Fang, H., Garrigues, S., Gobron, N., Lang, M., Lacaze, R., Leblanc, S., Meroni, M., Martinez, B., Nilson, T., Pinty, B., Pisek, J., Sonnentag, O., Verger, A., Welles, J., Weiss, M., Widlowski, J.-L., Schaepman-Strub, G., Roman, M., Nickeson, J., 2014. Global leaf area index product validation good practices. In: Fernandes, R., Plummer, S., Nightingale, J. (Eds.), Best Practice for Satellite-Derived Land Product Validation. Land product validation subgroup (committee on earth observation satellites working group on calibration and validation). <https://doi.org/10.5067/doc/ceoswgc/lpv/lai.002>.
- Fernandes, R., Brown, L., Canisius, F., Dash, J., He, L., Hong, G., Huang, L., Le, N.Q., MacDougall, C., Meier, C., Darko, P.O., Shah, H., Spafford, L., Sun, L., 2023. Validation of simplified level 2 prototype processor Sentinel-2 fraction of canopy cover, fraction of absorbed photosynthetically active radiation and leaf area index products over north American forests. *Remote Sens. Environ.* 293, 113600. <https://doi.org/10.1016/j.rse.2023.113600>.
- Fernandes, R., Djamaï, N., Harvey, K., Hong, G., MacDougall, C., Shah, H., Sun, L., 2024. Evidence of a bias-variance trade off when correcting for bias in sentinel 2 forest LAI retrievals using radiative transfer models. *Remote Sens. Environ.* 305, 114060. <https://doi.org/10.1016/j.rse.2024.114060>.
- Fuster, B., Sánchez-Zapero, J., Camacho, F., García-Santos, V., Verger, A., Lacaze, R., Weiss, M., Baret, F., Smets, B., 2020. Quality assessment of PROBA-V LAI, FAPAR and fCOVER collection 300 m products of Copernicus global land service. *Remote Sens.* (Basel) 12, 1017. <https://doi.org/10.3390/rs12061017>.
- García-Haro, F.J., Campos-Taberner, M., Muñoz-Marí, J., Laparra, V., Camacho, F., Sánchez-Zapero, J., Camps-Valls, G., 2018. Derivation of global vegetation biophysical parameters from EUMETSAT polar system. *ISPRS J. Photogramm. Remote Sens.* 139, 57–74. <https://doi.org/10.1016/j.isprsjprs.2018.03.005>.
- Garrigues, S., Allard, D., Baret, F., Weiss, M., 2006. Influence of landscape spatial heterogeneity on the non-linear estimation of leaf area index from moderate spatial resolution remote sensing data. *Remote Sens. Environ.* 105, 286–298. <https://doi.org/10.1016/j.rse.2006.07.013>.
- Garrigues, S., Lacaze, R., Baret, F., Morissette, J.T., Weiss, M., Nickeson, J.E., Fernandes, R., Plummer, S., Shabanov, N.V., Myneni, R.B., Knyazikhin, Y., Yang, W., 2008. Validation and intercomparison of global leaf area index products derived from remote sensing data. *J. Geophys. Res.* 113, G02028. <https://doi.org/10.1029/2007JG000635>.
- GCOS, 2019. Essential Climate Variables [WWW Document]. URL. <https://public.wmo.int/en/programmes/global-climate-observing-system/essential-climate-variables> (accessed 5.2.19).
- George, J.-P., Yang, W., Kobayashi, H., Biermann, T., Carrara, A., Cremonese, E., Cuntz, M., Fares, S., Gerosa, G., Grünwald, T., Hase, N., Heliasz, M., Ibrom, A., Knolh, A., Krujik, B., Lange, H., Limousin, J.-M., Loustau, D., Lukes, P., Marzuoli, R., Mölder, M., Montagnani, L., Neirynck, J., Peichl, M., Rebmann, C., Schmidt, M., Serrano, F.R.L., Soudani, K., Vincke, C., Pisek, J., 2021. Method comparison of indirect assessments of understory leaf area index (LAI<sub>u</sub>): a case study across the extended network of ICOS forest ecosystem sites in Europe. *Ecol. Indic.* 128, 107841. <https://doi.org/10.1016/j.ecolind.2021.107841>.
- Gielen, B., Acosta, M., Altimir, N., Buchmann, N., Cescatti, A., Ceschia, E., Fleck, S., Hörtznagl, L., Klumpp, K., Kolari, P., Lohila, A., Loustau, D., Marañón-Jiménez, S., Manise, T., Matteucci, G., Merbold, L., Metzger, C., Moureaux, C., Montagnani, L., Nilsson, M.B., Osborne, B., Papale, D., Pavelka, M., Saunders, M., Simioni, G., Soudani, K., Sonnentag, O., Tallec, T., Tuittila, E.-S., Peichl, M., Pokorný, R., Vincke, C., Wohlfahrt, G., 2018. Ancillary vegetation measurements at ICOS ecosystem stations. *Int. Agrophysics* 32, 645–664. <https://doi.org/10.1515/intag-2017-0048>.
- Gobron, N., Pinty, B., Verstraete, M.M., 1997. Theoretical limits to the estimation of the leaf area index on the basis of visible and near-infrared remote sensing data. *IEEE Trans. Geosci. Remote Sens.* 35, 1438–1445. <https://doi.org/10.1109/36.649798>.
- Gobron, N., Pinty, B., Aussedat, O., Chen, J.M., Cohen, W.B., Fensholt, R., Gond, V., Huemmrich, K.F., Lavergne, T., Mélin, F., Privette, J.L., Sandholt, I., Taberner, M., Turner, D.P., Verstraete, M.M., Widlowski, J.-L., 2006. Evaluation of fraction of absorbed photosynthetically active radiation products for different canopy radiation transfer regimes: methodology and results using joint research center products derived from SeaWiFS against ground-based estimations. *J. Geophys. Res.* 111, D13110. <https://doi.org/10.1029/2005JD006511>.
- Gobron, N., Morgan, O., Adams, J., Brown, L.A., Cappucci, F., Dash, J., Lanconelli, C., Marioni, M., Robustelli, M., 2022. Evaluation of sentinel-3A and sentinel-3B ocean land colour instrument green instantaneous fraction of absorbed photosynthetically active radiation. *Remote Sens. Environ.* 270, 112850. <https://doi.org/10.1016/j.rse.2021.112850>.
- Gorroño, J., Fomferra, N., Peters, M., Gascon, F., Underwood, C., Fox, N., Kirches, G., Brockmann, C., 2017. A radiometric uncertainty tool for the sentinel 2 Mission. *Remote Sens.* (Basel) 9, 178. <https://doi.org/10.3390/rs9020178>.
- Gorroño, J., Hunt, S., Scanlon, T., Banks, A., Fox, N., Wooliams, E., Underwood, C., Gascon, F., Peters, M., Fomferra, N., Govaerts, Y., Lamquin, N., Bruniquel, V., 2018. Providing uncertainty estimates of the Sentinel-2 top-of-atmosphere measurements for radiometric validation activities. *Eur. J. Remote Sens.* 51, 650–666. <https://doi.org/10.1080/22797254.2018.1471739>.
- Gorroño, J., Guanter, L., Valentín Graf, L., Gascon, F., 2024. A framework for the estimation of uncertainties and spectral error correlation in Sentinel-2 level-2A data products. *IEEE Trans. Geosci. Remote Sens.* 62, 1–13. <https://doi.org/10.1109/TGRS.2024.3435021>.
- Goryl, P., Fox, N., Donlon, C., Castracane, P., 2023. Fiducial reference measurements (FRMs): what are they? *Remote Sens. (Basel)* 15, 5017. <https://doi.org/10.3390/rs15205017>.
- Gower, S.T., Kucharik, C.J., Norman, J.M., 1999. Direct and indirect estimation of leaf area index, fAPAR, and net primary production of terrestrial ecosystems. *Remote Sens. Environ.* 70, 29–51. [https://doi.org/10.1016/S0034-4257\(99\)00056-5](https://doi.org/10.1016/S0034-4257(99)00056-5).
- Graf, L.V., Gorroño, J., Hueni, A., Walter, A., Aasen, H., 2023. Propagating Sentinel-2 top-of-atmosphere radiometric uncertainty into land surface phenology metrics using a Monte Carlo framework. *IEEE J. Sel. Top. Appl. Earth Obs. Remote Sens.* 16, 8632–8654. <https://doi.org/10.1109/JSTARS.2023.3297713>.
- Hassanpour, R., Majnooni-Heris, A., Fakheri Fard, A., Verrelst, J., 2024. Monitoring biophysical variables (FVC, LAI, LCab, and CWC) and cropland dynamics at Field scale using Sentinel-2 time series. *Remote Sens.* (Basel) 16, 2284. <https://doi.org/10.3390/rs16132284>.
- Hu, Q., Yang, J., Xu, B., Huang, J., Memon, M.S., Yin, G., Zeng, Y., Zhao, J., Liu, K., 2020. Evaluation of global decametric-resolution LAI, FAPAR and FVC estimates derived from Sentinel-2 imagery. *Remote Sens.* (Basel) 12, 912. <https://doi.org/10.3390/rs12060912>.
- Jacquemoud, S., Baret, F., 1990. PROSPECT: a model of leaf optical properties spectra. *Remote Sens. Environ.* 34, 75–91. [https://doi.org/10.1016/0034-4257\(90\)90100-Z](https://doi.org/10.1016/0034-4257(90)90100-Z).
- Jin, H., Li, A., Liang, S., Ma, H., Xie, X., Liu, T., He, T., 2022. Generating high spatial resolution GLASS FAPAR product from Landsat images. *Sci. Remote Sens.* 6, 100060. <https://doi.org/10.1016/j.srs.2022.100060>.
- Jonckheere, I., Fleck, S., Nackaerts, K., Muys, B., Coppin, P., Weiss, M., Baret, F., 2004. Review of methods for in situ leaf area index determination. *Agric. For. Meteorol.* 121, 19–35. <https://doi.org/10.1016/j.agrformet.2003.08.027>.
- Kanagawa, M., Hennig, P., Sejdinovic, D., Sriperumbudur, B.K., 2018. Gaussian processes and kernel methods: A Review on Connections and Equivalences. *arXiv Preprint*. <https://doi.org/10.48550/arXiv.1807.02582>.
- Kang, Y., Ozdogan, M., Gao, F., Anderson, M.C., White, W.A., Yang, Yun, Yang, Yang, Erickson, T.A., 2021. A data-driven approach to estimate leaf area index for Landsat images over the contiguous US. *Remote Sens. Environ.* 258, 112383. <https://doi.org/10.1016/j.rse.2021.112383>.
- Kao, R.H., Gibson, C.M., Gallery, R.E., Meier, C.L., Barnett, D.T., Docherty, K.M., Blevins, K.K., Travers, P.D., Azuaje, E., Springer, Y.P., Thibault, K.M., McKenzie, V. J., Keller, M., Alves, L.F., Hinckley, E.-L.S., Parnell, J., Schimel, D., 2012. NEON terrestrial field observations: designing continental-scale, standardized sampling. *Ecosphere* 3, art115. <https://doi.org/10.1890/ES12-00196.1>.
- Karan, M., Liddell, M., Prober, S.M., Arndt, S., Beringer, J., Boer, M., Cleverly, J., Eamus, D., Grace, P., Van Gorsel, E., Hero, J.-M., Hutley, L., Macfarlane, C., Metcalfe, D., Meyer, W., Pendall, E., Sebastian, A., Wardlaw, T., 2016. The Australian SuperSite network: a continental, long-term terrestrial ecosystem observatory. *Sci. Total Environ.* 568, 1263–1274. <https://doi.org/10.1016/j.scitotenv.2016.05.170>.
- Knyazikhin, Y., Martonchik, J.V., Myneni, R.B., Diner, D.J., Running, S.W., 1998. Synergistic algorithm for estimating vegetation canopy leaf area index and fraction of absorbed photosynthetically active radiation from MODIS and MISR data. *J. Geophys. Res. Atmos.* 103, 32257–32275. <https://doi.org/10.1029/98JD02462>.
- Kovács, D.D., Reyes-Muñoz, P., Salinero-Delgado, M., Mészáros, V.I., Berger, K., Verrelst, J., 2023. Cloud-free global maps of essential vegetation traits processed from the TOA Sentinel-3 catalogue in Google earth engine. *Remote Sens.* (Basel) 15, 3404. <https://doi.org/10.3390/rs15133404>.
- Lang, A.R.G., Yueqin, X., 1986. Estimation of leaf area index from transmission of direct sunlight in discontinuous canopies. *Agric. For. Meteorol.* 37, 229–243. [https://doi.org/10.1016/0168-1923\(86\)90033-X](https://doi.org/10.1016/0168-1923(86)90033-X).
- Leblanc, S.G., Chen, J.M., Fernandes, R., Deering, D.W., Conley, A., 2005. Methodology comparison for canopy structure parameters extraction from digital hemispherical photography in boreal forests. *Agric. For. Meteorol.* 129 (3-4), 187–207. <https://doi.org/10.1016/j.agrformet.2004.09.006>.
- Leblanc, S.G., Fournier, R.A., 2014. Hemispherical photography simulations with an architectural model to assess retrieval of leaf area index. *Agric. For. Meteorol.* 194, 64–76. <https://doi.org/10.1016/j.agrformet.2014.03.016>.
- Lewis, P., Gómez-Dans, J., Kaminski, T., Settle, J., Quaife, T., Gobron, N., Styles, J., Berger, M., 2012. An earth observation land data assimilation system (EO-LDAS). *Remote Sens. Environ.* 120, 219–235. <https://doi.org/10.1016/j.rse.2011.12.027>.
- Li, W., Weiss, M., Waldner, F., Defoury, P., Demarez, V., Morin, D., Hagolle, O., Baret, F., 2015. A generic algorithm to estimate LAI, FAPAR and fCOVER variables from SPOT4 HRVIR and Landsat sensors: evaluation of the consistency and comparison with ground measurements. *Remote Sens.* (Basel) 7, 15494–15516. <https://doi.org/10.3390/rs71115494>.
- Macfarlane, C., Grigg, A., Evangelista, C., 2007a. Estimating forest leaf area using cover and fullframe fisheye photography: thinking inside the circle. *Agric. For. Meteorol.* 146, 1–12. <https://doi.org/10.1016/j.agrformet.2007.05.001>.
- Macfarlane, C., Hoffman, M., Eamus, D., Kerp, N., Higginson, S., McMurtie, R., Adams, M., 2007b. Estimation of leaf area index in eucalypt forest using digital photography. *Agric. For. Meteorol.* 143, 176–188. <https://doi.org/10.1016/j.agrformet.2006.10.013>.
- Majasalmi, T., Rautiainen, M., 2016. The potential of Sentinel-2 data for estimating biophysical variables in a boreal forest: a simulation study. *Remote Sens. Lett.* 7, 427–436. <https://doi.org/10.1080/2150704X.2016.1149251>.

- Mathieu, P., O'Niell, A., 2008. Data assimilation: from photon counts to earth system forecasts. *Remote Sens. Environ.* 112, 1258–1267. <https://doi.org/10.1016/j.rse.2007.02.040>.
- Mederer, D., Feilhauer, H., Cherif, E., Berger, K., Hank, T.B., Kovach, K.R., Dao, P.D., Lu, B., Townsend, P.A., Kattenborn, T., 2025. Plant trait retrieval from hyperspectral data: collective efforts in scientific data curation outperform simulated data derived from the PROSAIL model. *ISPRS Open J. Photogramm. Remote Sens.* 15, 100080. <https://doi.org/10.1016/j.photo.2024.100080>.
- Meier, C.L., Thibault, K.M., Barnett, D.T., 2023. Spatial and temporal sampling strategy connecting <scop>NEON</scop> terrestrial observation system protocols. *Ecosphere* 14, 1–15. <https://doi.org/10.1002/ecs2.4455>.
- Meyer, G.E., Neto, J.C., 2008. Verification of color vegetation indices for automated crop imaging applications. *Comput. Electron. Agric.* 63, 282–293. <https://doi.org/10.1016/j.compag.2008.03.009>.
- Müller-Wilm, U., 2018. *Sen2Cor Configuration and User Manual*, 2nd ed. CS, Toulouse, France.
- Niro, F., Goryl, P., Dransfeld, S., Boccia, V., Gascon, F., Adams, J., Themann, B., Scifoni, S., Doxani, G., 2021. European Space Agency (ESA) calibration/validation strategy for optical land-imaging satellites and pathway towards interoperability. *Remote Sens. (Basel)* 13, 3003. <https://doi.org/10.3390/rs13153003>.
- Ogutu, B.O., Dash, J., Dawson, T.P., 2013. Developing a diagnostic model for estimating terrestrial vegetation gross primary productivity using the photosynthetic quantum yield and earth observation data. *Glob. Chang. Biol.* 19, 2878–2892. <https://doi.org/10.1111/gcb.12261>.
- Pedregosa, F., Varoquaux, G.A.G., Michel, V., Thirion, B., Grisel, O., Blondel, M., Prettenhofer, P., Weiss, R., Dubourg, V., Vanderplas, J., Passos, A., Cournapeau, D., Brucher, M., Perrot, M., Duchesnay, E., 2011. Scikit-learn: machine learning in Python. *J. Mach. Learn. Res.* 12, 2825–2830.
- Pekin, B., Macfarlane, C., 2009. Measurement of crown cover and leaf area index using digital cover photography and its application to remote sensing. *Remote Sens. (Basel)* 1, 1298–1320. <https://doi.org/10.3390/rs1041298>.
- Pisek, J., Kuusk, A., Borysenko, O., 2025. On the relationship between shoot Silhouette area to Total needle area ratio (STAR) and contour length. *Remote Sens. Environ.* 317, 114520. <https://doi.org/10.1016/j.rse.2024.114520>.
- Putzenlechner, B., Castro, S., Kiese, R., Ludwig, R., Marzahn, P., Sharp, I., Sanchez-Azofeifa, A., 2019. Validation of Sentinel-2 FAPAR products using ground observations across three forest ecosystems. *Remote Sens. Environ.* 232, 111310. <https://doi.org/10.1016/j.rse.2019.111310>.
- Rasmussen, C.E., Williams, C.K.I., 2006. *Gaussian Processes in Machine Learning*, 2nd ed. Massachusetts Institute of Technology, Cambridge, Massachusetts.
- Raupach, M.R., Rayner, P.J., Barrett, D.J., DeFries, R.S., Heimann, M., Ojima, D.S., Quegan, S., Schmullius, C.C., 2005. Model-data synthesis in terrestrial carbon observation: methods, data requirements and data uncertainty specifications. *Glob. Chang. Biol.* 11, 378–397. <https://doi.org/10.1111/j.1365-2486.2005.00917.x>.
- Revill, A., Florence, A., MacArthur, A., Hoad, S., Rees, R., Williams, M., 2019. The value of Sentinel-2 spectral bands for the assessment of winter wheat growth and development. *Remote Sens. (Basel)* 11, 2050. <https://doi.org/10.3390/rs11172050>.
- Reyes-Muñoz, P., Pipia, L., Salinero-Delgado, M., Belda, S., Berger, K., Estévez, J., Morata, M., Rivera-Caicedo, J.P., Verrelst, J., 2022. Quantifying fundamental vegetation traits over Europe using the Sentinel-3 OLCI catalogue in Google earth engine. *Remote Sens. (Basel)* 14, 1347. <https://doi.org/10.3390/rs14061347>.
- Richardson, A.D., Dail, D.B., Hollinger, D.Y., 2011. Leaf area index uncertainty estimates for model-data fusion applications. *Agric. For. Meteorol.* 151, 1287–1292. <https://doi.org/10.1016/j.agrformet.2011.05.009>.
- Richardson, A.D., Keenan, T.F., Migliavacca, M., Ryu, Y., Sonnentag, O., Toomey, M., 2013. Climate change, phenology, and phenological control of vegetation feedbacks to the climate system. *Agric. For. Meteorol.* 169, 156–173. <https://doi.org/10.1016/j.agrformet.2012.09.012>.
- Richter, K., Atzberger, C., Vuolo, F., Weihs, P., D'Urso, G., 2009. Experimental assessment of the Sentinel-2 band setting for RTM-based LAI retrieval of sugar beet and maize. *Can. J. Remote. Sens.* 35, 230–247. <https://doi.org/10.5589/m09-010>.
- Rivera-Caicedo, J.P., Verrelst, J., Muñoz-Marí, J., Camps-Valls, G., Moreno, J., 2017. Hyperspectral dimensionality reduction for biophysical variable statistical retrieval. *ISPRS J. Photogramm. Remote Sens.* 132, 88–101. <https://doi.org/10.1016/j.isprsjprs.2017.08.012>.
- Roberts, G., 2001. A review of the application of BRDF models to infer land cover parameters at regional and global scales. *Prog. Phys. Geogr.* 25, 483–511. <https://doi.org/10.1177/03091330102500402>.
- Schlterf, M., Atzberger, C., 2006. Inversion of a forest reflectance model to estimate structural canopy variables from hyperspectral remote sensing data. *Remote Sens. Environ.* 100, 281–294. <https://doi.org/10.1016/j.rse.2005.10.006>.
- Schraik, D., Hovi, A., Rautiainen, M., 2021. Crown level clumping in Norway spruce from terrestrial laser scanning measurements. *Agri. Forest Meteorol.* 296, 108238. <https://doi.org/10.1016/j.agrformet.2020.108238>.
- Sellers, P.J., Dickinson, R.E., Randall, D.A., Betts, A.K., Hall, F.G., Berry, J.A., Collatz, G. J., Denning, A.S., Mooney, H.A., Nobre, C.A., Sato, N., Field, C.B., Henderson-Sellers, A., 1997. Modeling the exchanges of energy, water, and carbon between continents and the atmosphere. *Science (80- )* 275, 502–509. <https://doi.org/10.1126/science.275.5299.502>.
- SEN4SCI, 2011. Assessing product requirements for the scientific exploitation of the Sentinel missions [WWW Document]. URL [http://www.geo.uzh.ch/microsite/se\\_n4sci/](http://www.geo.uzh.ch/microsite/se_n4sci/) (accessed 1.29.20).
- Serouart, M., Madec, S., David, E., Velumani, K., Lopez Lozano, R., Weiss, M., Baret, F., 2022. SegSeg: segmenting RGB images into green and senescent vegetation by combining deep and shallow methods. *Plant Phenomics* 2022. <https://doi.org/10.34133/2022/9803570>.
- Stenberg, P., 1996. Correcting LAI-2000 estimates for the clumping of needles in shoots of conifers. *Agric. For. Meteorol.* 79, 1–8. [https://doi.org/10.1016/0168-1923\(95\)02274-0](https://doi.org/10.1016/0168-1923(95)02274-0).
- Tian, Y., Woodcock, C.E., Wang, Y., Privette, J.L., Shabanov, N.V., Zhou, L., Zhang, Y., Buermann, W., Dong, J., Veikkanen, B., Häme, T., Andersson, K., Ozdogan, M., Knyazikhin, Y., Myneni, R.B., 2002. Multiscale analysis and validation of the MODIS LAI product I. Uncertainty assessment. *Remote Sens. Environ.* 83, 414–430. [https://doi.org/10.1016/S0034-4257\(02\)00047-0](https://doi.org/10.1016/S0034-4257(02)00047-0).
- Upreti, D., Huang, W., Kong, W., Pascucci, S., Pignatti, S., Zhou, X., Ye, H., Casa, R., 2019. A comparison of hybrid machine learning algorithms for the retrieval of wheat biophysical variables from Sentinel-2. *Remote Sens. (Basel)* 11, 481. <https://doi.org/10.3390/rs11050481>.
- Vanino, S., Nino, P., De Michele, C., Falanga Bolognesi, S., D'Urso, G., Di Bene, C., Pennelli, B., Vuolo, F., Farina, R., Pulighe, G., Napoli, R., 2018. Capability of Sentinel-2 data for estimating maximum evapotranspiration and irrigation requirements for tomato crop in Central Italy. *Remote Sens. Environ.* 215, 452–470. <https://doi.org/10.1016/j.rse.2018.06.035>.
- Verger, A., Baret, F., Camacho, F., 2011. Optimal modalities for radiative transfer-neural network estimation of canopy biophysical characteristics: evaluation over an agricultural area with CHRIS/PROBA observations. *Remote Sens. Environ.* 115, 415–426. <https://doi.org/10.1016/j.rse.2010.09.012>.
- Verhoef, W., 1984. Light scattering by leaf layers with application to canopy reflectance modeling: the SAIL model. *Remote Sens. Environ.* 16, 125–141. [https://doi.org/10.1016/0034-4257\(84\)90057-9](https://doi.org/10.1016/0034-4257(84)90057-9).
- Verhoef, W., Jia, L., Xiao, Q., Su, Z., 2007. Unified optical-thermal four-stream radiative transfer theory for homogeneous vegetation canopies. *IEEE Trans. Geosci. Remote Sens.* 45, 1808–1822. <https://doi.org/10.1109/TGRS.2007.895844>.
- Vermote, E., Justice, C., Claverie, M., Franch, B., 2016. Preliminary analysis of the performance of the Landsat 8/OLI land surface reflectance product. *Remote Sens. Environ.* 185, 46–56. <https://doi.org/10.1016/j.rse.2016.04.008>.
- Verrelst, J., Muñoz, J., Alonso, L., Delegido, J., Rivera, J.P., Camps-Valls, G., Moreno, J., 2012. Machine learning regression algorithms for biophysical parameter retrieval: opportunities for Sentinel-2 and -3. *Remote Sens. Environ.* 118, 127–139. <https://doi.org/10.1016/j.rse.2011.11.002>.
- Verrelst, J., Rivera, J.P., Moreno, J., Camps-Valls, G., 2013. Gaussian processes uncertainty estimates in experimental Sentinel-2 LAI and leaf chlorophyll content retrieval. *ISPRS J. Photogramm. Remote Sens.* 86, 157–167. <https://doi.org/10.1016/j.isprsjprs.2013.09.012>.
- Verrelst, J., Camps-Valls, G., Muñoz-Marí, J., Rivera, J.P., Veroustraete, F., Clevers, J.G. P.W., Moreno, J., 2015a. Optical remote sensing and the retrieval of terrestrial vegetation bio-geophysical properties – a review. *ISPRS J. Photogramm. Remote Sens.* 108, 273–290. <https://doi.org/10.1016/j.isprsjprs.2015.05.005>.
- Verrelst, J., Rivera, J.P., Veroustraete, F., Muñoz-Marí, J., Clevers, J.G.P.W., Camps-Valls, G., Moreno, J., 2015b. Experimental Sentinel-2 LAI estimation using parametric, non-parametric and physical retrieval methods – a comparison. *ISPRS J. Photogramm. Remote Sens.* 108, 260–272. <https://doi.org/10.1016/j.isprsjprs.2015.04.013>.
- Verrelst, J., Dethier, S., Rivera, J.P., Muñoz-Marí, J., Camps-Valls, G., Moreno, J., 2016. Active learning methods for efficient hybrid biophysical variable retrieval. *IEEE Geosci. Remote Sens. Lett.* 13, 1012–1016. <https://doi.org/10.1109/LGRS.2016.2560799>.
- Verrelst, J., Berger, K., Rivera-Caicedo, J.P., 2020. Intelligent sampling for vegetation nitrogen mapping based on hybrid machine learning algorithms. *IEEE Geosci. Remote Sens. Lett.* 1–5. <https://doi.org/10.1109/LGRS.2020.3014676>.
- Vuolo, F., Zóitak, M., Pipitone, C., Zappa, L., Wenning, H., Immitzer, M., Weiss, M., Baret, F., Atzberger, C., 2016. Data service platform for Sentinel-2 surface reflectance and value-added products: system use and examples. *Remote Sens. (Basel)* 8, 938. <https://doi.org/10.3390/rs8110938>.
- Wan, L., Ryu, Y., Dechant, B., Hwang, Y., Feng, H., Kang, Y., Jeong, S., Lee, J., Choi, C., Bae, J., 2024. Correcting confounding canopy structure, biochemistry and soil background effects improves leaf area index estimates across diverse ecosystems from Sentinel-2 imagery. *Remote Sens. Environ.* 309, 114224. <https://doi.org/10.1016/j.rse.2024.114224>.
- Weiss, M., Baret, F., 2016. *S2ToolBox Level 2 Products: LAI, FAPAR, FCOVER*, 1.1. ed. Institut National de la Recherche Agronomique, Avignon, France.
- Weiss, M., Baret, F., Myneni, R.B., Pragnère, A., Knyazikhin, Y., 2000. Investigation of a model inversion technique to estimate canopy biophysical variables from spectral and directional reflectance data. *Agronomie* 20, 3–22. <https://doi.org/10.1051/agro:2000105>.
- Weiss, M., Baret, F., Block, T., Koetz, B., Burini, A., Scholze, B., Lecharpentier, P., Brockmann, C., Fernandes, R., Plummer, S., Myneni, R., Gobron, N., Nightingale, J., Schaeppman-Strub, G., Camacho, F., Sanchez-Azofeifa, A., 2014. On line validation exercise (OLIVE): a web based Service for the Validation of medium resolution land products. Application to FAPAR Products. *Remote Sens.* 6, 4190–4216. <https://doi.org/10.3390/rs60504190>.
- Widłowski, J.-L., 2015. Conformity testing of satellite-derived quantitative surface variables. *Environ. Sci. Policy* 51, 149–169. <https://doi.org/10.1016/j.envsci.2015.03.018>.
- Woodgate, W., Armston, J.D., Disney, M., Jones, S.D., Suarez, L., Hill, M.J., Wilkes, P., Soto-Berelov, M., 2016. Quantifying the impact of woody material on leaf area index estimation from hemispherical photography using 3D canopy simulations. *Agric. For. Meteorol.* 226–227, 1–12. <https://doi.org/10.1016/j.agrformet.2016.05.009>.
- Working Group 1 of the Joint Committee for Guides in Metrology, 2008. *Evaluation of Measurement Data — Guide to the Expression of Uncertainty in Measurement*. Bureau International des Poids et Mesures, Paris, France.

- Wulder, M.A., Roy, D.P., Radeloff, V.C., Loveland, T.R., Anderson, M.C., Johnson, D.M., Healey, S., Zhu, Z., Scambos, T.A., Pahlevan, N., Hansen, M., Gorelick, N., Crawford, C.J., Masek, J.G., Hermosilla, T., White, J.C., Belward, A.S., Schaaf, C., Woodcock, C.E., Huntington, J.L., Lymburner, L., Hostert, P., Gao, F., Lyapustin, A., Pekel, J.-F., Strobl, P., Cook, B.D., 2022. Fifty years of Landsat science and impacts. *Remote Sens. Environ.* 280, 113195. <https://doi.org/10.1016/j.rse.2022.113195>.
- Xie, Q., Dash, J., Huete, A., Jiang, A., Yin, G., Ding, Y., Peng, D., Hall, C.C., Brown, L., Shi, Y., Ye, H., Dong, Y., Huang, W., 2019. Retrieval of crop biophysical parameters from Sentinel-2 remote sensing imagery. *Int. J. Appl. Earth Obs. Geoinf.* 80, 187–195. <https://doi.org/10.1016/j.jag.2019.04.019>.
- Xie, R., Darvishzadeh, R., Skidmore, A.K., Heurich, M., Holzwarth, S., Gara, T.W., Reusen, I., 2021. Mapping leaf area index in a mixed temperate forest using Fenix airborne hyperspectral data and Gaussian process regression. *Int. J. Appl. Earth Obs. Geoinf.* 95, 102242. <https://doi.org/10.1016/j.jag.2020.102242>.
- Yan, K., Park, T., Yan, G., Chen, C., Yang, B., Liu, Z., Nemani, R., Knyazikhin, Y., Myinen, R., 2016a. Evaluation of MODIS LAI/FPAR product collection 6. Part 1: consistency and improvements. *Remote Sens.* 8, 359. <https://doi.org/10.3390/rs8050359>.
- Yan, K., Park, T., Yan, G., Liu, Z., Yang, B., Chen, C., Nemani, R., Knyazikhin, Y., Myinen, R., 2016b. Evaluation of MODIS LAI/FPAR product collection 6. Part 2: validation and Intercomparison. *Remote Sens.* 8, 460. <https://doi.org/10.3390/rs8060460>.
- Yan, K., Park, T., Chen, C., Xu, B., Song, W., Yang, B., Zeng, Y., Liu, Z., Yan, G., Knyazikhin, Y., Myinen, R., 2018. Generating global products of LAI and FPAR from SNPP-VIIRS data: theoretical background and implementation. *IEEE Trans. Geosci. Remote Sens.* 56, 2119–2137. <https://doi.org/10.1109/TGRS.2017.2775247>.
- Yin, F., Lewis, P.E., Gómez-Dans, J.L., 2022. Bayesian atmospheric correction over land: Sentinel-2/MSI and Landsat 8/OLI. *Geosci. Model Dev.* 15, 7933–7976. <https://doi.org/10.5194/gmd-15-7933-2022>.
- ### Datasets
- Arndt, S., Hinko-Najera, N., Griebel, A., 2021. Digital Hemispherical Photography (DHP) from TERN Wombat Stringybark Eucalypt SuperSite. Version 1.0. Terrestrial Ecosystem Research Network. (Dataset). <https://portal.tern.org.au/metadata/TERN/0578e1ac-8e24-48c6-be5b-bc3e64e8824b>.
- Arriga, N., Dell'Acqua, A., Matteucci, M., 2022. Digital Hemispherical Pictures, San Rossore 2, 2022-12-21. ICOS RI. [https://hdl.handle.net/11676/4nnlCl51MTdbNiV9ri-K\\_uB](https://hdl.handle.net/11676/4nnlCl51MTdbNiV9ri-K_uB).
- Aurela, M., Hatakka, J., Laurila, T., Lohila, A., Mäkelä, T., Rainne, J., Tuovinen, J., 2020. Digital Hemispherical Pictures, Sodankyla, 2020-08-09. ICOS RI. <https://hdl.handle.net/11676/3dkglrsE66ZMShjsDEIND-wU>.
- Beringer, J., McHugh, I., Arndt, S., 2021c. Digital Hemispherical Photography (DHP) from Whroo Dry Eucalypt SuperSite. Version 1.0. Terrestrial Ecosystem Research Network (Dataset). <https://portal.tern.org.au/metadata/TERN/9f0e05df-10a9-4b8d-895e-e906f5a5ae4b>.
- Beringer, J., Moore, C., Lardner, T., 2021a. Digital Cover Photography (DCP) from TERN Boyagin Wandoo Woodland SuperSite. Version 1.0. Terrestrial Ecosystem Research Network (Dataset). <https://portal.tern.org.au/metadata/TERN/0e044a42-1704-450b-9f46-81ad45226e87>.
- Beringer, J., Moore, C., Lardner, T., 2021b. Digital Hemispherical Photography (DHP) from TERN Boyagin Wandoo Woodland SuperSite. Version 1.0. Terrestrial Ecosystem Research Network (Dataset). <https://portal.tern.org.au/metadata/TERN/7e5970c8-b4ad-4817-8d94-24d85155a5d9>.
- Bernhofer, C., Grünwald, T., Hehn, M., Moderow, U., Prasse, H., 2021. Digital Hemispherical Pictures, Tharandt, 2021-09-22, ICOS RI. <https://hdl.handle.net/11676/XB6WyUQ78Cxa0rLh-lubgK>.
- Berveiller, D., Delpierre, N., Morfin, A., Vincent, G., Dufrêne, E., Bazot, S., Soudani, K., 2022. Digital Hemispherical Pictures, Fontainebleau-Barbeau, 2022-10-31, ICOS RI. <https://hdl.handle.net/11676/xEWalvAVzQN8Jsts-cfpTsH4>.
- Cleverly, J., Boulain, N., Grant, N.M., Faux, R., Nolan, R., Ewenz, C., Gallegos Carboneras, J., 2021. Digital Cover Photography (DCP) from TERN Alice Mulga SuperSite. Version 1.0. Terrestrial Ecosystem Research Network. (Dataset). <https://portal.tern.org.au/metadata/TERN/6ee47825-1a8d-46d8-8316-d7e1a19cf36>.
- Cuntz, M., Joetzer, E., Aiguier, T., Courtois, P., 2022. Digital Hemispherical Pictures, Hesse, 2022-07-20, ICOS RI. <https://hdl.handle.net/11676/-8teqkWsZ6BxAbmOPokjMso>.
- Fares, S., Conte, A., Ilardi, F., Moretti, V., Sorgi, T., 2022. Digital Hemispherical Pictures, Castelporziano2, 2022-08-11. ICOS RI. <https://hdl.handle.net/11676/k27jtQcHJFGctA5XBh2Dx1cv>.
- Feigenwinter, I., Etzold, S., Hortnagl, L., Meier, P., Liechti, K., Stutz, T., Burri, S., Buchmann, N., Zweifel, R., Baur, T., Gessler, A., Hug, C., Marty, M., Schmitt Oehler, M., Staudinger, M., Sutter, F., Thimonier Rickenmann, A., Trotsiuk, V., Waldner, P., Zhu, J., Zimmermann, S., 2022. Digital Hemispherical Pictures, Davos, 2022-09-22, ICOS RI. <https://hdl.handle.net/11676/M8qx22QWFIDjuLT2xVppkOjq>.
- Grace, P., Tucker, D., Rowlings, D., Christensen, B., 2021. Digital Cover Photography (DCP), Samford Peri-Urban Site. Version 1.0. Terrestrial Ecosystem Research Network (Dataset). <https://portal.tern.org.au/metadata/TERN/7bbe3a0-85df-460c-9f37-bba452add0ef>.
- Heliasz, M., Kljun, N., Biermann, T., Holst, J., Holst, T., Mölder, M., 2022. Digital Hemispherical Pictures, Hyltemossa, 2022-09-08, ICOS RI. [https://hdl.handle.net/11676/Ly7PT-Ffa\\_nNNdgmPgIg2UtK](https://hdl.handle.net/11676/Ly7PT-Ffa_nNNdgmPgIg2UtK).
- Hero, J., Lollback, G., 2021. Digital Cover Photography (DCP) from TERN Karawatha Peri-Urban SuperSite. Version 1.0. Terrestrial Ecosystem Research Network (Dataset). <https://portal.tern.org.au/metadata/TERN/20902d03-e979-409a-90e5-dee5e5d86698>.
- Hutley, L., Northwood, M., Maier, S., 2021. Digital Cover Photography (DCP) from TERN Litchfield Savanna SuperSite. Version 1.0. Terrestrial Ecosystem Research Network (Dataset). <https://portal.tern.org.au/metadata/TERN/2d9cbe90-3782-4656-9e43-b22d5d275a3a>.
- Ibrom, A., Lange Rønn, E., Møller, F., Pilegaard, K., Schaarup Sørensen, J., 2022. Digital Hemispherical Pictures, Sorøe, 2022-12-02, ICOS RI. [https://hdl.handle.net/11676/TszeSlpkU82C\\_D3WZL565xCVY](https://hdl.handle.net/11676/TszeSlpkU82C_D3WZL565xCVY).
- Janssens, I., De Meuler, T., Lefevre, L., Roland, M., Segers, J., Van Look, J., 2022. Digital Hemispherical Pictures, Brasschaat, 2022-12-02. ICOS RI. <https://hdl.handle.net/11676/x5uLY5sUs4O7JdyEFu1pFro>.
- Lange, H., Zhao, J., Meissner, H., 2022. Digital Hemispherical Pictures, Hurdal, 2022-06-03, ICOS RI. [https://hdl.handle.net/11676/yyandy.YC5\\_ATeGucCNA8Xh](https://hdl.handle.net/11676/yyandy.YC5_ATeGucCNA8Xh).
- Liddell, M., Bradford, M., Weigand, N., 2016. Digital Hemispherical Photography (DHP) from TERN Robson Creek Rainforest SuperSite. Version 1.0. Terrestrial Ecosystem Research Network (Dataset). <https://portal.tern.org.au/metadata/TERN/2fe86586-10b1-4776-85f7-d3b846016388>.
- Limousin, J., Kempf, J., Ourcival, J., 2022. Digital Hemispherical Pictures, Puechabon, 2022-08-11, ICOS RI. [https://hdl.handle.net/11676/u9H4xJsfC\\_IQn-S3XpTH2AYF](https://hdl.handle.net/11676/u9H4xJsfC_IQn-S3XpTH2AYF).
- Loustau, D., Alouane, C., Chipeaux, C., Denou, J., Garrigou, C., Kruszewski, A., Lafont, S., 2022. Digital Hemispherical Pictures, Bilos, 2022-07-04, ICOS RI. <https://hdl.handle.net/11676/1q1pnZAti23FrJ8E2N53XnQQ>.
- Mammarella, I., Aalto, J., Back, J., Kolaric, P., Laakso, H., Matilainen, T., Pihlatie, M., Taipale, R., Vesala, T., 2022. Digital Hemispherical Pictures, Hytytiala, 2022-11-04, ICOS RI. [https://hdl.handle.net/11676/b57zAQDWwEdFbbnvVz\\_q7OmK](https://hdl.handle.net/11676/b57zAQDWwEdFbbnvVz_q7OmK).
- Meyer, W., Koerber, G., 2021. Digital Cover Photography (DCP) from TERN Calperum Mallee SuperSite. Version 1.0. Terrestrial Ecosystem Research Network (Dataset). <https://portal.tern.org.au/metadata/TERN/a16b3324-8358-415a-82d8-3e684672cefe>.
- Mölder, M., Kljun, N., Lehner, I., Båth, A., Holst, J., 2022. Digital Hemispherical Pictures, Norunda, 2022-08-18, ICOS RI. [https://hdl.handle.net/11676/GwQ27ALttlfT9wW5\\_w0ISIU](https://hdl.handle.net/11676/GwQ27ALttlfT9wW5_w0ISIU).
- Montagnani, L., Bortoli, M., Cobbe, I., Stecher, M., Tenca, F., 2021. Digital Hemispherical Pictures, Renon, 2021-10-03, ICOS RI. [https://hdl.handle.net/11676/wlm140Yk24\\_NJAM\\_N23eHe\\_d](https://hdl.handle.net/11676/wlm140Yk24_NJAM_N23eHe_d).
- National Ecological Observatory Network, 2022. Digital hemispheric photos of plot vegetation (DP1.10017.001). <https://data.neonscience.org/> (accessed April 24, 2023).
- Peichl, M., Nilsson, M., Smith, P., Marklund, P., De Simon, G., Löfvenius, P., Dignam, R., Holst, J., Mölder, M., Larmanou, E., 2022. Digital Hemispherical Pictures, Svartrøget, 2022-07-09, ICOS RI. <https://hdl.handle.net/11676/r0Dx7mEUJoxVdfrXua1Tr9>.
- Pendall, E., Boer, M., Metzen, D., 2020. Digital Cover Photography (DCP) from TERN Cumberland Plain SuperSite. Version 1.0. Terrestrial Ecosystem Research Network (Dataset). <https://portal.tern.org.au/metadata/TERN/db766c37-f00d-4dc4-aa1a-325b284da1a0>.
- Prober, S.M., Macfarlane, C.K., Wiehl, G., 2020. Digital Cover Photography (DCP) from Great Western Woodlands Site. Version 1.0. Terrestrial Ecosystem Research Network (Dataset). <https://portal.tern.org.au/metadata/TERN/7cd80502-9f5a-4c7b-a692-2945f190389>.
- Rebmann, C., Dienstbach, L., Schmidt, P., Wiesen, R., Meis, J., Paasch, S., 2022. Digital Hemispherical Pictures, Hohes Holz, 2022-11-02, ICOS RI. [https://hdl.handle.net/11676/So6d1\\_zxrNLbSe25BqpKZHx](https://hdl.handle.net/11676/So6d1_zxrNLbSe25BqpKZHx).
- Silberstein, R., Lardner, T., Mahabbati, A., Just, M., Kunadi, A., Eckersley, J., Galalizadeh, S., 2021. Digital Hemispherical Photography (DHP) from TERN Gingin Banksia Woodland SuperSite. Version 1.0. Terrestrial Ecosystem Research Network (Dataset). <https://portal.tern.org.au/metadata/TERN/5847f424-781b-4b1f-ba48-c182119d52b5>.
- Simioni, G., Marloie, O., Martin-Saint Paul, N., 2022. Digital Hemispherical Pictures, Font-Blanche, 2022-11-29, ICOS RI. [https://hdl.handle.net/11676/jQHZNV\\_321Rof8fmqsF2CdW](https://hdl.handle.net/11676/jQHZNV_321Rof8fmqsF2CdW).
- Stol, J., Kitchen, M., Hodgson, J., Nadelko, A.J., Woodgate, W., 2021. Digital Cover Photography (DCP) from TERN Tumbarumba Wet Eucalypt SuperSite. Version 1.0. Terrestrial Ecosystem Research Network (Dataset). <https://portal.tern.org.au/metadata/TERN/de27e9bb-c7cb-43ae-8780-9fdc59da5d86>.
- Vincke, C., Bogaerts, G., Chopin, H., Demoulin, L., Faurès, A., Heinesch, B., Manise, T., Orgun, A., 2022. Digital Hemispherical Pictures, Vielsalm, 2022-11-25, ICOS RI. [https://hdl.handle.net/11676/4D5Y06yAB7JBswhF\\_000qqFX](https://hdl.handle.net/11676/4D5Y06yAB7JBswhF_000qqFX).
- Wardlaw, T., 2021. Digital Hemispherical Photography (DHP) from TERN Warra Tall Eucalypt SuperSite. Version 1.0. Terrestrial Ecosystem Research Network (Dataset). <https://portal.tern.org.au/metadata/TERN/37fefe41-eaf5-4286-ba7d-3af47ef132cc>.